NTNU

Norwegian University of
Science and Technology

Conceptual structural design of footbridges

A case study of asymmetrically suspended
bridges using parametric modelling

Herman Enger Aas
Kristian Mathias Eick

Department of Structural Engineering
Faculty of Engineering Science and Technology
NTNU- Norwegian University of Science and Technology

ACCESSIBILITY
PUBLIC

MASTER THESIS 2017

ENGINEERING ARCHITECTURE	2 July 2017	NO. OF PAGES: 134

TITLE:

Conceptual structural design of footbridges: *A case study of asymmetrically suspended bridges using parametric design*

Konseptuelt design av gangbroer: *En undersøkelse av asymmetrisk opplagte broer ved bruk av parametrisk design*

BY:

Herman Enger Aas

Kristian Mathias Eick

SUMMARY:
The thesis uses parametric design software tools to investigate relevant structural aspects to be used for development of a conceptual design phase of a footbridge, taking part in the conference "Footbridge 2017" in Berlin. Through a sequence of tests that looked into how the different ways of solving a one-sided suspended deck worked mechanically were performed, in addition to tests on how to conceptualize them. The process has provided the authors with knowledge on one of the many applications to which parametric design tools can be used, which have been shown through hypothesis testing. The utilized parametric design tool in this thesis is mainly Grasshopper 3d including the plug-in tool Karamba.

The footbridge was designed on a site between the districts of Kreuzberg and Fredrichsthain in Berlin, requiring several design parameters to be met. During the design of this bridge a number of different bridge concepts were conceived, and the final concept was accepted by the Conference Committee. The bridge's decks are suspended on only one side of the, the mechanical implications of which are documented inside. After delivering the conceptual design, a series of shallow analysis was performed. The analysis investigated how the structure was influenced by changes inspired by previous hypothesis testing, as well as new found curiosities.

Once the analysis was completed, discussions outline how the design might be optimized based on the findings. Furthermore, the potential future role of parametric design in structural engineering is discussed. Lastly, the thesis summarizes potential and interesting fields for further work related the use parametric tools in structural engineering.

RESPONSIBLE TEACHER:

PROF. ANDERS RÖNNQUIST

CARRIED OUT AT: THE DEPARTMENT OF STRUCTURAL ENGINEERING

Problem statement

The subject of this thesis is conceptual structural design in a parametric software environment. The domain of conceptual design has traditionally been limited to functional problems solved by using heuristics and design knowledge acquired through experience, and been guided by principles from all disciplines within the scope of a project. In conceptual design, the usual mode of presentation would be drawings and solid models, whereas structural analysis' outputs definite results as numbers and graphs.

Parametric design offers a possibility for designers to continuously make rapid changes to their designs, in order to qualitatively accommodate functional needs. It also offers deeper technical analysis of daylight and other building physics, crowd movements, acoustics, and of course structural analysis.

With this thesis we seek to explore the possibilities of parametric design software in conceptual structural design, both with respect to building intuition and testing heuristics, but also using it through the duration of a case to assess design changes accurately on the fly. By the end of the thesis, we should be able to give an assessment of the possibilities of parametric design and its future use in the field of structural engineering. Key activities to create a foundation for the thesis will be

- Hypothesis testing of relevant structures.
- Participation in the "Footbridge 2017 Berlin" through delivering a conceptual footbridge design contribution.
- Further analysis and hypothesis testing of the conceptual design contribution.

Abstract

The thesis uses parametric design software tools to investigate relevant structural aspects to be used for development of a conceptual design phase of a footbridge, taking part in the conference "Footbridge 2017" in Berlin. Through a sequence of tests that looked into how the different ways of solving a one-sided suspended deck worked mechanically were performed, in addition to tests on how to conceptualize them. The process has provided the authors with knowledge on one of the many applications to which parametric design tools can be used, which have been shown through hypothesis testing. The utilized parametric design tool in this thesis is mainly Grasshopper 3d including the plug-in tool Karamba.

The footbridge was designed on a site between the districts of Kreuzberg and Fredrichsthain in Berlin, requiring several design parameters to be met. During the design of this bridge a number of different bridge concepts were conceived, and the final concept was accepted by the Conference Committee. The bridge's decks are suspended on only one side of the, the mechanical implications of which are documented inside. After delivering the conceptual design, a series of shallow analysis was performed. The analysis investigated how the structure was influenced by changes inspired by previous hypothesis testing, as well as new found curiosities.

Once the analysis was completed, discussions outline how the design might be optimized based on the findings. Furthermore, the potential future role of parametric design in structural engineering is discussed. Lastly, the thesis summarizes potential and interesting fields for further work related the use parametric tools in structural engineering.

Sammendrag

Oppgaven undersøker bruk av parametriske designverktøy i utviklingen av et konseptuelt design av en gangbru gjennom deltagelse i gangbrokonferansen "Footbrigde 2017 Berlin". En serie av hypotesetester som undersøker ulike måter å gjennomføre et ensidig opplagt brodekke er utført, i tillegg til tester for å undersøke konseptualiseringen av dem. Denne prosessen har gitt forfatterne kunnskap om én av de mange bruksområdene til parametriske designverktøy. Den parametriske programvaren benyttet i denne oppgaven er i hovedsak Grasshopper 3d med utvidelsen Karamba.

Et konseptuelt gangbrodesign ble utarbeidet og levert som bidrag til gangbrokonferansen "Footbridge 2017 Berlin". Broen er satt til å krysse over elven Spree mellom distriktene Kreuzberg og Fredrichtshain i Berlin. I løpet av designprosessen ble det utviklet en rekke ulike konsept, og det endelige brokonseptet ble akseptert av konferansekomiteen. Broen er opphengt i kabler kun på én side av hvert av sine to dekker og mekaniske implikasjoner er dokumentert i denne oppgaven. Det er gjennomført en rekke tester som undersøker ulike måter å løse dette ensidige opphenget av dekket på, i tillegg til forbedringer på det innleverte brodesignet.

Etter gjennomførelse av videre analyse er det diskutert hvordan brodesignet kan optimaliseres basert på de analytiske funnene. Videre er den potensielle, fremtidige rollen til parametrisk design i konstruksjonsteknikk diskutert. Til slutt oppsummerer oppgaven mulige og interessante områder for videre arbeid knyttet til bruken av parametrisk design i konstruksjonsteknikk.

Preface

This master's thesis is written in the spring of 2017, and is the concluding part of a five years master's program in Structural Engineering at the Norwegian University of Science and Technology. The thesis is written on the subject of parametric modelling in conceptual design, which suits both signatories' interests.

Chapter I of this thesis is an introduction to the subject of parametric design, giving a general assessment of its current use.

Chapter II shows the use of Grasshopper 3D and gives examples to provide the reader with insight as to how parametric design works.

Chapter III consists of an array of hypothesis tests on relevant footbridge designs, in order for the authors to conceptualize how asymmetrically suspended footbridges work, for their design contribution to the Footbridge 2017 Berlin Conference.

Chapter IV introduces the process of participation in the Footbridge 2017 Berlin Conference, showing details from the early design phase to the finalized conceptual design.

Chapter V contains further analysis of the design delivered to the Footbridge Conference. The chapter shows quick analyses as to how the proposed design reacts to certain changes in the design.

Chapter VI summarizes the thesis' main findings and provides relevant discussions on both the use of parametric design in this thesis as well as potential future use in the field of structural engineering.

First and foremost, the authors would like to thank our supervisor, Professor Anders Rønnquist, for his insightful guidance, and for allowing us to undertake such an interesting subject, whilst at the same time giving us the opportunity to partake in the Footbridge 2017 Berlin as a part of our master's thesis.

We would also like to thank postgraduate student Marcin Luczkowski at the Department of Structural Engineering for all his help with learning the Grasshopper, Karamba and Robot software. Thank you also for your continuous guidance in using the software and in solving a variety of problems throughout work on the thesis.
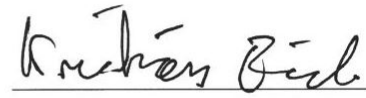
Lastly, thanks to our families, friends and student colleagues for their help and support during the entirety of our studies.

2 July 2017, Trondheim

Herman Enger Aas

Kristian Mathias Eick

Conceptual structural design of footbridges:

Definition of axis systems

Unless anything else is specified, references made with regards to axis' throughout this thesis will be done according to axis systems as defined below.

For any bridge seen as a global structure, the direction of the bridge's main span will be along the x-axis. The direction of the bridge's width will be along the y-axis, while the z-axis will be in the direction of the bridge height.

When discussing a specific structural part, as for example an arch or a deck as an isolated part, references will be made according to that part's local axis system based on the same principle as above.

The same applies for any specific smaller structural component, such as a transverse beam, a stiffener or such.

Should a smaller component be referred to as for example "spanning in y-direction" due to the component being discussed in a global context, this shall be made clear and illustrated where necessary.
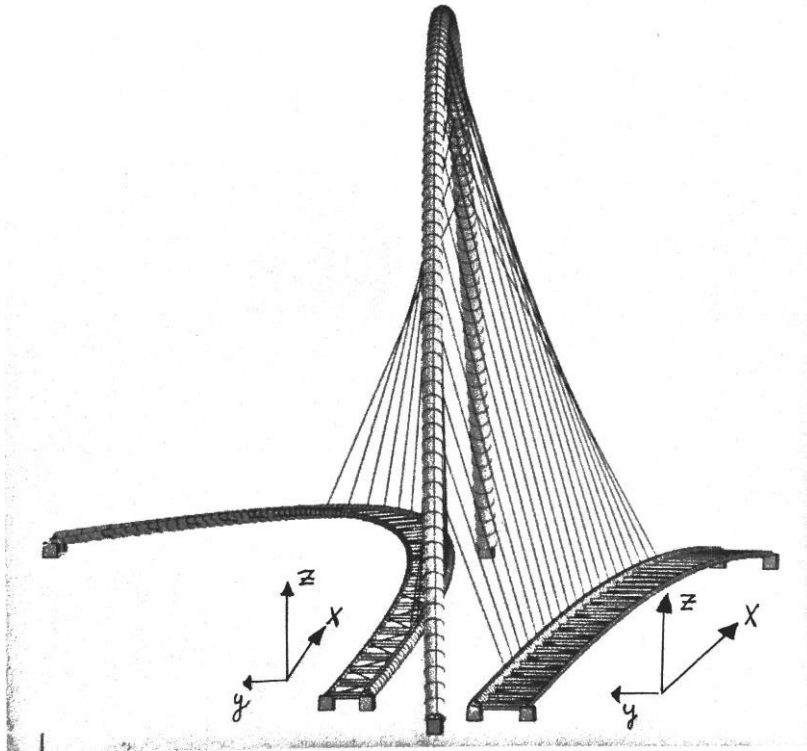
Figure 1: Global axis system for bridges and local system for structural parts.
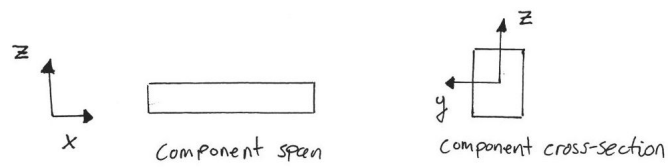

Figure 2: Local axis system for components.

Conceptual structural design of footbridges:

Contents

1. <u>INTRODUCTION</u>

Parametric design and its integration into the work flow of engineering offices around the world is gradually taking over for the older methods on how to conduct design of complex projects, especially buildings. As building projects are designed by teams from a large array of discipline, the continuous sharing of documentation of changes made for their respective fields of expertise traditionally takes a lot of time. This is especially due to the fact that team members are not always acquainted with the specifics, or even generalities of each others' work. Parametric design represents the natural continuation of this sharing of information, not through transfer of documentation, but through rule-based boundary conditions for changes or through clear indicators on whether the changes made are feasible or not. This thesis will investigate whether parametric design tools are applicable when designing a conceptual footbridge design. This chapter will provide information on parametric design and its use today.

1.1   Parametric design

Firstly, an introduction to the use of BIM (building information modeling) is necessary to be able to relate an almost universally adopted method of engineering, to parametric design. BIM involves keeping all documentation in a database which is view able on a common model to give quick assessment of all its content. The content range from plumbing to meta data about deliveries from different vendors, with schedules for installment of prefabricated elements among others. The total integration of the building into computer models in practice makes us able to do a huge amount of real life changes with very few manipulations, but most manifestations of BIM in use at the moment work mainly through manual manipulations in 3d space through a modern GUI (graphical user interface).

A computer, much different from a human, would understand the world not through the 3d or 2d space, but through numerical representations of it. In its earlier manifestations, one would communicate with the computer

through various levels of languages on a command line. This requires some learning, but gives the possibility of very efficient use as there is usually a big variety of commands to choose from. Modern GUIs almost entirely bridge the gap between human and computer, as you interact with buttons that initiate the commands or move files around with the mouse in your hand.

Relating this to the use of parametric design moves the design thinking back one step from interacting with what you see to a more abstract, algorithmic form. In general, architects, engineers and designers have been applying this line of thinking throughout the centuries, the most famous example being the catenary line, constructed by hanging a chain or strings with lead weights, guaranteeing a form with only tensile forces. This is in essence an algorithm (gravity, sum of forces in a non-accelerating system equals zero, strings have no bending stiffness) and parameters (length of string, spacing and weight of weights) resulting in a design satisfying the criteria of only handling its forces in tension. Inverting this form leads to a form necessarily carrying all its forces in compression.

The exemplified algorithm operates on a level directly linked to the structural performance of the object and the designer redistributes forces to get the desired form with a guarantee of structural performance. This, summarized in a short sentence, represents the foundation of parametric design.

1.2 Grasshopper 3d

The parametric design software used in this thesis is called Grasshopper 3d with the plug-in Karamba. Using Grasshopper, one has the opportunity of form finding a-la Gaudi through various plug-ins such as Kangaroo and Karamba. However, the algorithms used throughout this thesis use a more formal approach, where the geometry generated is based on rules depending on lengths, points, divisions. Tinkering and evolutionary algorithms are used to arrive at the final form. This is done because grasshopper does not lend itself very well to recursive algorithms, which requires scripting or creative use of FEM-software such as Karamba.

Geometry can be imported from Rhinoceros or created in Grasshopper itself. For our purposes, executing everything inside Grasshopper gives the greatest level of flexibility. Is it worth mentioning, however, that designing in Grasshopper for structural engineering can be range from being easy and cumbersome depending on the level of ambition in what one wants to produce. The algorithms documented in this thesis belong somewhere in

the middle. The main benefit which makes it so attractive for design, and one of the reasons this and similar concepts see such widespread adaptation, is the fact that once an algorithm is produced, it can be reused with slight modifications for any similar application it was intended to. Additionally, the information the components contain can be easily discerned when reusing parts of an algorithm.

The next chapter, chapter II, will provide several examples on how these algorithms have been utilized in this thesis' use of parametric design. The algorithms form the basis to perform hypothesis testing in chapter III.

2. <u>EXAMPLE ALGORITHMS</u>

The following chapter presents some simple algorithms that can be applied for trivial structural analysis. The aim of this chapter is to more clearly showcase how the Grasshopper software can be used for structural analysis by giving a more detailed presentation of how the software can be used to perform common structural requirement checks.

By choosing basic requirement checks, a more detailed approach on how these can be incorporated into the software can be presented. The hope is that this chapter may become a useful guide for designers on how one can apply simple algorithms in the software in order to easily and continuously perform requirement checks to the developing structure when using the software for conceptual design of structures.

2.1   Drawing geometry

In Grasshopper, a comprehensive set of components for making geometry is put to our disposal. In bridge design, several examples have turned out to be especially useful and will be documented in practical use in this section.

2.1.1   Kite cross-section arch

The kite cross-section became relevant when working on the Gateshead Millennium Bridge, as shown further in section 3.4, as the sideways forces induce varying moments across the arch. This implies that for minimal material usage, material spent one place in a uniform cross-section might be better spent somewhere else, which in the Gateshead millennium Bridge is solved by having a kite-shaped cross-section.

This can be drawn in a lot of different ways in Grasshopper and the method chosen could be made simpler by using the "PerpFrames" component instead of the plane-averaging method used. The part of the algorithm pictured in 2.2 is treating three planes drawn along a NURB.
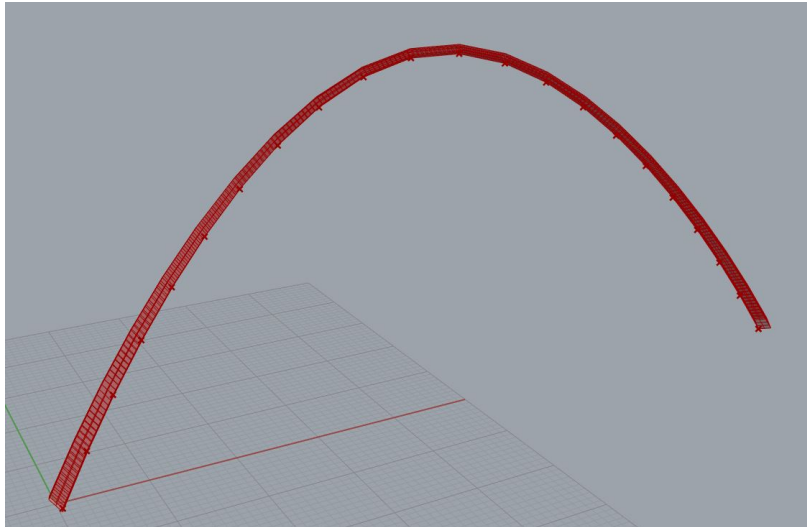
Figure 2.1: Arch with varying cross-section.

To get a varying cross-section, in this case smaller in the top and bigger at its ends, the two planes at the ends are sorted out to the bottom of the algorithm and the middle plane is separated out to the top, both using the "list item" component. Points representing the corners of the cross-section are drawn on the three planes, and a curve representing the longitudinal edges of the arch is interpolated through its respective points.

To create an easily handled geometry, both in terms of connecting cables to it and in terms of meshing, these interpolated curves are divided into straight segments drawing polylines. The polylines are then made into a set of straight lines using the "explode" component, and the points representing the divisions are output for attachment of cables etc.. Ruled surfaces are drawn between the neighboring line-segments, which are in turn meshed. These meshes are output to Karamba where they will represent plate-elements and surfaces to be loaded. the surfaces are automatically meshed with a snippet of algorithm that seeks to make each element as square as possible in combination with the "meshUV" component.

2.1.2 Box-section

A box-section can easily be produced in Grasshopper if one is satisfied with certain limitations. This box-section can not be produced from extruded profiles as the geometry is defined on the mating surfaces, as defined from planes in the "PerpFrames" component. If the structural part has to follow a curve with varying curvature, this will result in cross-sections with dimensions varying along its length. if one wishes to make an extruded-type
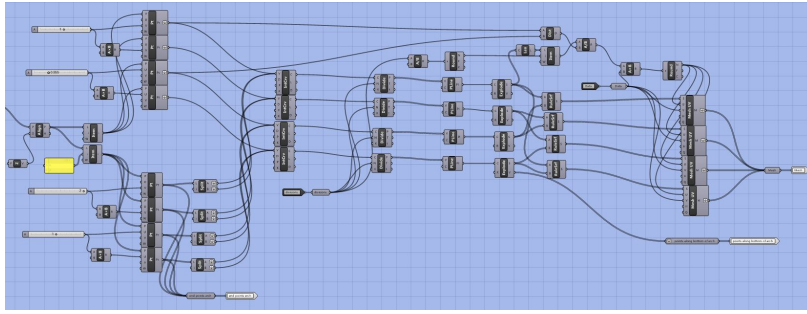
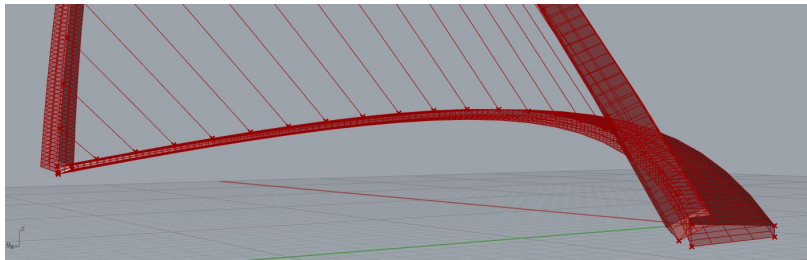Figure 2.2: Algorithm drawing an arch with varying cross-section.

Figure 2.3: A box-type deck pictured with the arch from the previous section.

section, more work has to be done.

A curve is input in the algorithm, which is then divided into the desired amount of divisions. Planes, perpendicular to the curve, are drawn on the points that represent the divisions. The "Point oriented" component is used to draw points on this set of planes at the desired corners of the box. In this case four points are drawn on the set of planes, resulting in four sets of points. Each set of points is then used to draw polylines, that are used to draw surfaces using the "RuleSrf" component. The end points of the polylines are output to be used as supports in a FE-analysis. A snippet similar to the one used in the last section is used to mesh the surfaces, and the meshes are output to represent elemnts and loaded surfaces in a FE-analysis.
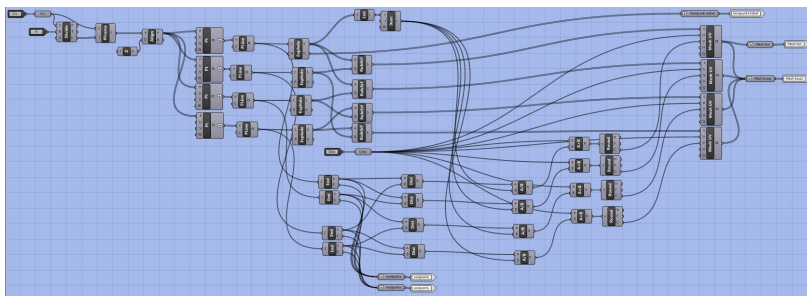

Figure 2.4: A box-type deck pictured with the arch from the previous section.

2.1.3 Suspension system

To make a catenary suspension system in Grasshopper, an algorithm was made that projects NURB lines onto a surface drawn between a top point and the line one intends to attach the hanger cables to.

The algorithm takes in the polyline outlining the desired side of the deck and two lines drawn between each of the ends and the desired top point using the "EdgeSrf"-component. NURBs are drawn with the end points and top point as control points for their ends, and a common point as the control point for their middle. The NURBS are then projected onto the edged surface using the "Project" component. the curves are projected along a vector between the center of area and a point.
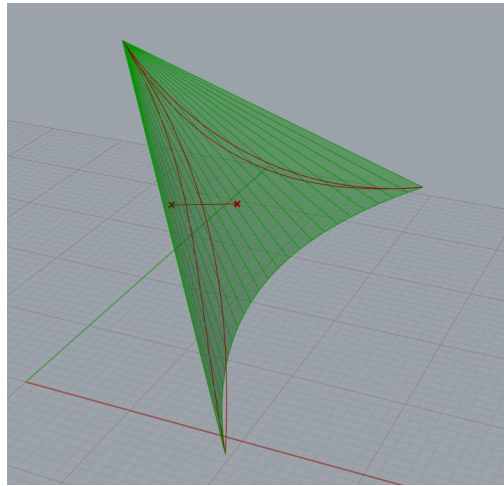

Figure 2.5: Edged surface, NURBSs and vector used to project the NURB.

To draw cables, represented by lines between the main cable and the deck, the "PCX" (plane curve intersection) component is used on the projected curves with planes used to draw the deck. This outputs the points where the planes intersect the curves. These points can then be connected with points along the deck with the "Line" component to draw hanger cables. The points are also sorted along the curve ("AlongCrv" component) and connected with the "polyline" component to form the lines that will represent the catenary.

As can be seen in Figure 2.6, the top-point of the polyline does not coincide with the original top-point. The top point of the polyline is found using the "closest point" component, and can now, for example, be used to draw a tower to which the catenary is attached.
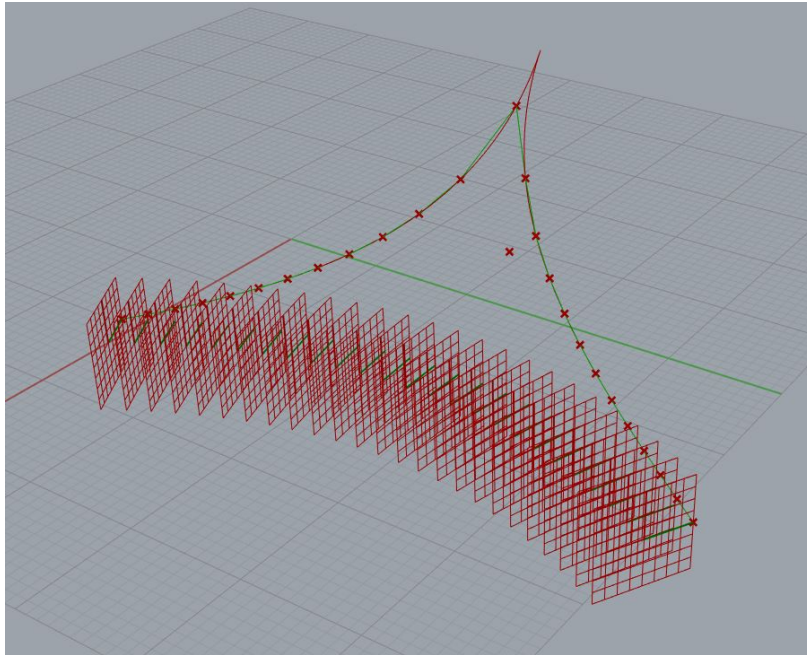
Figure 2.6: Planes from deck, projected NURBs and polyline representing the NURBs (green).
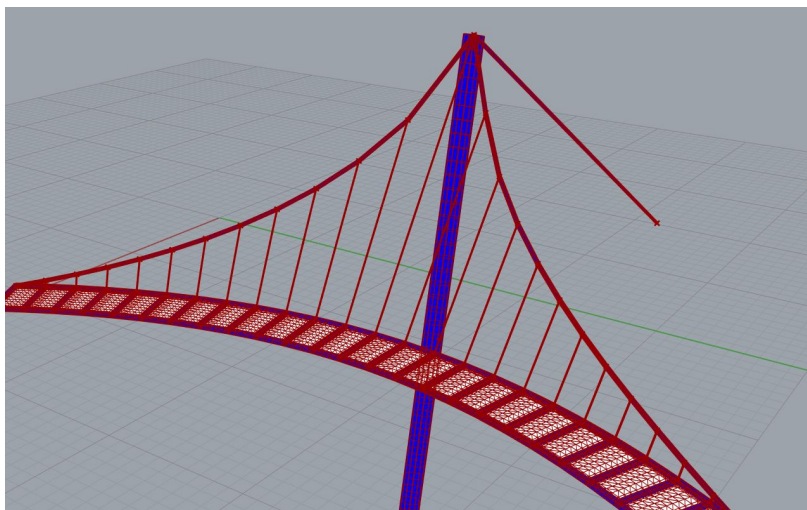

Figure 2.7: A catenary with hanger cables placed on one side of the deck of a bridge.
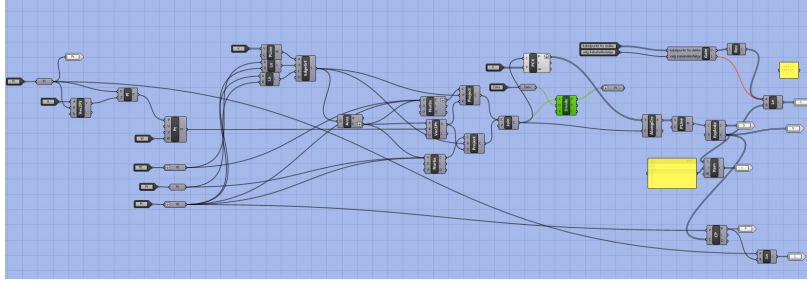
Figure 2.8: The algorithm used to draw a catenary.

2.2 Serviceability Limit State (SLS)

A common requirement check is that of maximum allowed deformation of structural elements in the Serviceability Limit State. In this example a check that can be applied for the deformation of load-carrying transverse beams in a deck will be presented.

Figure 2.9 shows an algorithm created in the Grasshopper and Karamba software that constructs a beam as shown in figure 2.10.

The beam is simply supported and has a length of 4 m, an IPE240 cross-section and S355 steel quality. The loading applied is that which corresponds to the servicability limit state loading for a pedestrian bridge, i.e. the characteristic traffic (crowd) load [1]. This load, of value $q_{fk} = 5.00$ $\frac{kN}{m^2}$, can be found in table 5.1 and attachment B. For the sake of simplicity, permanent load from self-weight and any potential deck is neglected, but should be part of the load-combination for an actual SLS requirement check for deformation in accordance with NS-EN 1992 (6.4). In this example it is initially assumed that the spacing between each transverse beam is 4 m, resulting in each beam carrying the planar crowd load 2 m in each direction perpendicular to the beam span. The result becomes a uniform line load of

$$q_{fk} = 5.00 \frac{kN}{m^2} \times (2+2)m = 20.00 \frac{kN}{m} \tag{2.1}$$
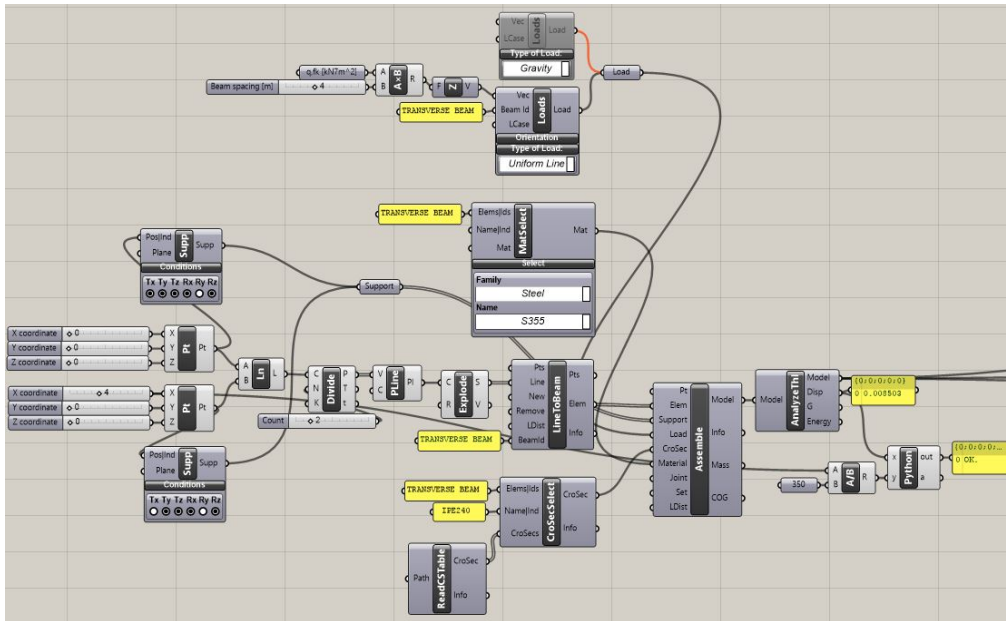
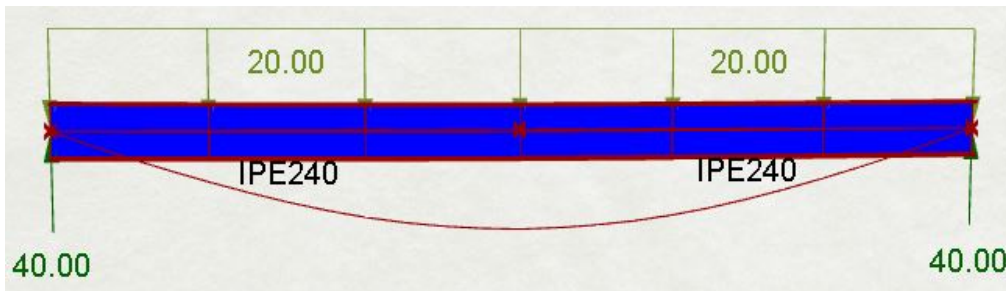Figure 2.9: SLS deformation control algorithm.

Figure 2.10: The produced beam resulting from the algorithm.

According to Eurocode NS-EN 1992 A1.4, the vertical displacement of a structural steel component in the SLS should not surpass a value in the range of

$$\frac{L}{250} < w < \frac{L}{200}, \tag{2.2}$$

while the vertical displacement of a bridge span should not surpass the value of

$$w < \frac{L}{350} \tag{2.3}$$

in neither vertical directions (downward nor upward displacement) according to Statens Vegvesen [1]. As this thesis focuses on bridges, it is chosen to evaluate the displacement of the transverse beams against the latter requirement found in equation 2.3.
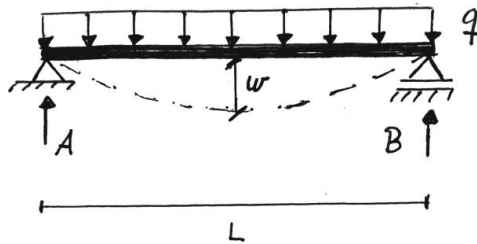
2.2.1 Beam theory

Figure 2.11: Simply supported beam.

From beam theory, we know that the reaction forces A and B of a simply supported beam with a uniform line load equals $\frac{qL}{2}$, and that the maximum vertical displacement of value $\frac{5qL^4}{384EI}$ occurs at mid-span $\frac{L}{2}$ [2].

By inserting data for the above example, the following results are achieved

Results for the example beam using beam theory

Data	Forces A, B	Max. moment	Displ.
S355 IPE 240 $E = 210000\ MPa$ $I_y = 38.9 \times 10^6\ mm^4$ $Q_{fk} = 20.00\ \frac{kN}{m}$ $L = 4\ m$	$40\ kN$	$40\ kNm$	$8.161\ mm$

Table 2.1: Calculated results for the transverse beam using beam theory.
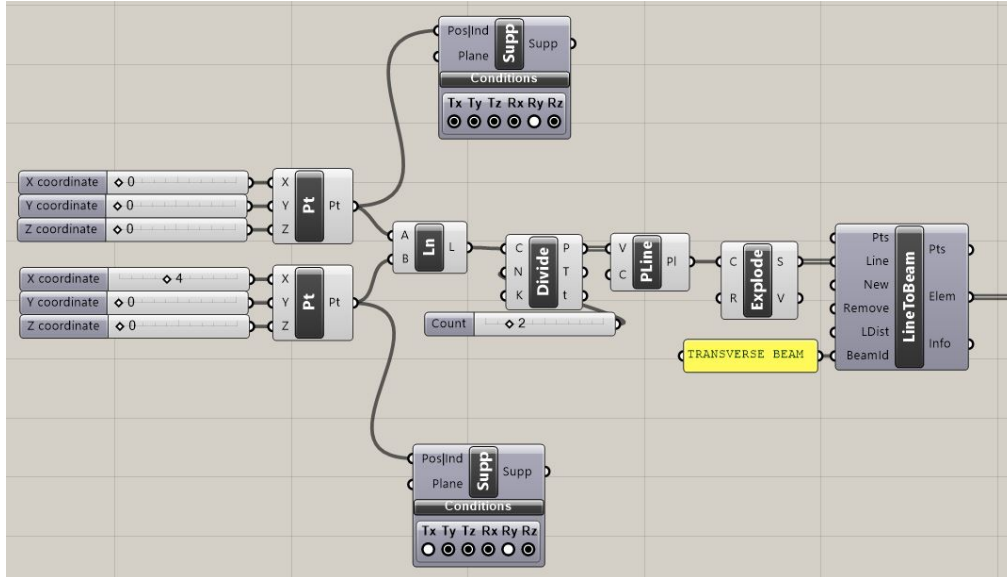
2.2.2 Detailed look at the algorithm

Figure 2.12: Definition of geometry, support types, and element creation.

The first part of the algorithm, seen in figure 2.12, defines the desired geometry of the beam - in this case a 4 m long line between two points in the xy-plane. The length of this line is easily adjusted by pulling the slider, now set to 4, to the left or right in order to decrease or increase the length respectively. Support conditions are then applied to each of the two points, in this case to create a simply supported beam by allowing rotation about the y-axis for one of the supports, and allowing rotation about y-axis and movement in x-direction for the other. If a fixed support was desired in one or both points, one would simply need to tick the remaining boxes of the support definer. Lastly, the line that represents the beam are divided in two and fed into a line-to-beam converter in order to get a 3-node element that can be analyzed by the Karamba plug-in. A 3-node element is needed in order to enable results from the mid-span of the beam, while the line-to-beam converter is needed for Karamba to recognize the geometry as an element.

The second part of the algorithm is defining the material, cross-section and load-situation as seen in figure 2.13. The material is chosen by using a material-selection-tool which allows the selection between steel, aluminum, wood and concrete with a variety of options for material qualities. The cross-section may be chosen from a list of standard cross-sections as chosen in this example, or it may be customized freely. A third option would be to download additional standard cross-sections from the internet. Here,

IPE240 is called in the cross-section selector.

For the loading in this example it has been chosen to turn off the gravity load, i.e. the self-weight of the beam, in order to more easily compare the results to the ones from the beam theory calculation above. However, the gravity load can be turned on for a more realistic result by the click of a button. The uniform line load has been made using the 'Loads' tool and choosing 'uniform line'. The size of load has then been made using a multiplication box with one fixed value of $q_{fk} = 5.00 \ \frac{kN}{m^2}$ to be multiplied with a number slider which has been renamed 'Beam spacing'. The result is then given a directional vector (-z). What this achieves is the option to change the crowd loading applied to each transverse beam as a result of the spacing distance between each of the beams automatically, simply by pulling a slider to the left or to the right to decrease or increase the beam spacing respectively.

The definition boxes in figure 2.13 have all been given the same element ID 'TRANSVERSE BEAM' as the beam element in order to specify that the material, cross-section and uniform line load applies to that specific element.
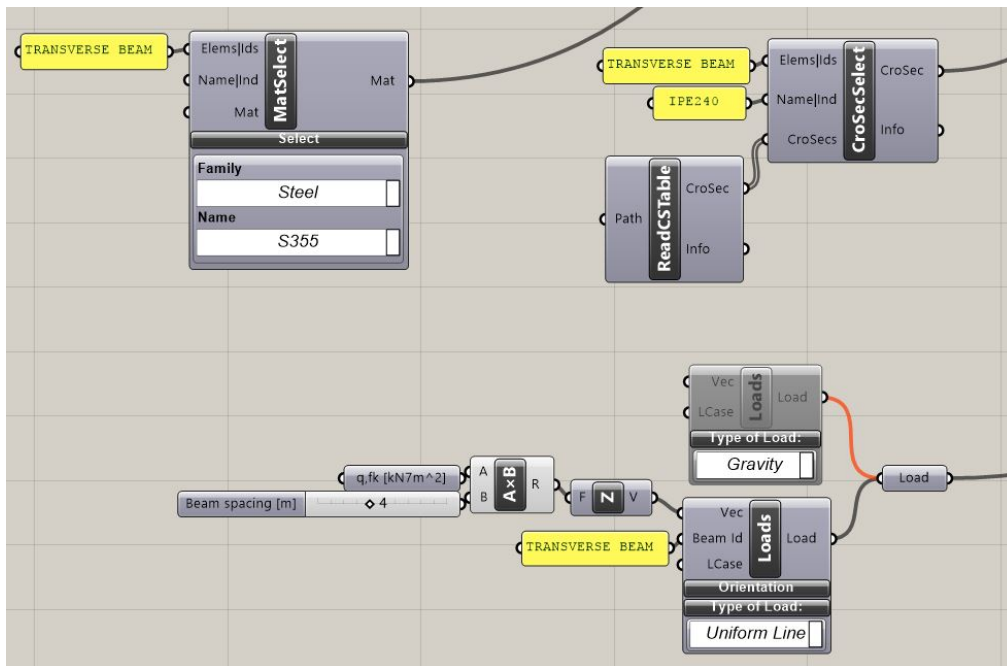

Figure 2.13: Definition of material, cross-section and load-situation.

The third, and last, part of the algorithm combines all the different components in the algorithm and performs the calculations and requirement check. Figure 2.14 shows, from left to right, how the components are fed

into the Karamba Assembly component, which collects all the data and transfers it to the Analysis Th1 tool, which performs the analysis. A panel has been connected to display the output 'Disp' which shows the maximum displacement of a node in the element.

The displacement is then fed into a python script in order to perform the requirement check. The python tool takes the displacement as an input x, and the result of a division tool box as an input y. The division box takes the slider with the length of the beam along the x-axis as input A, and divides it with a fixed value of 350 as input B, in order to calculate the value of the maximum allowed displacement of the beam as output 'R'. This means that if the length of the beam is changed, the control value for the requirement check automatically adjusts itself as a result.
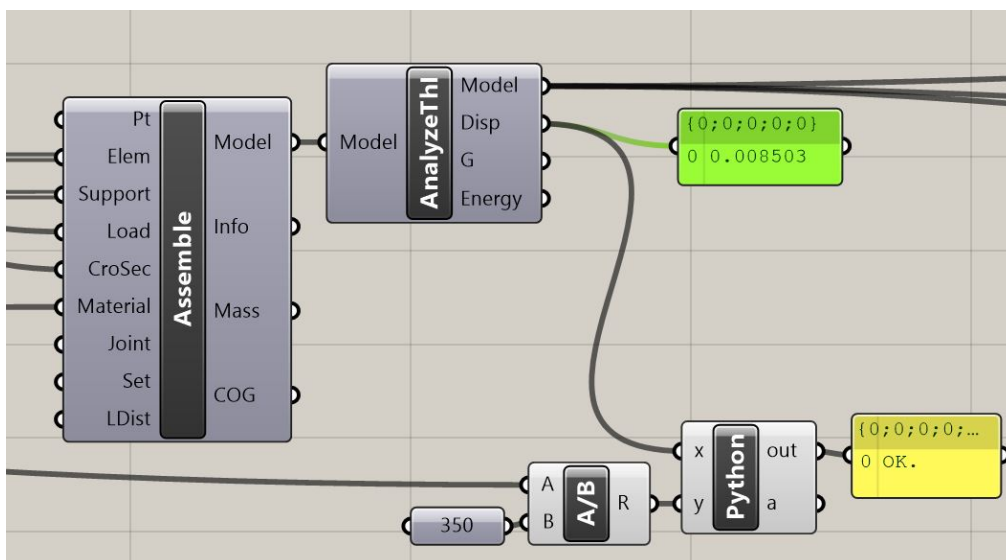

Figure 2.14: Analysis and requirement check.

The python script then performs the quite simple check of controlling whether or not the input x, i.e. the displacement of the beam, is larger than the input y, i.e. the requirement value for maximum allowed displacement of the beam in SLS. A panel is then used to display the output 'OK' or 'NOT OK' based on the result of the requirement check performed in the script. Figure 2.15 shows the code for the python script.

To achieve the display that was shown in figure 2.10 of the beam's cross-sectional geometry, cross-section tags, load values and load symbols as a figure in Rhinoceros 5, one can use Karamba tools such as 'ModelView' and 'BeamView', and connecting them to the 'Model' output seen in figure 2.14. To control the reaction forces, largest moments and forces in the element the Karamba tool 'BeamForces' may be applied in the same

manner. These functions are not shown in this presentation, as it strictly speaking is unnecessary in order to perform or use the requirement check algorithm. It may however be wise to control these values, together with controlling the calculated displacement by the software, in order to verify that the algorithm is working properly. Verification can be carried out on a simple example, as done in this chapter, and the superfluous components (or tool-boxes) may then be removed after the verification.

```python
import rhinoscriptsyntax as rs

if x < y:
    print('OK.')
else:
    print('NOT OK.')
```

Figure 2.15: The code in the python script tool-box.

A comparison between the results for the beam using the algorithm, presented in table 2.2, and the results calculated using beam theory, presented in table 2.1 seems to be within the margin of error and is if anything more conservative with regards to the displacement.

Results for the example beam using the algorithm

Data	Forces A, B	Max. moment	Displ.
S355 IPE 240 $E = 210000\ MPa$ $Q_{fk} = 5.00\ \frac{kN}{m^2} \times 4.00\ m$ $L = 4\ m$	$40\ kN$	$40\ kNm$	$8.503\ mm$

Table 2.2: Calculated results for the transverse beam using the algorithm (Karamba).

2.2.3 Applications

The SLS requirement check algorithm has a variety of applications. It can be incorporated into larger algorithms for different specific conceptual designs in order to get continuous results on whether or not the chosen combination of beam length (span), spacing and cross-section is OK or NOT OK with regards to displacement in SLS. Alternatively it can be used as an external requirement check, i.e. that it is not inserted into a

larger algorithm, for checking what sort of combination that is appropriate whenever the need occurs.

To sum up, the following attributes are available in the algorithm for the requirement check of the displacement in the Serviceability Limit State:

•Change the support conditions with the click of a button and get instant results

•Adjust the span of the beams by pulling a slider to decrease or increase the span

•Automatic adjustment of loading applied to each beam when changing the spacing between the beams by pulling a slider to decrease or increase the spacing

•Change the dimensions of the cross-section by typing its name

•Instant and continuous results of the deformation as changes are made

•Automatic adjustment of the maximum displacement requirement as the span changes

•Instant and continuous display of whether or not the chosen solution is OK or NOT OK with regards to the requirement for maximum displacement

How the algorithm can be used

The algorithm can be used to determine the maximum distance of the spacing between each transverse beam. If there is a predefined requirement for the width of the bridge deck for the design, the length of the transverse beam span becomes a constant. The slider for the spacing between each transverse beams can then be pulled until the panel for the displacement requirement check switches between OK and NOT OK, hence determining the maximum spacing allowed with the given cross-sectional data for the transverse beams.
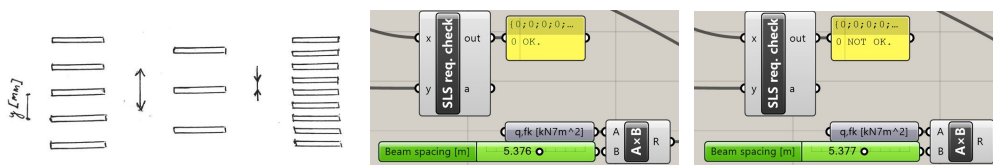

Figure 2.16: Determination of maximum spacing.

Figure 2.16 shows that the result of the requirement check switches when

the spacing distance reaches 5.377 m, thus making 5.376 m the maximum spacing to fulfill the SLS requirement check for vertical deformation.

If a specific or desired spacing between each of the transverse beams exists due to symmetry or restrictions from the deck material, one may decrease or increase the size of the cross-section until the panel for the requirement check switches between OK and NOT OK in order to efficiently find the minimal cross-section that fulfills the requirements for displacement in SLS. Figure 2.17 shows the changing between IPE240 and IPE300 with corresponding values for displacement (in meter), and the result for the SLS requirement check for a beam with 4 m span and an arbitrary, yet constant spacing between each beam of 5.960 m. The crowd load is still 5 $\frac{kN}{m^2}$.
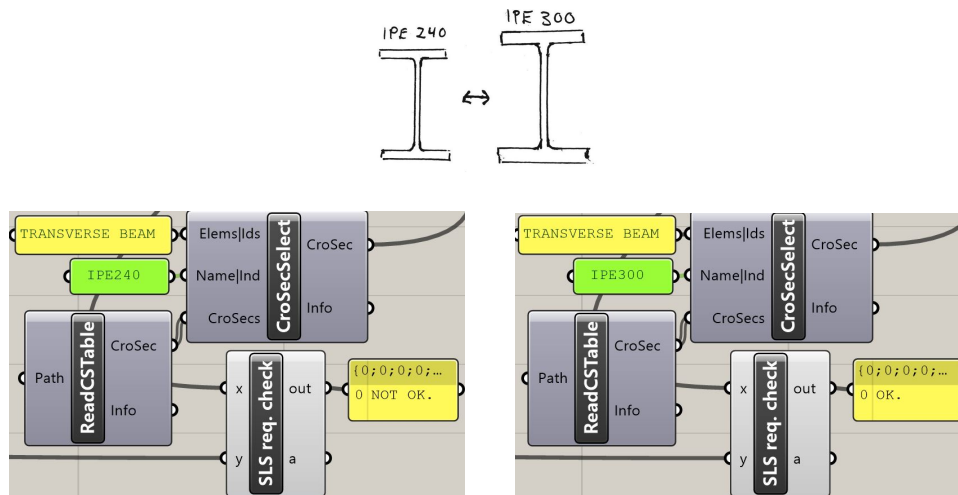

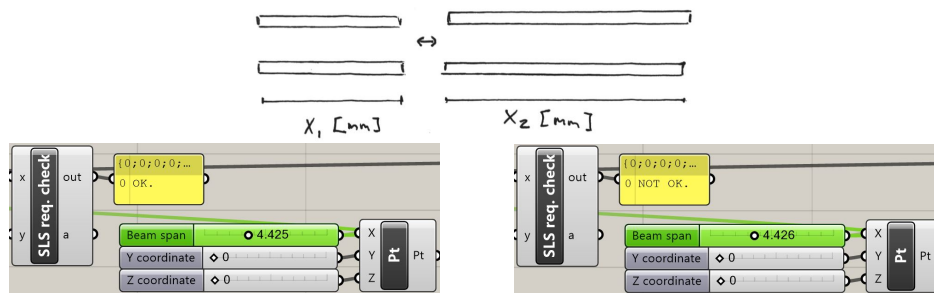Figure 2.17: Determination of minimum cross-section.

Figure 2.18: Determination of maximum span.

The algorithm can also be used for determining maximum length of the transverse beams, thus the maximum width of the bridge. This is achieved by increasing the length of the beams until the requirement check displays

'NOT OK'. Figure 2.18 shows that the requirement check changes from fulfilled to unfulfilled between beam spans 4.425 m and 4.426 m. Thus a maximum beam span of 4.425 m is found to fulfill the SLS vertical displacement requirement based on the specified crowd load, when the beam spacing is 4 m and the cross-section is IPE240.

As a tool, this algorithm may prove quite practical in the process of conceptual design, where the parameters constantly change. Once implemented, the algorithm saves quite a lot time in comparison to hand-calculations for each time the design changes. All sorts of combinations can very rapidly be created and instantly evaluated against some specified requirement once the user has defined the relationships through an algorithm, as shown in the above example.

3. <u>HYPOTHESIS TESTING</u>

In the development of the bridge delivered as part of the Footbridge Conference, a common theme among all the different design concepts considered was one sided suspension of the bridge deck. To check how the general shapes of the different ways to solve a single-sided suspended bridge affect the observed deflections and dispersion of forces, a series of tests will be performed in the following chapter, along with presentations of real world examples of these structures.

Table 3.1 shows the structures considered throughout this chapter:

Structure name	Year
Clavières footbridge, Boncourt	2013
Jiak Kim Bridge	1999
Gateshead Millenium Bridge	2001
Liberty bridge	2004

Table 3.1: Example structures that are discussed.

3.1 General assertions

Bridges suspended on one side have been constructed for some time, though without creating a great fuzz. Regardless, bridges and footbridges of this design have been produced for the latter half of the last century with decent success. One obvious weakness they all presumably share is the longitudinal torsion experienced by the bridge's deck - which in principle is somewhat of a voluntary weakness, as no one is forced to use this kind of design.

This torsion, or rather the one sided sagging that is caused by it, can be alleviated through many measures hereby considered external to the cross-
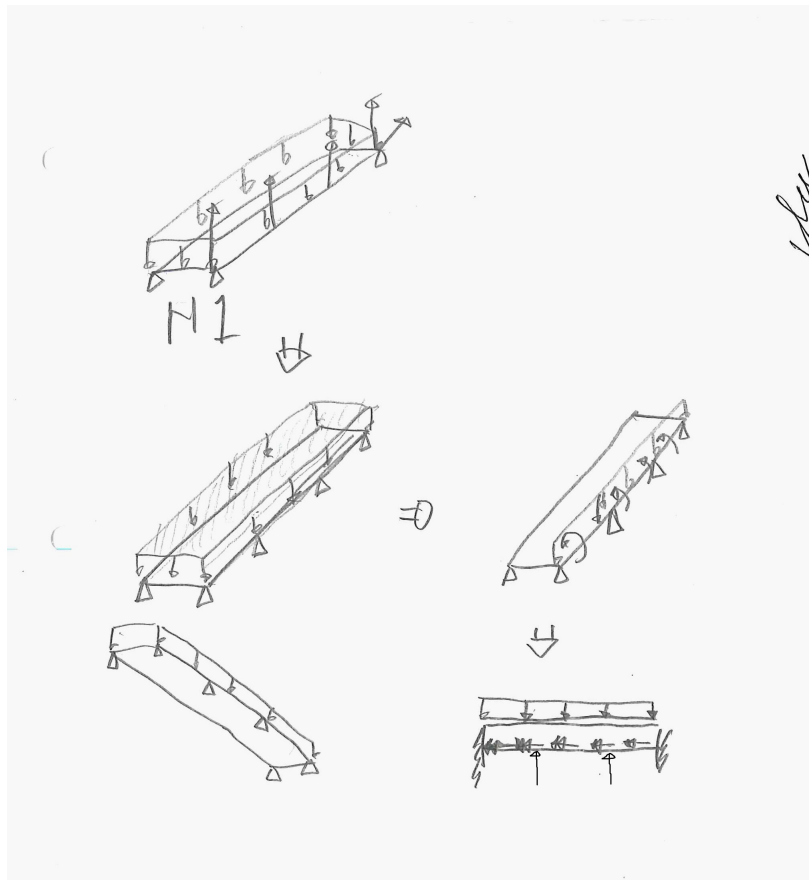
Figure 3.1: Effect on cross-section close to cable-side.

Conceptual structural design of footbridges:

Figure 3.2: The Boncourt footbridge. Photo credit: [3].

section of the deck or internal to it. The former concerns the general layout of the bridge, and the latter concerns the deck specifically.

The decks and superstructures also, in most cases, experience sideways forces that can be exploited to our benefit or are detrimental to the designs and have to be alleviated.

Bridges with asymmetric attachment of superstructure come in three main varieties: cable-stayed, suspension and arch bridges. Designs of all types will be looked at, in addition to different curvatures of the decks and shape of the superstructure.

3.2 Straight deck - cable stayed

To assess the function of asymmetrically suspended bridges we start off with an intuitively easy example, the Clavières footbridge in Boncourt, Jura, Switzerland. This is a simple and elegant footbridge, its 2,2 m wide deck spanning 31,88 m over the A16 highway. The distal end of the cable works as anchoring to the forces led over the tower at 1/3 out, from the cable attachment at 2/3 out. The cable attachment can be considered pinned while the point where the deck meets the tower is welded, making it a fixed connection [4].

To sort out how the bridge works, we approximate the deflection on the

outer edge by hand, followed by a simulation where the load-effects can be observed and assessed.
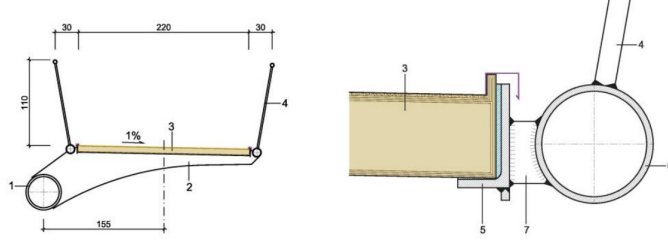

Figure 3.3: Sectional view of the Claviere footbridge, Jura, Switzerland figure taken from [4].

The smaller 114/7 pipes that hold the COLEVO balsa/carbon fiber deck-section are laid upon consoles that in turn are fixed to the main tubular beam. Seeing as (the second moment of area of main circular beam) $I_m >> I_s$ (the second moment of area of the secondary circular beams), we simulate the deck with a main circular cross-section with consoles of IPE200.

For ease of calculation, the point where the main beam intersects the tower is modelled as pinned, knowing that the fixed configuration present on the actual bridge will result in smaller deformations. As circular cross-sections do not warp, integrating the angular deformation per infinitesimal piece of beam due to torsion over half of the length is sufficient to calculate the rotation at midpoint for our proposed system. Multiplying the rotation with the width and adding this to the deflection due to moments in the beam and consoles will yield an approximation of the deflection at the outer edge of the deck.

Using a distributed load of 5 kN/m^2 and no gravity, we get a deflection at the outer edge of 30.1 mm by scripted "hand-calculations", ignoring self-weight. The rotation due to torsion at midspan is calculated to be $M_t/(I_t * G) * 3 * L/4$, M_t being the torsion per length ($q * w^2/2$ kNm/m). This means that for every doubling in length you would need to double the torsional resistance to keep deflections along the outer edge the same.

A general model for bridge deck geometry is made in Grasshopper and modified slightly to represent the geometry of the Clavières footbridge, and with cross-section dimensions assigned in Karamba. The cross-sections for the tower are set to be 450 mm in diameter and 40 mm in thickness for the bottom section and 350 mm in diameter and 40 mm in thickness for the top section. The cables are set to be 10 cm in diameter.

A test is made on the assumptions done in the hand calculations. The FE-model pictured in Figure 3.5 a) returns a maximum deflection along
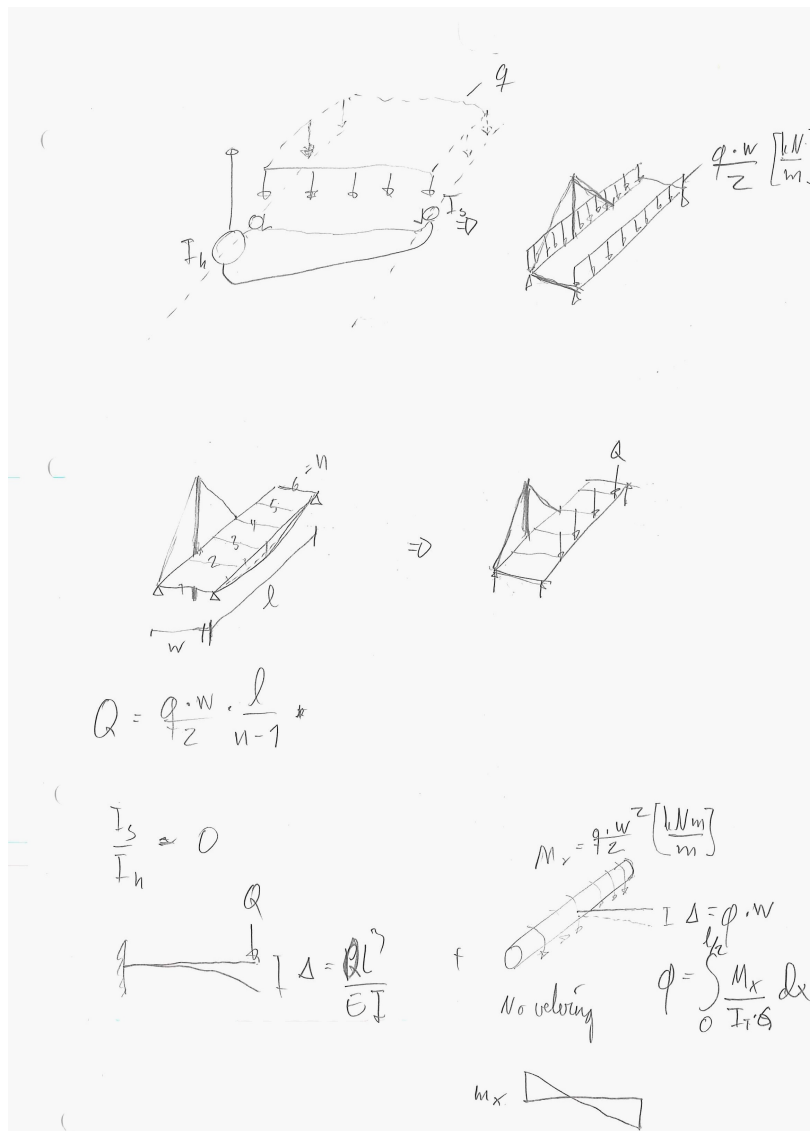
Figure 3.4: Simplifications made.
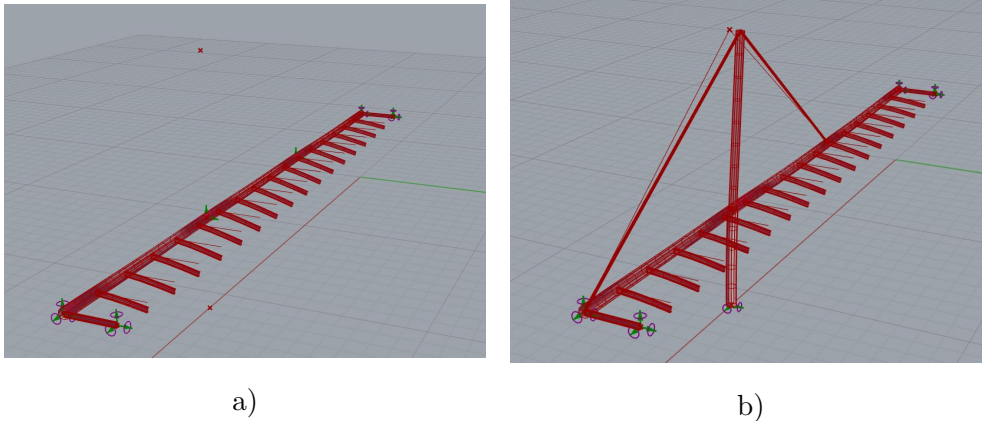
a)   b)

Figure 3.5: a) Model as calculated on paper b) model of Boncourt footbridge.

its free edge of 31.6 mm, 1.5 mm more than the hand-calculations. The model in 3.5 b) has a maximum deflection of 28 mm. It is limited by the tower, that absorbs moments at 1/3rd out, and enlarged a little by the cable elongating. the tower deflects 22 mm sideways.

3.2.1 Hypothesis

The tubular beams rotations are expected to double as the span doubles. To test this the parametric model (found in the electronic annex) is simply pulled to double its length. it is also expected that the tower deflects to twice its current deflection. The deflection of the ends of the consoles is estimated to 81 mm by hand-calculation.

3.2.2 Result

As can be seen in Figure 3.6, the elongation of the cables increases drastically, which leads to bigger deflections than estimated. The maximum deflection is 127 mm at the tip of the console at 2/3rds out. The top of the tower deflects 62 mm which is 3 times bigger than the previous results. This indicates that the assumed model for hand-calculation can only be used after stringent care has been taken on all other structural parts. Maximum rotation of the main tubular beam increases from 0.05 to 0.02 rad, most likely due to the tower exhibiting bigger deflection than expected.
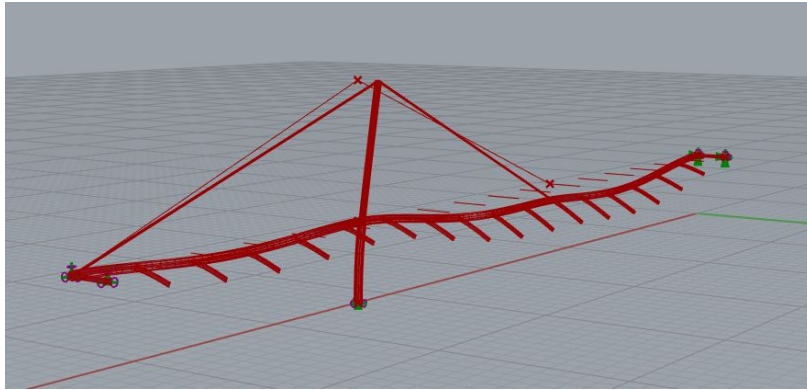
Figure 3.6: Clavieres footbridge, double length.

Figure 3.7: Jiak kim Bridge, vaguely longitudinal view. Photo credit: [6].

3.3 Curved deck - suspended on outer edge, with arch

The Jiak Kim bridge is a modest footbridge in Singapore finished in 1999 by the CPG coorporation. The arch, attached to the outer side of the curved deck, spans 40,6 meters and leans over the deck [5]. Unsuccessful attemps were made at acquiring more information than what can be seen with the naked eye, thus this section relies exclusively on assumptions about the size of the structural parts for its calculations.

Looking closer at the design, the Jiak Kim bridge's curved deck alone could
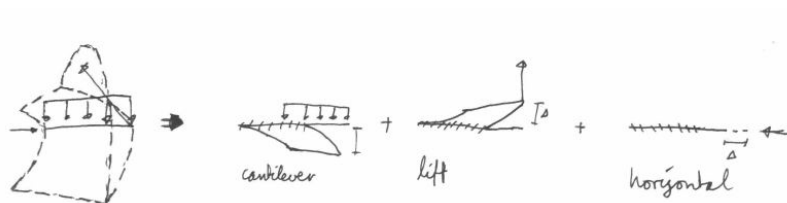
Figure 3.8: Jiak kim Bridge, assumed modes of deformation.

be expected to deflect more on the protruding edge. Thus one would also
expect this to be the edge on which it would be most beneficial to place
the cables. One would also expect the arch to lean away from the overhang
to counter the global overturning moment caused by the deck's lateral
overhang. Furthermore, since leaning the arch inwards induces lateral loads
on the walkway, one would expect to see bending moments about the global
z-axis and lateral shearing forces induced in the deck, with corresponding
deformations. It is expected that the Jiak Kim bridge's design is a healthy
compromise between these effects.

As no information on the cross-sections and dimensions of the bridge except
the most rudimentary were available, the cross-sections of the tubular beam
was set to be the same as in the Clavières footbridge (457/40 mm) and the
arch, looking very similar to the tubular beam in size, is set to the same.
Cables are set to 10 cm diameter and crossbeams are set to IPE200. The
walkway itself is set to 3 meters width.

3.3.1 Hypothesis

It is believed that the arch leans inwards because it counterbalances the
deck's cantilever action, and that this is the main purpose of leaning it
over. To counterbalance the deck without inducing moments where the arch
meets the ground, the arch is set free to rotate. The apex is moved inwards
until no movement of the arch is seen in the deformed state, subjected
to self weight only. An algorithm accounting for second order effects is
used to let the solution settle in equilibrium. This is a crude imitation
of form-finding a-la Gaudi, and it is wished to see if it performs well in
comparison to configurations that are not balanced in the unloaded state.
It is presumed that more lean is beneficial under load as this directs the
forces acting on the arch to pull it with a less oblique angle.

Figure 3.9: Jiak kim Bridge, balanced form, longitudinal view.

3.3.2 Results

Running a finite element analysis in Karamba using an algorithm that accounts for second degree effects, we discover that the form in which the arch counterbalances the cantilevering on the deck is the expected inwards lean. The final form is pictured in 3.9, with an overlay of how it deforms under self-weight scaled to 100x. Note the similarity to the actual geometry of the Jiak Kim bridge.

Curious to how it reacts under load, a parameter study is done where the control point of the NURB that draws the arch is moved from one side to the other. The top point of the NURB in the balanced configuration is referred to as 0. Positive values leans the arch over, negative values straighten it up.

Loading it with loads of 5 and 10 kN/m^2 yields maximum deformations as illustrated in 3.10. It can be seen that for the lighter load, the arch actually reaches an optimal amount of lean. This would be where the weight of the arch counterbalances the cantilever-deflections just enough to not induce more prominent vertical deflections. The big problem with this is that the lean is too strong to make for a practical bridge at all (see figure 3.11). for designers seeking to make such a bridge, as much lean as possible without
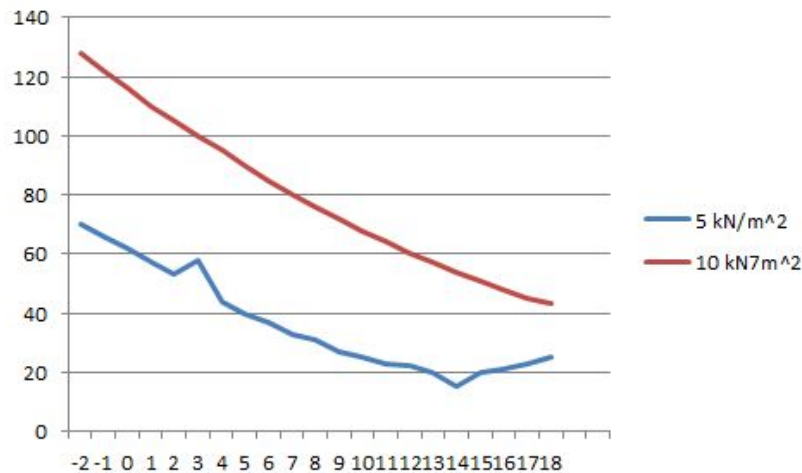
Figure 3.10: x-axis) Lean, y-axis) Deflection.

disturbing traffic should be sought, and more effort should be put into making the arch stiff out of its plane.

3.4 Curved deck - suspended on inner edge, with arch

Gateshead Millennium bridge was planned in anticipation of the new millennium and erected by a large floating crane in November 2000 over the river Tyne, connecting the cities Newcastle and Gateshead, England. It possesses a large array of peculiar design features, particularly the tilting mechanism that rotates around the ties of its arch, and the kite cross-section of said arch. Aesthetically it communicates with its environment most strikingly when viewed from the river, exaggerating the arch drawn by the Tyne bridge's arch and mimicking the lines drawn by its cables [9] [?].

The deck has a stronger curvature than that of the Jiak Kim bridge, which leads to the cables pulling with comparatively bigger force components perpendicular to the arch. As the deck is suspended on its inner side, the cables can lean over more without disturbing traffic on the bridge. This also enables the use of surprisingly small motors to tilt it since the arch counter-weighs the deck as it leans over.

From a more detailed perspective, the arch presents an interesting solution to a very real problem that surfaced when looking at the configuration with the arch on the outer side in the last subsection. The kite-shaped
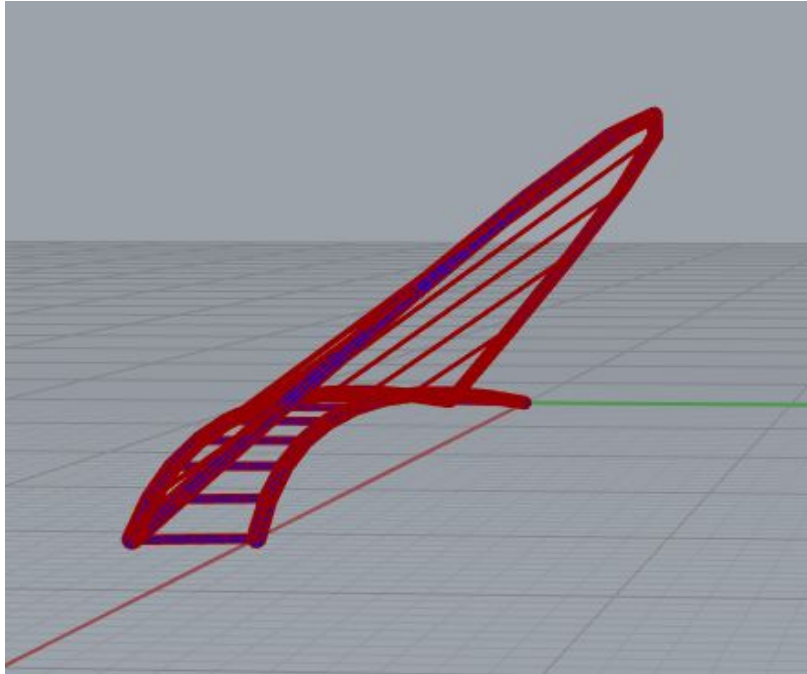
Figure 3.11: Model with a lean of 14.

Figure 3.12: View from Gateshead Quayside. Photo credit: Andy Williamson [7].

Figure 3.13: Gateshead Millennium Bridge with Tyne Bridge in the background. Photo credit: Ramboll [8].

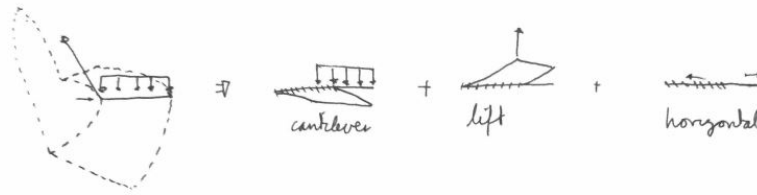Figure 3.14: Gateshead Millennium Bridge, tilted. Photo credit: [10].

Figure 3.15: Gateshead Millennium Bridge, assumed modes of deformations.

cross-section (Figure 3.21 is presumed to lessen the lateral deflection of the arch through making it stiffer in out of plan bending. The "width" of the cross-section also changes from the apex to the bottom, increasing from 2 meters at the apex to 4 meters at the bottom. The metal plates from which the arch is welded are up to 35 mm thick.

The deck is a box-type section for the pedestrian lane with cantilevered beams supporting the bike lane as seen in Figure 3.21.

3.4.1 Hypothesis

Large deflection at the outside edge when cables are placed on the inner side of the deck.

Looking at a diagram over the forces acting on a deck section and its assumed deflection-patterns (Figure 3.15, it can be seen that the lift provided by the cables is placed on the inner side - the side that experiences the least deflection in cantilever-action. This implies that we would see a a larger deflection at the outside edge than that of a bridge configured like the Jiak Kim. That is, if we make a model with the exact same geometry as Jiak Kim, but with the arch tied on the inside and not on the outside, we would expect rotations due to cantilever action and lift both to work against the favour of the bridge.

To isolate the effects of this change, the points along the arch are set to be free to rotate, but fixed in translation. This effectively makes the arch infinitely stiff. The model used in the analysis of the Jiak Kim Bridge is manipulated to assume the shape of the Gateshead Millenium Bridge, albeit scaled down to the span of 41 meters.
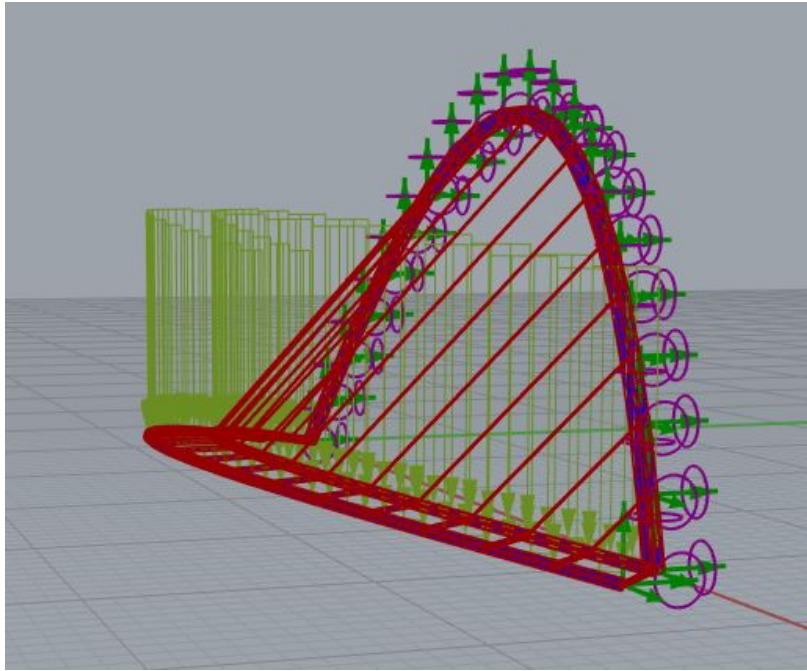
Figure 3.16: Gateshead Millennium Bridge, model used to check one-sided sag of deck.

3.4.2 Results

The model is loaded with line-loads corresponding to a distributed load of $10 \ kN/m^2$ along the outer and inner pipes. It is seen that the assumptions seem to be right, yielding 0,028 meters deflection on the inside of the deck with cables attached on the outside and 0,041 meters deflection with the cables attached to the inside.
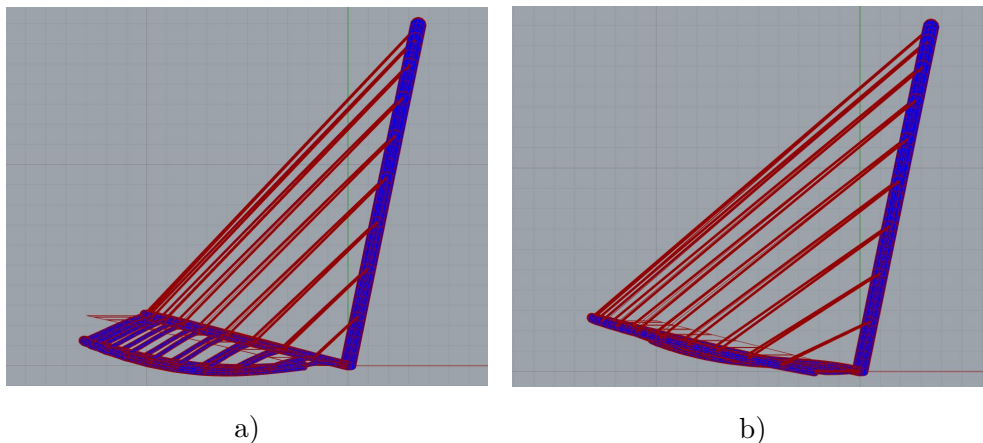
Figure 3.17: a) Cables attached to inside of deck-curvature b) Cables attached to outside of deck-curvature.

3.4.3 Hypothesis

Moments in arch taking a cantilever-like nature when tall and narrow, clamped-beam nature when wide and low.

An arch is normally thought of as a structural part that leads vertical forces over a horizontal span into the ground through compression. It will also most likely display moments and shear in plane. The arch of the Gateshead Millennium Bridge (and the Jiak Kim bridge for that matter) however, has cables pulling out of plane. The intention of this subsection is to take a closer look at the moments these forces induce and the solution chosen to cope with said moments.

The arch can be thought of as both a cantilever and as a fixed-end beam with regards to out of plane forces. The implied moments are pictured in figure 3.18

Because the orientation of single sections of arch changes over the span, we would expect the moments induced to manifest as both torsion and out-of-plane bending moments. The moments induced in fixed-edge beam perspective are expected to manifest as torsional moments close to the ends of the arch and bending moments close to the top, whereas the moments induced in cantilever perspective are expected to manifest as bending moments close to the bottom and torsional moments closer to the top

To test this, the model used in last subsection is subjected to line loads along the deck corresponding to 10 kN/m^2, and the arch is set free to deform. For the above assertions to hold true, tall and narrow arches would have to have more cantilever-like characteristics, whereas low and
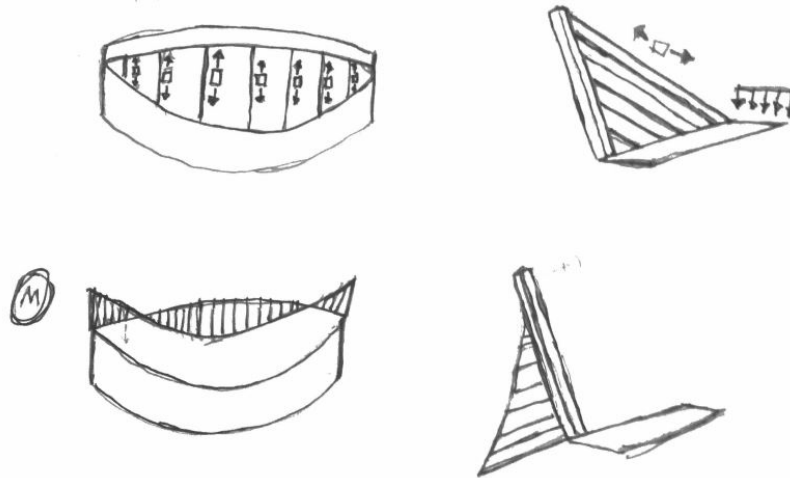
Figure 3.18: Sketch of moments in arch due cable forces when thought of as a clamped beam and when thought of as a cantilever.

wide arches would have to have characteristics more similar to a clamped beam. The results are expected to be somewhat obfuscated by the fact that the cables change their angle of pull as the height of the arch is changed

3.4.4   Results

Running the Karamba FE-analysis on the generic pipe-model returns moments corresponding to the moment-diagrams pictured in Figure 3.19. It is also observed that the torsional moments through the arch vary slightly differently: for the tall configuration the torsion at the bottom is 125 kNm and the maximum torsion is 400 kNm at approximately 1/3 of the length. This constitutes a ratio of 0,3125. For the wide configuration the torsion is 262 kNm at the ends and 886 kNm at approximately one third of the length. This constitutes a ratio of 0.2957. The diagrams affirm the assertion that long, narrow arches subjected to horizontal loads do indeed work more like cantilevers, whereas wide, low arches act more like clamped beams.

An interesting revelation is that for the the geometry that imitates the actual geometry of the Millennium bridge, the out of plane moments are approximately 4 times bigger than the in plane moments (1210 kNm versus 4641 kNm). This is mirrored in the actual design of the arch, pictured in Figure 3.20. Since the out-of-plane bending moments are bigger towards the ends of the arch, the cross-section is bigger and more stretched there. In the middle, the moments in and out of plane are almost equal, resulting

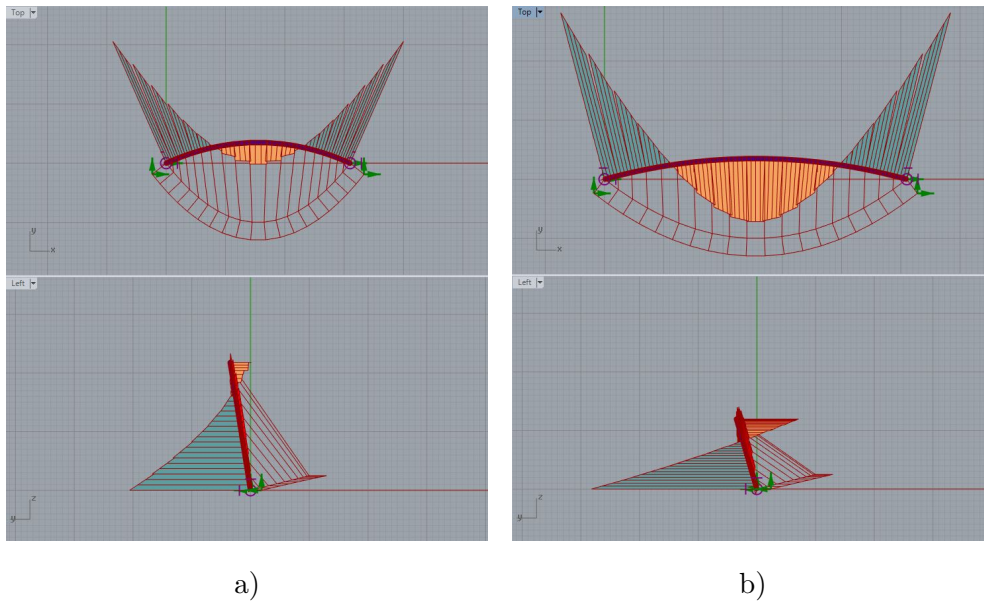a)   b)

Figure 3.19: a) Out of plane moments, tall configuration b) Out of plane moments, wide configuration.

in a more square cross-section

The deck, pictured in Figure 3.21, is a box-section on which the pedestrians walk, with beams cantilevered outwards that support the deck where cyclists bike. it can be imagined that this works in unison similarly to the tubular beam with consoles as seen in the Boncourt footbridge, with its much bigger dimensions being much stiffer

To simulate the Gateshead from this point onwards, a model using the box-section from 2.1.2 and the arch with varying cross-section from 2.1.1 is used from this point onwards. the thickness of all steel plates is set to 40mm. Subjected to a load of 5 kN/m^2 this results in a maximum deflection of 0,24 meters and maximum utilization 0,29. When subjected to gravity in addition to the same distributed load these values increase to 0,25 and 0,36 respectively. During the work on this model it is observed that the deck displays remarkably small deflections when the deck assumes certain inclinations to to the cables. the next hypothesis is based around these observations.

3.4.5   Hypothesis

The curve of the bridge's deck can be thought of as an arch - this is the assumption made earlier, along with the assumption that it mostly provides stiffness horizontally. It can be thought that it works in unison with the
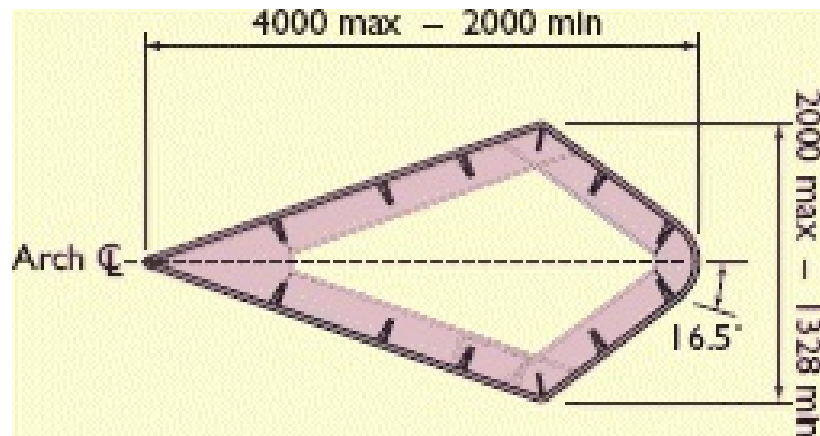
Figure 3.20: Cross-section of arch, Gateshead Millennium Bridge. Photo credut: Johnson Curran 2003 [11].
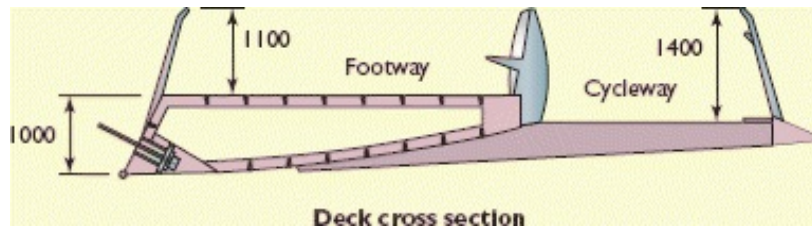

Figure 3.21: Cross-section of deck, Gateshead Millennium Bridge, Johnson Curran 2003 [11].
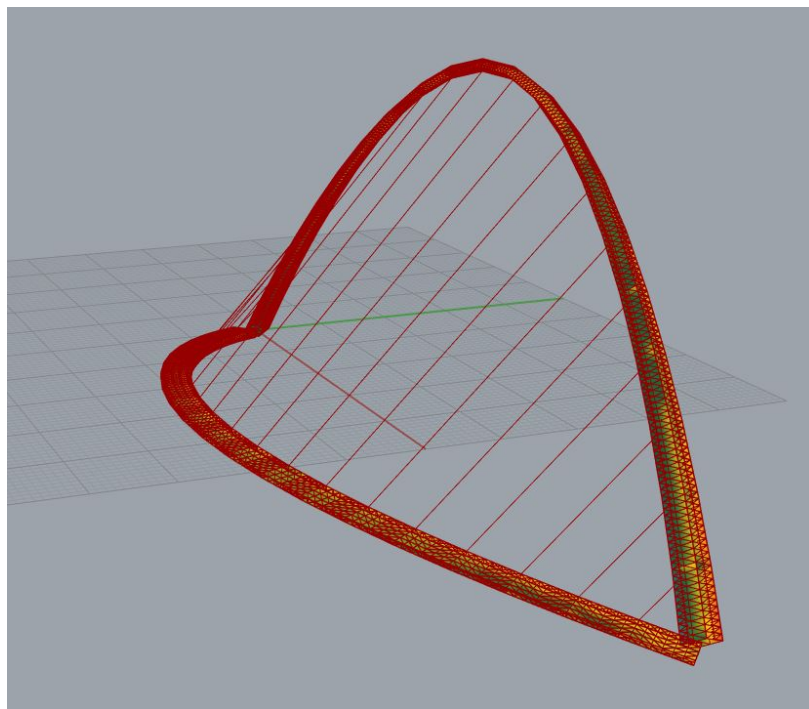

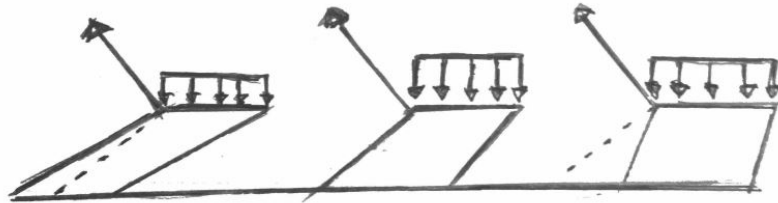Figure 3.22: Gateshead Millennium bridge, utilization plot on model.

Figure 3.23: Cables and deck, main stiffness direction.

cables most effectively when it provides the most stiffness in the direction where the cables provide the least stiffness.

The cables are free to swing, that is, they provide no stiffness in a direction perpendicular to their own lengths (dotted lines in Figure 3.23). It is hypothesized that a configuration where the arc drawn by the footway is meeting the cables at approximately 90 degrees will perform better than other configurations in terms of deflection. To test this, the algorithms presented in sections 2.1.1 and 2.1.2 are used to represent the bridge. Beams carrying bike deck are added to the model and subjected to line-loads corresponding to 5 kN/m^2. The arch is locked in place as in Section 3.4.1

3.4.6   Results

Since the arch is immovable, the results achieved are only due to interaction between the arch and the cables. It can clearly be seen that a configuration where the cable meets the plane drawn by the arch at approximately 90 degrees is beneficial for the observed deformations of the deck. This effect should be kept in mind by designers, although it will require an arch leaning over a lot to achieve this without making the decks unclimbable.
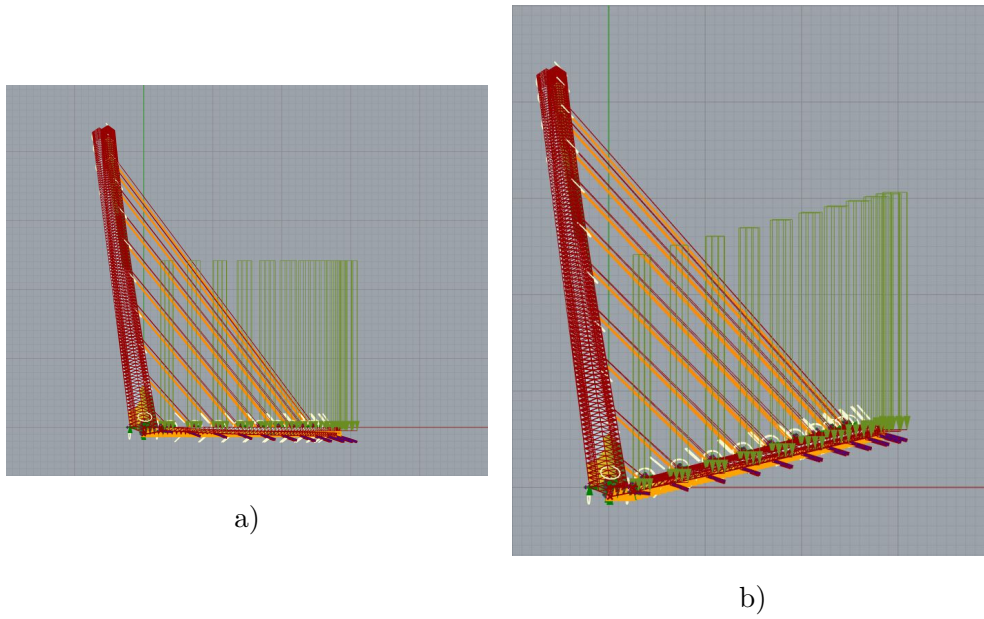
Figure 3.24: a) Narrow angle of incidence, deflection: 0.08428 b) Standard angle of incidence, deflection: 0.057.
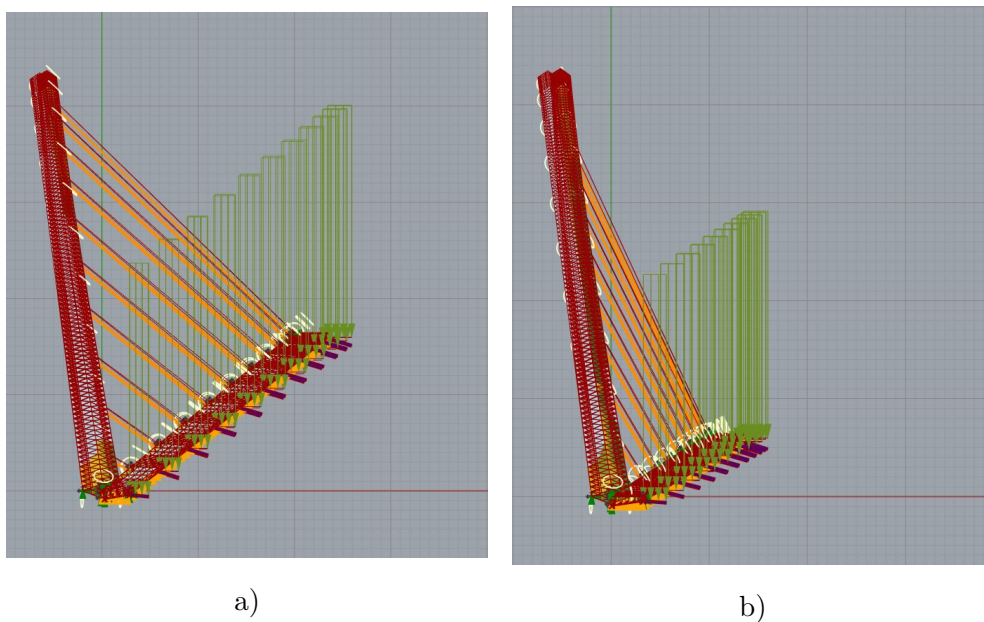

Figure 3.25: a) Best performing angle of incidence, deflection: 0.038 b) Open angle of incidence, deflection: 0.067.
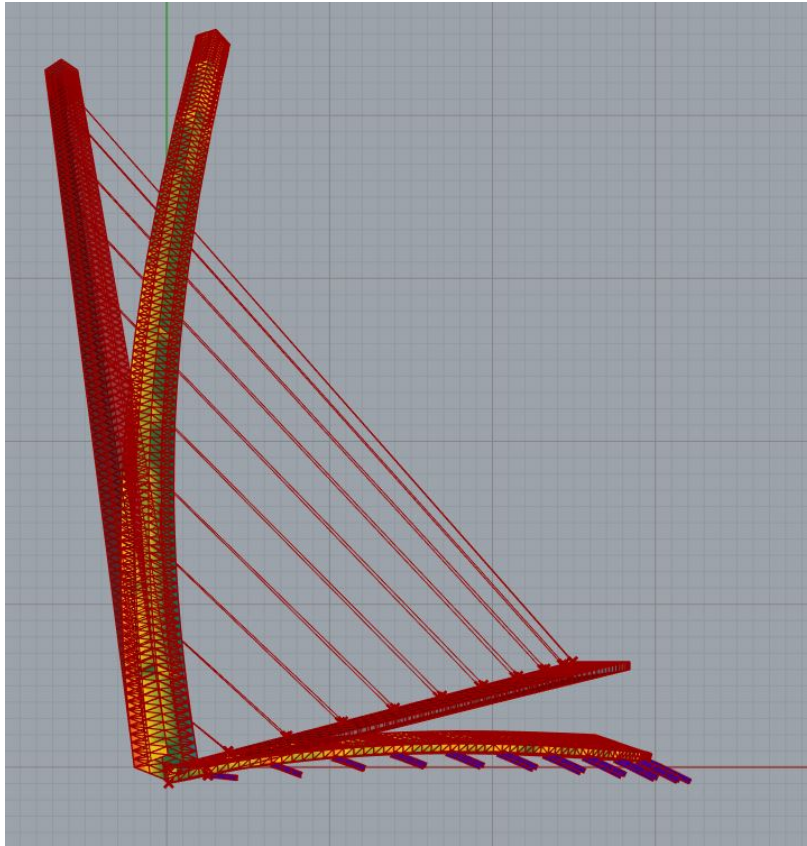
Figure 3.26: Deflection of the Gateshead with bike-deck.

3.5 Liberty bridge, Reedy river

Throughout this testing it has been dealt with bridges that rely on passive solutions to the sag on the unsupported side. A very elegant solution to this sag is the Liberty Bridge, in Greenville, South Carolina, over the river in the Falls Park. It is an asymmetrically suspended catenary bridge with a tension ring running along its underside, an invention of Jörg Schlaich (responsible engineer for the Olympiastadion in Munich, among others).

The design of the bridge solves the sag that one would expect on the unsupported by having the cables on the underside be pre-stressed. The cables are fastened to a truss 1.3 meters below the deck. This provides a moment arm for the radial components of tension in the cables - thus creating uplift on the unsupported side (Figure 3.28, leftmost load effect).

Figure 3.27: Liberty Bridge, Greensville. Photo credit: [12].

Figure 3.28: Liberty Bridge, Greensville - interpretation.

4. <u>FOOTBRIDGE 2017 BERLIN</u>

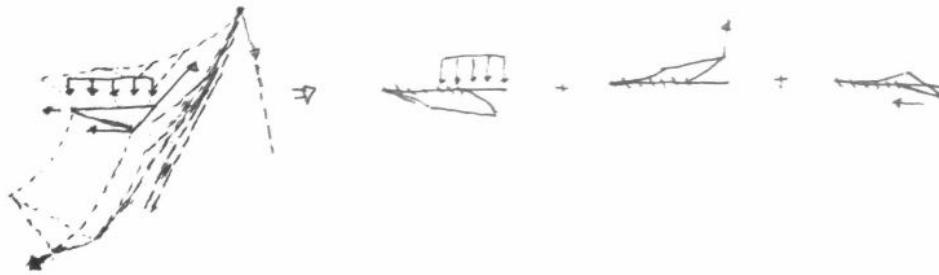As a point of departure for this master thesis, it was chosen to participate at a conference taking place in Berlin, called "Footbridge 2017 Berlin", concerning footbridges and their peculiarities. The process from start to finish, along with specifics on design considerations, is documented in this chapter.

4.1 Brief overview

Footbridge 2017 Berlin is the 6th international Footbridge conference, taking place in Berlin. One of the aims of the conference is to acquire a variety of footbridge designs of interesting, well-functioning, technically challenging or innovative art from architects and engineers all over the world. By "telling a story" with their bridge designs combined with other aspects of the conference (such as cultivating debates and paper-submissions and lectures in dynamics and innovation), all participants contribute to increased knowledge about the future possibilities of footbridges.

All bridge design contributions are vetted by a panel of professionals and either accepted or rejected from being part of a book show-casing the footbridge designs. The conference will be held from the 6th of September until the 8th of September in 2017, where the best contribution will win a prize.

4.2 Participation

As previously mentioned, the reason for participating was to have a point of departure for this master thesis. In participating, a bridge design would have to be developed. The idea was to use parametric design to achieve this, and explore the opportunities thereof during the work on the bridge. In so doing, there would be an exciting task at hand to complete, making sure as many of the technical requirements as possible were fulfilled, in addition

to creating an interesting, functional and aesthetically sound design. The participation offered a great opportunity to explore and gain insight into how one can use parametric design tools in conceptual design, thus creating a solid foundation for the thesis.

4.3   Tools and software

4.3.1   Rhinoceros 5 and Grasshopper 3d

To best be able to develop a feasible footbridge design, a series of suitable tools and software would have to be learned. The first step was to learn how to draw in Rhinoceros 5 using Grasshopper 3d, the latter being a software that enables drawing geometry through a canvas with different modules combined to an algorithm represented visually. The advantage of this drawing method is that all commands can be linked together and affect each other. In effect this means that if one has created a smart algorithm, it can be reused and ease the workload. Once making drastic changes to the design, that would normally lead to chain events resulting in the need to redraw, one could now be linked together in such a way that all relevant changes would automatically be done when pulling a slider, or a lever, to make the parameter change. All dependent parameters with it would also follow. Compared to a "normal" drawing program, the types of which are usually used in BIM such as Autodesk Revit and Autocad, this is very efficient and flexible. One small drawback is the fact that it is a single core application, meaning that it only uses the data power from one of the processor cores in multicore systems.

4.3.2   Karamba 3d

Once a bridge geometry is drawn the next step would be to undertake a finite element analysis of the bridge design. Karamba 3d is a Grasshopper plug-in software which does just that. By connecting drawn lines, points and meshed surfaces to its' components, converting the lines to beams that can be given different cross-sections and the surfaces to plates, one can now get a number of results from a structural FE-analysis. Also here, changing of cross-sections and dimensions will be just as easily done by changing the parameters, leading the software to instantaneously recalculate and showing the results change as you pull the parameter levers.

Karamba utilizes simple beam elements as a default for lines output from Grasshopper, with an option of disabling bending, turning them into simple

rods. For surfaces, it utilizes kirchhoff plate elements.

4.3.3 Galapagos

The Grasshopper and Karamba software used in combination with another plug-in named Galapagos allows for evolutionary optimization of the design. Galapagos is a tool that can be fed with parameters that constitute a genotype and an outcome that represents the phenotype. The genotypes are random combinations of parameters defined by sliders. The phenotype fed into Galapagos is a number, for example deflection, rotation, weight, forces or any conceivable combination of these. Galapagos then runs a standard evolutionary optimization that can minimize or maximize the phenotype by making random sets of genotypes leading to corresponding phenotypes that are compared. The genotypes producing the most desirable phenotypes are then paired to produce new, (hopefully) more desirable phenotypes.

As an example, Galapagos can be connected with the sliders for parameter values of the position of an arch's end-support as well as sliders for the height and positioning of the arch mid-point to optimize for the minimum displacement in an arch bridge. The run-time of the optimization will depend on the amount of sliders, the range of the sliders and the convergence of the phenotypes that are fed into the tool. After completion, the most desirable (with regards to the value being minimized or maximized for) combinations of parameters are displayed and can be chosen between.

Evolutionary, genetic optimization algorithms are generally considered slow, and for on-the-fly optimization rule based algorithms are considered more efficient use of data-power. In addition to this, the single core operation of Rhinoceros 5 also applies to Galapagos and Karamba. To the authors' experience, the results are produced faster on older systems with fewer cores and higher clock-frequencies than newer systems with multiple weaker cores.

4.3.4 Robot 3d

For verification of the Karamba model, it was chosen to design the structure in Robot Structural Analysis for comparing results. Robot Structural Analysis is a traditional modelling FE-software used in the engineering industry. This software also allows for generation of load combinations.

To sum up, the following software is used in designing the bridge:

Software	Purpose
Rhinoceros 5	Manual drawing and rendering
Grasshopper 3d	Parametric drawing
Karamba 3d	FE Analysis
Galapagos	Optimization
Robot 3d	FE Analysis: Load comb. etc.

Table 4.1: Software used in the bridge design

4.4 Conceptual design process

The design process of the developed arch bridge began in February of 2017. Starting by exploring different types of inspiring bridge structures as a means to learn the different software, certain types of structural designs were found more appealing than others. As the chosen bridge site and technical requirements were more thoroughly examined, the concept of the suspended arch bridge as a structure was especially found to be appealing and purposeful. In this section, the process of the development of the design will be described.

4.4.1 Site

The bridge site, "Brommy", was chosen out of six possible locations. Most of these locations offered interesting possibilities, however none the historical appeal and feeling of importance as the site of the old "Brommybrücke".

Once bridging the river "Spree" between the downtown districts of Kreuzberg and Friedrichshain until its demolition in 1945, the remaining pylon gives historical value to the site. It was this in combination with the close positioning to the remains of the historical Berlin Wall as well as the areas being in development that made for an intriguing place to develop a concept for a footbridge design.

Figure 4.1: The Brommy Bridge.

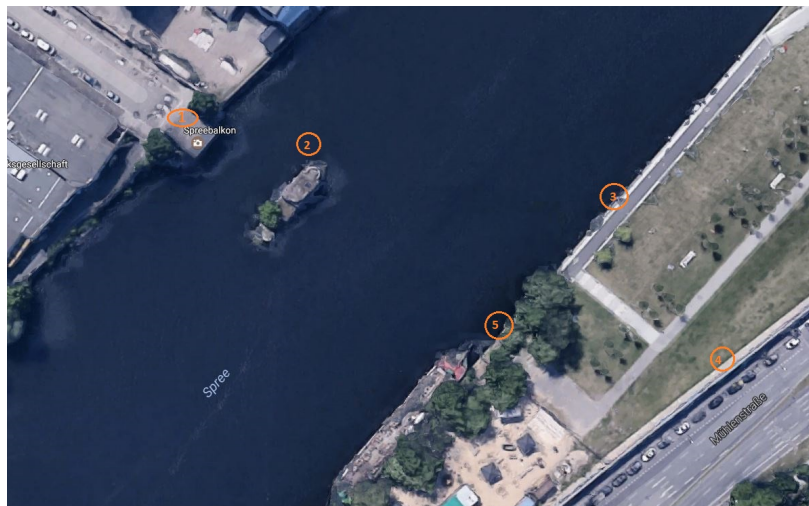Figure 4.2: Airphoto of the Brommy site today.

Figure 4.1 shows the old Brommy Bridge and figure 4.2 shows the site as is today.

The orange circled numbers in figure 4.2 marks the following:

- 1 and 5 are the suggested start and end points of the bridge

- 2 is the remaining ruins of the abutment of the old Brommybrücke

- 3 is a pedestrian and bicycle path

- 4 is the remains of the Berlin Wall

4.4.2 Technical requirements

Each site for the conference contributions comes with certain technical specifications and general requirements specific to the different sites. These requirements are guidelines for the design concepts to further ensure feasible structure designs, i.e. a design that could potentially be built. In effect, these requirements imply that the more of the requirements fulfilled, the better. However, it does not mean that a great concept cannot be developed without meeting all the specified requirements. What is important is to keep them in mind, and try to come up with alternative solutions if certain requirements are not directly met in the design. "If the total impression of a design leaves a great overall impression, though at the cost of one of the requirements not being fulfilled - it might still be amongst the strongest contenders."

For the Brommy site, the technical specifications were as follows in table 4.2:

•The bridge should serve pedestrian and biking purposes.

•Bicycle traffic should be able to cross both ways while pedestrians should be able to stroll and linger to appreciate the view.

•Traffic should be able to pass continuously.

•The design can include platforms.

•The bridge should serve as a local landmark and tourist attraction.

•A width of at least 4 m is necessary, and the railing needs to be at least 1.3 m high.

Table 4.2: Technical specifications for the bridge design.

The general requirements were stated as listed in table 4.3:

●No piers within 4.5 m of the water edges.

●Maximum ramp gradient 6 %.

Lighting req. due to ship traffic

●The height of the point of light is between 3 and 5 m.

●The setting angle is 0 degrees.

●The glass cover is flat and clear.

●There are reflectors.

●The discharging lamps are tubular.

Req. due to ship radar systems

●Big, parallel areas should be avoided.

●Cavities should be avoided.

●A radar-absorbing coating should be applied.

Table 4.3: General requirements for the bridge design.

In addition, a text containing the following aspects was to be considered;

Extraordinary strains, such as a ship collision, should be factored into the design. The construction should be accessible to all people, also those with special needs or disabilities. Vibrations from side winds and traffic must be considered. The construction of new piers are prohibited due to disruption of ship traffic. The remaining pier in the water can be used, but should not carry any weight, which results in a river span of 110 m without any supports in the water. The lower edge of the construction should be at least 4.5 m above the river's water level. A 20 cm height difference to the bridge's surroundings is sufficient.

Since the purpose of the participation was to create a foundation for this master thesis, the requirements have been weighted against their relevance to the thesis. For example, little effort has been made concerning the lighting requirements due to ship traffic, since it bears little relevance to conceptual structural design. Nonetheless, all requirements have been considered, and taken into account if possible. As the evolution of the design is presented in the following section, requirement considerations will be commented where they are relevant and have affected the decision.

4.4.3 Design evolution

Since the design process was not separate from the learning of the computer tools, the successive designs emerged out of a pool of gradually improving designs and their interesting features being cobbled together into one end

result, doing changes along the way as challenges arose. Many observations made during this period were used to formulate hypotheses tested in the relevant chapter.

As the authors see it, the development went through a couple of distinct concepts that will be expanded upon, considering their benefits and drawbacks as they were seen at the time.

In the beginning, much attention was paid to the remaining pylon and how to accentuate it. With this in mind, a series of concepts were thought up and preliminarily tested and tweaked in Grasshopper with the help of Karamba and Octopus. These concepts sought to emphasize the pylon by starting off in the tracks of the old Brommybrücke and subsequently curving out of the straight line following the old bridge in Figure 4.2.

Realizing that because the bikers' relatively high velocity and the relatively small width of the Brommystraße would make lanes with small radii in their curvature less desirable, the concepts started assuming a perpendicular orientation to the river on the Brommystraße-side.

The concepts differed mostly in their choice of superstructure and arrangement thereof. A keen interest was taken in systems in which the bridge was suspended, and only suspended on one side on the walkway. These were interesting systems to the authors, as they provide unobstructed view to one side. Two different families of designs for the superstructure were considered: Cable stayed and tied arch (4.3).
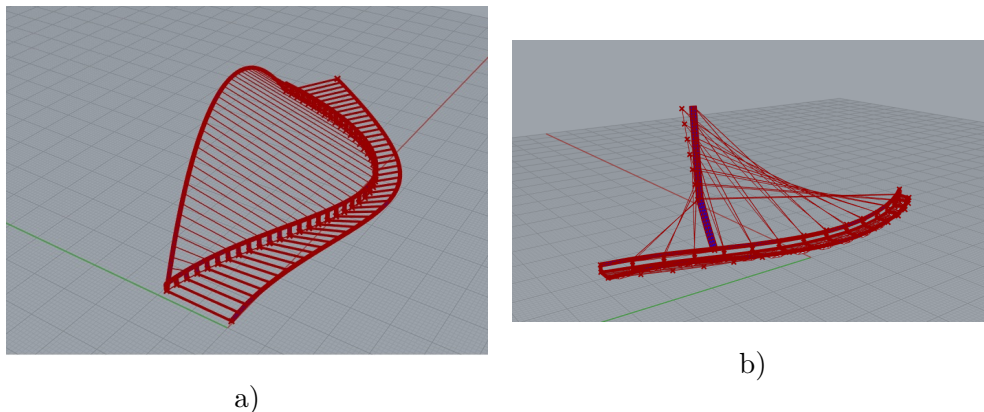

a)

b)

Figure 4.3: a) Early concept with arch b) Early cable-stayed concept.

Observing that the variants with an arch displayed somewhat large side-to side deformations under vertical loads of different magnitudes, a variety with a tethered arch (Figure 4.4) was tested. Towards the end of the early design phase it was decided to make use of two footways, one for cyclists and

one for pedestrians. This separates the cyclists and pedestrians, and also allows the bike deck to have a somewhat more exaggerated curvature as one does not need to consider wheel-chair users ad other movement-challenged users. In turn it requires more area of walkway since the flexibility in use of the walkways is minimized. A catenary and a free-standing arch were considered for the superstructure, and the solution with a free-standing arch was decided superior as it did not necessitate any obstructions in the river. After a bit of tuning, the delivered concept can be seen in figure 4.5. The concept with a tethered arch and the concept with a catenary-type solution can be seen in Figure 4.4
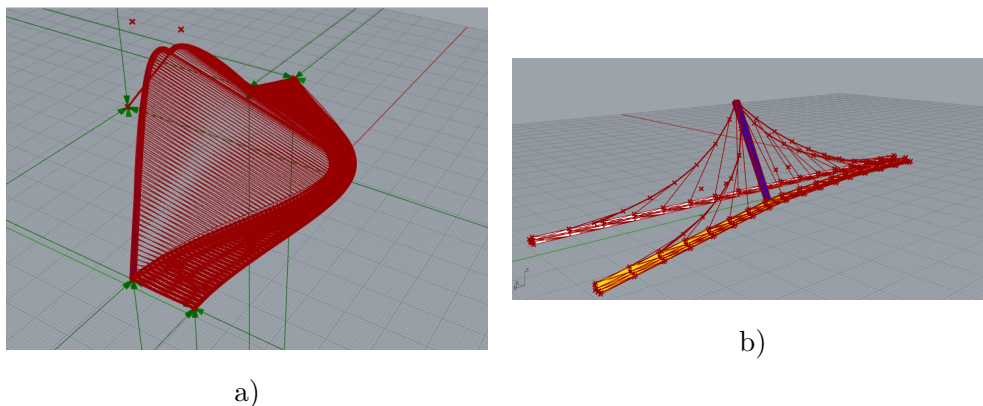

a)

b)

Figure 4.4: a) Tethered arch b) Double catenary.

4.4.4   Reasoning of final design

This section should be seen together with the contribution delivered to the Footbridge 2017 Berlin Conference found as attachment A at the end of this thesis.

As a concept, the arrived upon bridge design first and foremost achieves to connect the two areas in development in an efficient manner. The design consists of two decks that could either be separate, as they are in the current model, or joined together by stairs. In either option, the two decks serve their own purpose; the straight deck with the shortest walking distance and lowest gradient (6 % as per the gradient requirement) as a crossing for pedestrians, and the curved deck with a slightly longer walking distance and steeper gradient as a crossing for cyclists. This way, pedestrians lingering to take in the views will not interfere with the bicycle traffic.

Furthermore, the curved deck is connected to an already existing bicycle path, making the flow of the bicycle traffic more natural and efficient.

Figure 4.5: Top view of rendered model of the final bridge design.

Figure 4.5 shows the top view of a rendered model of the final bridge design concept placed on the actual site.

Each of the two decks are suspended on one side by cables attached to an arch positioned between the two decks. This allows for the crossing to seem open and spacious, and results in an attractive aesthetic expression. It also results in an intriguing structural system that is likely to trigger the bridge's users' curiosity, while at the same time contributing to the bridge potentially becoming a tourist attraction in itself.

Underneath the bridge there is planned for a platform to surround the remaining abutment of the old Brommybrücke and be connected to the pedestrian bridge deck. The idea is for the users to be able to walk down and view the historic remains up-close, and possibly for there to be informational signs or posters describing the history of the site. This, in combination with the nearby Berlin wall and the peculiar aesthetic expression of the bridge might achieve for the Brommy crossing to become a tourist attraction.

In the model there has been chosen to use a wooden surface for the pedestrian deck and a concrete surface for the bicycle deck. The reason being to show that different sort of themes can be chosen based on what sort of look one desires. It should be mentioned that wet wood may be less ideal as a surface for cycling.

The ramps are planned to be made out of concrete, but are however not further analyzed. They are simply added to the rendered models as a suggestion to give more of a full picture to the concept.

Figure 4.6 shows the top view of a rendered model of the final bridge design depicting the one-sided suspension of the decks and the platform surrounding the ruins of the old Brommy Bridge's abutment.

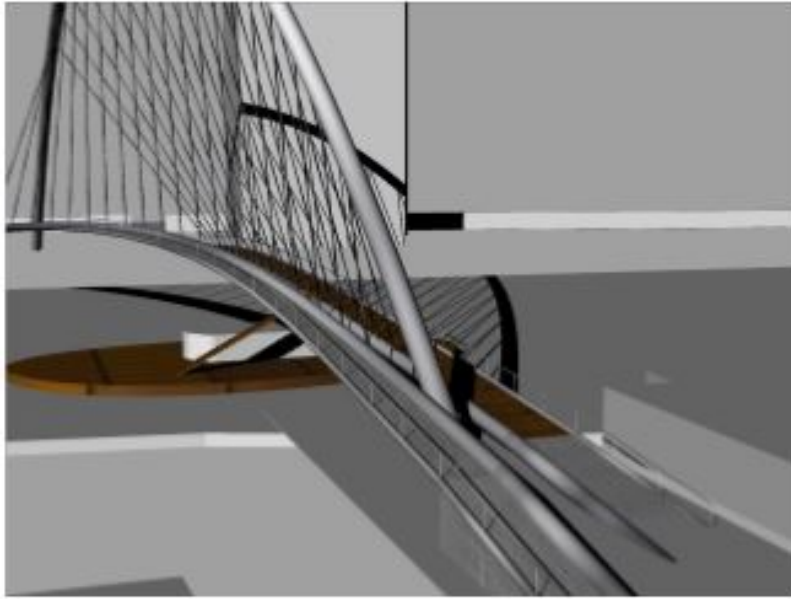Choosing the arch as a structural load-bearing system for the design pro-

Figure 4.6: One-sided suspension of decks and the platform surrounding ruins.

vides the possibility of not having any abutments, or new piers, in the water as per the site requirements, by suspending the decks through cables.

The two separate decks allows for each of the decks to be narrower as the total traffic of the bridge is divided between the two decks. Placing each of the decks on different sides of the arch achieves increased balance, improving the situation for horizontal displacements. In addition, it offers an interesting solution for the torsional situation of the decks that have single-sided suspension.

A compression eliminating tool has been applied to the algorithm, removing cables that would have experienced a state of compression. As a result the cables have been positioned in accordance.

The circular cross-sections, i.e. the tubular beams, for the decks have mainly been chosen as a result of their benefits regarding torsional capacity [13], seeing as large amounts of torsion were expected especially at the inner tubular beams of the decks due to their single-sided suspension.

4.5   Submission of contribution

The finished design has been rendered using Photoshop and presented in accordance with the Conference templates. Submission was completed within the due date and was approved by the Conference Committee. The par-

ticipation will end by attending the Conference in Berlin in September 2017, as a courtesy of the Norwegian University of Science and Technology (NTNU), more specifically through Professor Anders Rönnquist.

5. <u>CONTRIBUTION ANALYSIS</u>

As the thesis work has progressed after submitting the contribution to Footbridge 2017 Berlin, the submitted bridge design has been analyzed further. The analysis' carried out and presented in the following chapter includes the effects of more realistic loads, changes to geometry and support conditions. The chapter also presents possible solutions to deal with identified concerns as they are observed.

5.1   Load values and combinations

As per the deadline for the submission of the contributions for the Footbridge Conference, the considered load situation was simply the self-weight of the structure and a rough estimate of 10 $\frac{kN}{m^2}$ loading to deck surfaces thought unlikely to surpass. In order to better determine the plausibility of the footbridge design, it is necessary to account for a more accurate load situation for the structure at the actual building site.

Table 5.1 shows the calculated values for characteristic loads as well as the safety factor and corresponding design value for each load.

As the available standards to the authors applies to Norway and Norwegian regions for the most part, certain assumptions and simplifications has been unavoidable. This section presents the main assumptions and results for the load calculations, and should be seen together with the detailed argumentation and calculation of the loads which can be found in attachments B through E.

For determination of the thermal load's effect on the bridge, it has been assumed that the bridge will be built so that there is no thermal loading working on the structure at the temperature at the mid-point between the maximum and minimum temperature, 8°C. This implies that the thermal loading will appear as tensile or compressive forces in the structure as the steel contracts or expands due to the change in temperature from 8°C. These forces can then be accounted for by inserting $\pm\frac{\Delta T}{2}$ as a thermal

loading input in the footbridge model, using either the Karamba or Robot 3d software.

The calculated value for thermal loading accounts for the extreme situations $T = 58°$C and $T = -42°$C as summer and winter temperatures respectively, in Berlin. It should be mentioned that the control of these forces will be valid even if the temperatures found for Berlin is slightly wrong. The control still accounts for a temperature change of $\pm\frac{\Delta T}{2} = \pm 50°C$ regardless of the mean temperature in the given environment, which can be argued to be quite conservative temperature changes for Berlin, Germany.

To determine the wind load acting on the bridge, it is assumed that Berlin weather conditions can be compared to Oslo in Norway, as the available standards merely contained data regarding Norwegian regions. Furthermore, the effect of the wind velocity as a function of height has been accounted for by developing a conservative and simplified model of the wind load, dividing the structure into 4 different parts with regards to the height. The simplified model can be found as "Figure E.1" in attachment E. This results especially in the arch being increasingly loaded as the height increases, over the three parts that the arch is divided into.

Load values for the footbridge

Load type	Characteristic value	SF	Design value
Snow load	$q_{sk} = 0.963\ \frac{kN}{m^2}$	1.5	$q_{sd} = 1.451\ \frac{kN}{m^2}$
Crowd loading			
Vertical	$q_{fk} = 5.00\ \frac{kN}{m^2}$	1.35	$q_{fd} = 6.75\ \frac{kN}{m^2}$
Horizontal	$Q_{flk,1} = 225\ kN$	1.35	$Q_{fld,1} = 303.75\ kN$
Service vehicle			
Vertical	$Q_{SV1.1} = 40\ kN$	1.0	”
	$Q_{SV1.2} = 40\ kN$	1.0	”
	$Q_{SV2.1} = 20\ kN$	1.0	”
	$Q_{SV2.2} = 20\ kN$	1.0	”
Horizontal	$Q_{flk,2} = 72\ kN$	1.0	”
Accidental loads			
To pier:			
$\parallel$ *direction of traffic*	$500\ kN$	1.0	”
$\perp$ *direction of traffic*	$250\ kN$	1.0	”
To deck:			
Horizontal $\perp$ *deck span*	?	1.0	”
Thermal load	$\pm \frac{\Delta T}{2} = \pm 50°C$	-	-
Wind load			
To deck:			
Vertical $\perp$ *deck surface*	$q_{W,ver} = 0.320\ \frac{kN}{m^2}$	1.5	$q_{W,ver,d} = 0.480\ \frac{kN}{m^2}$
Horizontal $\perp$ *deck span*	$q_{W,hor} = 0.356\ \frac{kN}{m^2}$	1.5	$q_{W,hor,d} = 0.534\ \frac{kN}{m^2}$
To arch:			
Horizontal $\perp$ *arch span*	$Q_{W,arch,lower} = 0.687\ \frac{kN}{m}$	1.5	$Q_{W,a,l,d} = 1.031\ \frac{kN}{m}$
	$Q_{W,arch,middle} = 0.923\ \frac{kN}{m}$	1.5	$Q_{W,a,m,d} = 1.385\ \frac{kN}{m}$
	$Q_{W,arch,upper} = 1.073\ \frac{kN}{m}$	1.5	$Q_{W,a,u,d} = 1.610\ \frac{kN}{m}$

Table 5.1: Calculated load values that will act on the footbridge structure.

To determine the worst likely load combinations, three different scenarios have been proposed that would logically appear to be most undesirable yet still possible to occur, before allowing the software to run an automatic combination of the specified loads to determine the software's result for worst possible load combination. That way, the least desirable load combination is to some degree tested against an initial and logical understanding. After the automatic combination of the loads by the software, new insight may be given. If the worst case found through the computer is more desirable than the proposed combination, i.e. that the software algorithm has not found that given combination, a more conservative design case for the bridge has been achieved through not blindly accepting the software's generated combinations. Alternatively, the software creates a more undesirable combination that has been deemed too unlikely to occur in the proposal, and one can then choose not to use that combination when optimizing the structure. The goal of doing this approach has been to maximize awareness and apply some degree of common sense when choosing design case for worst load combination.
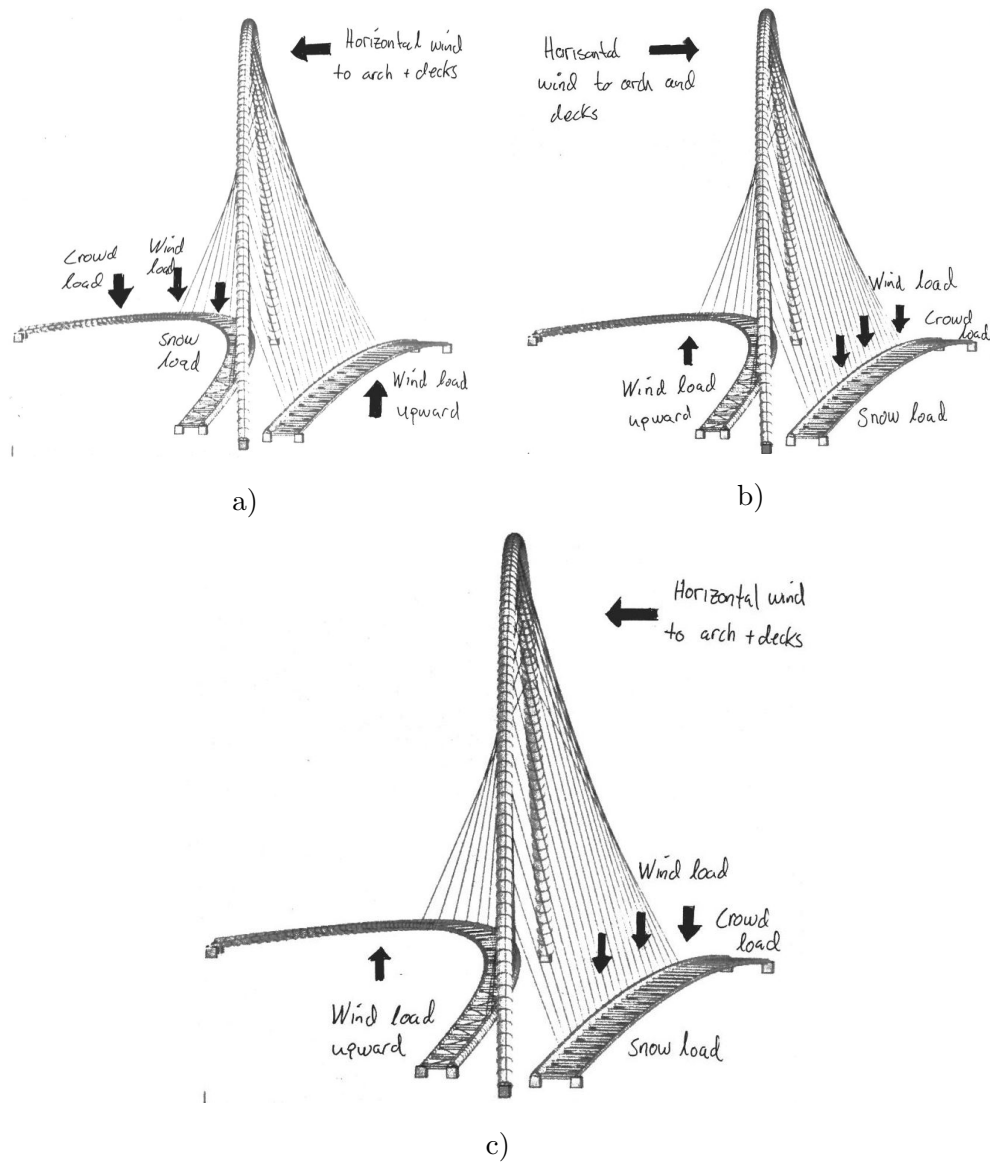
Figure 5.1: a-c) Proposed worst load combinations likely to occur.

Figure 5.1 a-c) shows the first, second and third proposed worst load combination likely to occur. In all instances, load from self-weight and horizontal wind perpendicular to the deck span in the same direction as the wind to the arch is naturally present.

5.1.1 Automatic load combination generation in Robot Structural Analysis

After developing a proposal for what the worst load combination should look like, there has been automatically generated 306 load combinations in Robot Structural Analysis. Ideally, one could produce a much larger number of combinations by dividing the structural parts into smaller sections, allowing for more specific load applications. However, due to both computer processing capacity and in order to achieve a simplified and more applicable set of combinations, it has been chosen that the different loads are either applied for an entire structural part or not at all.

The automatically generated load combinations that results in the largest values of forces, moments and displacements in the structure are the ones that has been assumed most unfavourable for the bridge structure. The largest values with corresponding load combinations are presented in figure 5.2 below.

Worst automatically generated load combinations

Force/displ.	min.	LComb.	max.	LComb.
$\mathbf{F}_x$	-3251 kN	162(C)	16050 kN	16(C)
$\mathbf{F}_y$	-648 kN	112(C)	710 kN	112(C)
$\mathbf{F}_z$	-788 kN	168(C)	1290 kN	132(C)
$\mathbf{M}_x$	-4092 kNm	162(C)	3905 kNm	162(C)
$\mathbf{M}_y$	-5792 kNm	132(C)	12774 kNm	132(C)
$\mathbf{M}_z$	-12779 kNm	168(C)	13383 kNm	132(C)
$\mathbf{U}_x$	-74 mm	132(C)	53 mm	112(C)
$\mathbf{U}_y$	-414 mm	180(C)	413 mm	112(C)
$\mathbf{U}_z$	-383 mm	168(C)	26 mm	162(C)

Table 5.2: Worst automatically generated load combinations

The six different load combinations identified in table 5.2 are: 16(C), 112(C), 132(C), 162(C), 168(C) and 180(C).

Before presenting the content of each of these load combinations, it is necessary to define each of the load cases the combinations can contain. The potential load cases and their abbreviations can be found in table 5.3.

Definition of load cases and their abbreviations

Abbreviation	Load case
S	Self-weight + weight of deck
CP	Crowd load to pedestrian deck
CB	Crowd load to bicycle deck
C2	Crowd load to both decks
SP	Snow load to pedestrian deck
SB	Snow load to bicycle deck
S2	Snow load to both decks
WP	Horizontal wind load to both decks and the arch in direction from pedestrian to bicycle deck (positive y-direction) + vertical wind working upward on pedestrian deck + vertical wind working downward on bicycle deck
WB	Horizontal wind load to both decks and the arch in direction from bicycle to pedestrian deck (negative y-direction) + vertical wind working downward on pedestrian deck + vertical wind working upward on bicycle deck

Table 5.3: Abbreviations for different load cases

The definition of each of the load combinations, which is automatically generated in Robot Structural Analysis and based on NS-EN 1990:2002/NA:2008, is as follows in table 5.4

Definition of load combinations

Load combination	Definition
16(C)	S*1.35+(C2+S2)*1.05+WP*0.90
112(C)	S*1.20+C2*1.50+WP*0.90+S2*1.05
132(C)	S*1.20+CB*1.50+WP*0.90+SB*1.05
162(C)	S*1.20+C2*1.50+WB*0.90+S2*1.05
168(C)	S*1.20+CP*1.50+WB*0.90+SP*1.05
180(C)	S*1.00+CP*1.50+WB*0.90+SP*1.05

Table 5.4: Definition of load combinations generated in Robot S. A.

As becomes clear from the results in tables 5.4 and 5.2, simultaneous loading of both decks, 112(C), becomes the critical combination for shear forces, which in retrospect is quite natural, and also for maximum values of deformation in x- and y-direction, which was not assumed when the proposing the worst combinations.

It is chosen to define all the above load combinations as design cases for the structure in Karamba when evaluating the Footbridge 2017 Berlin contribution bridge further. As may be noticeable, the thermal load is not included in the combinations above. It has been decided to add the thermal loading to each of these cases in Karamba where it is considered appropriate by the authors, as one should account for the thermal load to be present at the same time as other loads according to the Eurocodes.

Since the combinations above are generated for the bridge as it was when delivered to Berlin, it is reasonable to assume that the combinations that gives the worst cases based on the results from the tables above might change as the bridge design is being modified. It is however not generated new load combinations for each time changes are made to the bridge, although doing so might have provided valuable insight in regards to the changes made.

5.2 Verification of model

The final design was largely based on optimization with regards to deformation using the Galapagos plug-in. The result of this creates quite large cross-sections in order to achieve less than 100 per cent utilization for each of the structural components. The geometry of the bridge model can be seen in figure 5.2, with the pedestrian deck on the right-hand side and the bicycle deck on the left-hand side. The spacing distance between each transverse beam the bridge decks longitudinal direction is c-c 4 meters in the pedestrian deck, and c-c 5 meters in the bicycle deck. Specification of measurements and cross-sections can be found in table 5.5 and table 5.6.

Before further analyzing the bridge, it has been considered relevant to perform a verification of the Grasshopper Karamba bridge model, using Robot structural Analysis to control the quality of the model. A verification such as this may be useful and important in order to ensure that the structure is behaving properly, and to ensure results of a good quality.
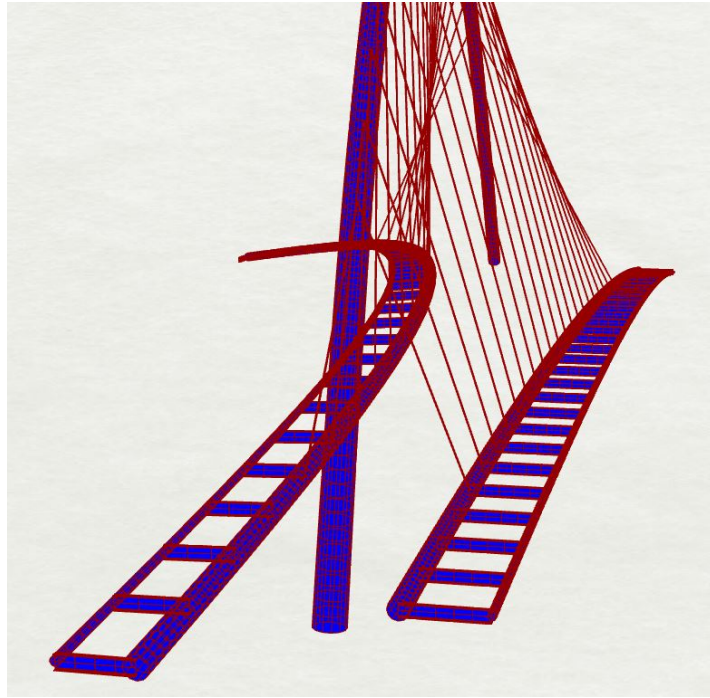
Figure 5.2: The initial bridge design model.

Measurements for the initial bridge's structural parts

Structural part	Span [m]	Length [m]	Width [m]	Height [m]
Arch	136	169.2	-	46
Pedestrian deck	120	120.15	4	-
Bicycle deck	141.4	147.5	3	-

Table 5.5: Measurements for the initial bridge's structural parts.

Cross-sectional data for the initial bridge components

Structural component	Cross-section [mm]	Material
Arch	Tubular beam 1500/150	Steel/S355
Inner deck pipes	Tubular beam 1000/100	Steel/S355
Outer deck pipes	Tubular beam 400/50	Steel/S355
Transverse beams	IPE600	Steel/S355
Cables	Circular section 70	Steel/S355

Table 5.6: Cross-sectional data for the initial bridge components.

When modelling, it is important to do so in such a way that the model representing the structure simulates the chosen design in the best way possible. The model being used to simulate and perform calculations on the conference contribution design does not account for wind load to cables. The reason for this is that the modelling of this phenomenon is quite a complex problem, and has not been focused on in this thesis. As the model is at this point, all supports at the arch and deck ends are fixed. The transverse beams are modelled using fixed connections, and the cables are modelled using pinned joints for connection between the arch and decks. All components steel of quality S355 as material, except the cables. The cables have customized material properties, increasing the tensile, or ultimate strength, to better simulate the characteristics of the cable. The material properties are based on a galvanized strand cable available on the market from manufacturer "TriPyramid", with Young's modulus 124 GPa and ultimate strength 1055 MPa [14]. The software seemingly has some flaws when it comes to the scaling of deformations of the cables when modelling them this way and having turned on gravitational force. Being unable to overcome this issue, it is chosen to show deformations from the Karamba software without the presence of the cables.

The verification is done by modelling the bridge in both Karamba 3d and Robot Structural Analysis and comparing the results first using only self-weight, and then using a defined load combination. What it achieves, is to determine whether the model calculates and behaves the same way in both FE-programs, and in so doing controlling that the assumptions made regarding the joining (joints) of structural members, support conditions and so forth are modelled properly in Karamba. It does however not control the validity of the assumptions made in order to simulate a realistic structure.

For presentation of the results, it is chosen to limit the amount of presented values to the sectional maximum values of the bending moment about the y-axis for the arch and inner pipe beam on the pedestrian deck only. Even though all values have been controlled, a presentation of all result would be irrelevant to the reader, and the presented data should be sufficient in giving an impression of the coherence between the results from the two different programs. See figure 1 after the table of contents for the bridge's axis system. The comparison is done using first self-weigh, which should produce close to equal results in the two programs, and then using a load combination, where one might except some deviation in the results.

5.2.1   Comparison of results from Robot and Karamba with self-weight
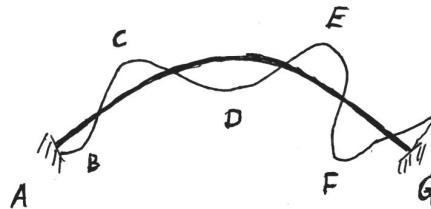
Bending moment about y-axis for the arch

Figure 5.3: Sectioning of the moment diagram for the arch.

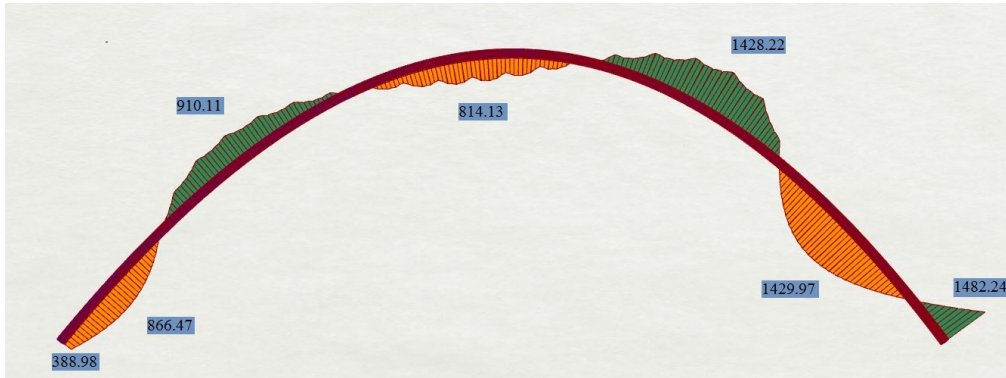**Diagram of M_y for the arch using Robot**

Figure 5.4: Diagram of M_y for the arch using Robot. Loading: self-weight

Values of M_y at sectional points along the arch using Robot

M_y at sectional points	Value [kNm]
M_A	378.65
M_B	861.81
M_C	-907.74
M_D	795.49
M_E	-1431.79
M_F	1445.61
M_G	-1480.78

Table 5.7: Values of M_y at sectional points along the arch using Robot

Notice that the moment diagram for the arch in figure 5.9, produced in Robot is drawn on a horizontal projection of the arch.

Diagram of M_y for the arch using Karamba

Figure 5.5: Diagram of M_y for the arch using Karamba. Loading: self-weight.

Notice that the moment diagram for the arch in figure 5.9, produced in Karamba is drawn on the arch's actual geometry. Using the same sectioning for the moment diagram for the arch as in 5.3, the results are presented in table 5.8.

Values of M_y at sectional points along the arch using Karamba

M_y at sectional points	Value [kNm]
M_A	388.98
M_B	866.47
M_C	-910.11
M_D	814.13
M_E	-1428.22
M_F	1429.97
M_G	-1482.24

Table 5.8: Values of M_y at sectional points along the arch using Karamba

Comparing the results from the tables above, the largest identified deviation in results at the sectional points between the two FE-programs when loading with self-weight, in per cent, is that of M_A. This value deviates with 2.7 per cent from the results in Robot for the Karamba model. The largest difference as a numeric value is that of M_D, having a difference of 18.64 kNm.

Note 1: The deviation in results for bending moment about y-axis in the arch when loaded with only self-weight are reasonably small. The fairly small deviations in addition to the two diagrams having the same nature of behavior, and given the fact that the same is true for other controlled force

diagrams and deformations not presented here, the conclusion is coherence in results for the arch in the two programs when loaded with only self-weight.

Bending moment about y-axis for the inner tubular beam of the pedestrian deck

When looking at the moment diagram and values for the inner tubular beam, the sectioning of the diagram shown in figure 5.6 is used.
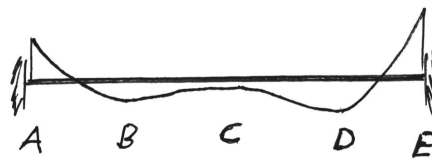

Figure 5.6: Sectioning of the moment diagram for inner tubular beam of the pedestrian deck.

Diagram of M_y for the inner tubular beam of the pedestrian deck using Robot
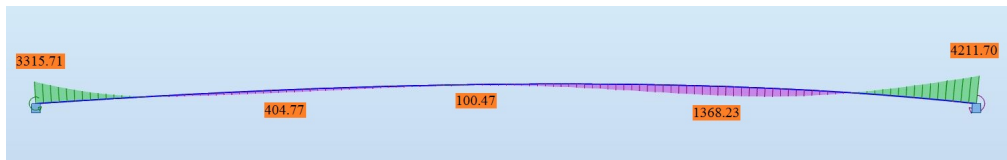
Figure 5.7: Diagram of M_y for the inner tubular beam of the pedestrian deck using Robot. Loading: self-weight.

Values of M_y at sectional points along the inner tubular beam of the pedestrian deck using Robot

M_y at sectional points	Value [kNm]
M_A	3315.71
M_B	-404.77
M_C	-100.47
M_D	-1368.23
M_E	4211.70

Table 5.9: Values of M_y at sectional points along the inner tubular beam of the pedestrian deck using Robot

Diagram of M_y for the inner tubular beam of the pedestrian deck using Karamba
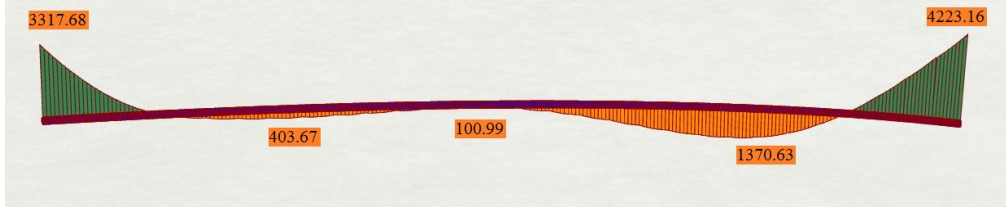
Figure 5.8: Diagram of M_y for the inner tubular beam of the pedestrian deck using Karamba. Loading: self-weight.

Using the same sectioning for the moment diagram for the inner tubular beam of the pedestrian deck as in 5.6, the results are presented in table 5.10.

Values of M_y at sectional points along the inner tubular beam of the pedestrian deck using Karamba

M_y at sectional points	Value [kNm]
M_A	3317.68
M_B	-403.67
M_C	-100.99
M_D	-1370.63
M_E	4223.16

Table 5.10: Values of M_y at sectional points along the inner tubular beam of the pedestrian deck using Karamba

Comparing the results from the tables 5.9 and 5.10, the largest identified deviation in results at the sectional points when loading with self-weight, in per cent, is that of M_C. This value deviates with 0.52 per cent from the results in Robot for the Karamba model. The largest difference as a numeric value is that of M_E, having a difference of 11.46 kNm.

Note 2: The deviation in results for bending moment about y-axis in the inner tubular beam of the pedestrian deck when loaded with only self-weight are also reasonably small. Given the diagrams' nature of behaviour, and given the same standard of results when controlling for the remaining force diagrams and deformations not presented here, the conclusion is coherence in results for the inner tubular beam of the pedestrian deck as well, when loaded with only self-weight.

5.2.2 Comparison of results from Robot and Karamba with load combination 16(C)

Bending moment about y-axis for the arch

Using the same sectioning for the moment diagram for the arch as in 5.3, the results are presented in table 5.11 5.12.
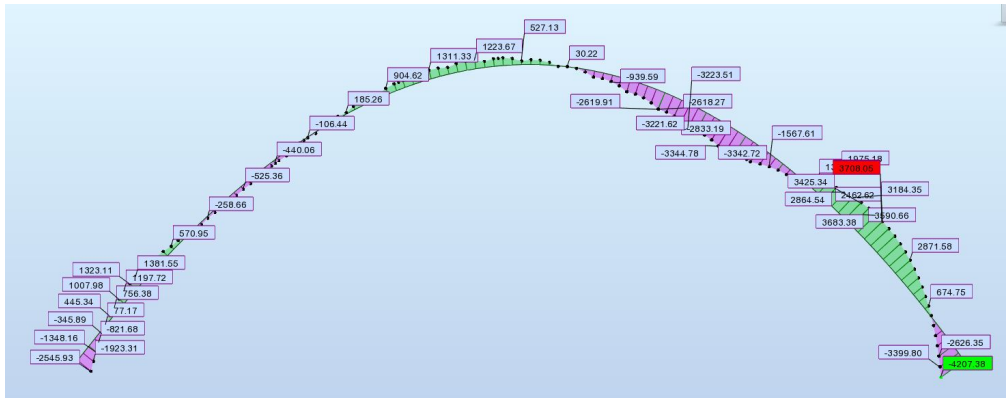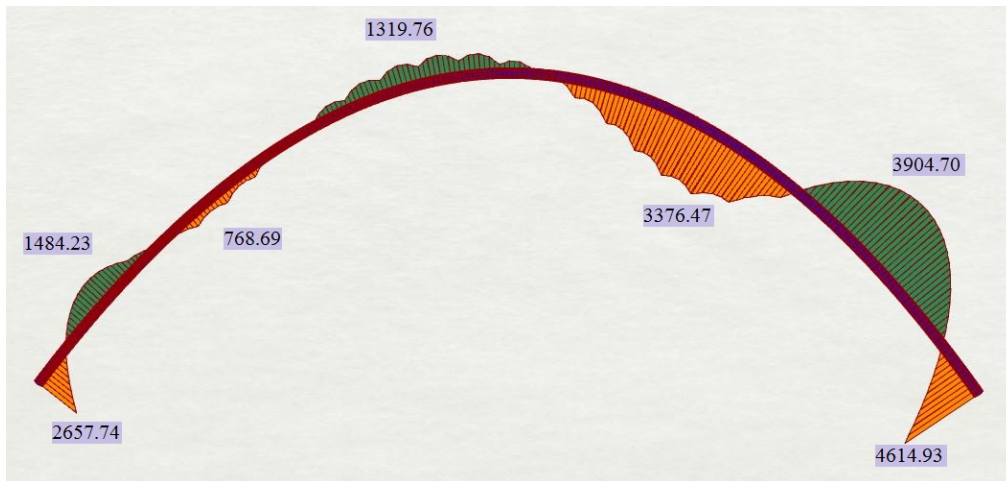
Diagram of M$_y$ for the arch using Robot

Figure 5.9: Diagram of M$_y$ for the arch using Robot. Loading: 16(C)

Values of M$_y$ at sectional points along the arch using Robot

M$_y$ at sectional points	Value [kNm]
M$_A$	-2545.93
M$_B$	1381.55
M$_C$	-525.36
M$_D$	1311.33
M$_E$	-3344.78
M$_F$	3708.05
M$_G$	-4207.38

Table 5.11: Values of M$_y$ at sectional points along the arch using Robot

Diagram of M_y for the arch using Karamba

Figure 5.10: Diagram of M_y for the arch using Karamba. Loading: 16(C).

Values of M_y at sectional points along the arch using Karamba

M_y at sectional points	Value [kNm]
M_A	-2657.74
M_B	1484.23
M_C	-768.69
M_D	1319.76
M_E	-3376.47
M_F	3904.70
M_G	-4614.93

Table 5.12: Values of M_y at sectional points along the arch using Karamba

When applying load combination16(C) to the bridge structure, comparison of the results in the tables above now shows a largest identified deviation in results between Robot and Karamba, in per cent, to be that of M_C. The values for M_C deviates with 46.3 per cent. The largest difference as a numeric value is that of M_G, having a difference of 407.55 kNm.

Note 3: The deviation in results for bending moment about y-axis in the arch when applying load combination 16(C) are somewhat larger than when only applying the structure's self-weight. With closer examination of the tables, one will find that the largest identified deviation of 46.3 per cent is an exception to the rest of the results, which deviates between 0.5-10.0 per cent. Seen in perspective, the largest deviation as a numeric value of 407.55 kNm represents a 9.7 per cent deviation from the result in Robot

in Karamba. Combined with a solid equality of behavioural nature for the diagrams, it is fair to suggest that the differences in results have increased, but seem to have valid coherence for the arch also when load combination 16(C) is applied.

Bending moment about y-axis for the inner tubular beam of the pedestrian deck

Using the same sectioning for the moment diagram for the inner tubular beam as in 5.6, the results are presented in table 5.13 5.14.

Diagram of M_y for inner tubular beam of the pedestrian deck using Robot
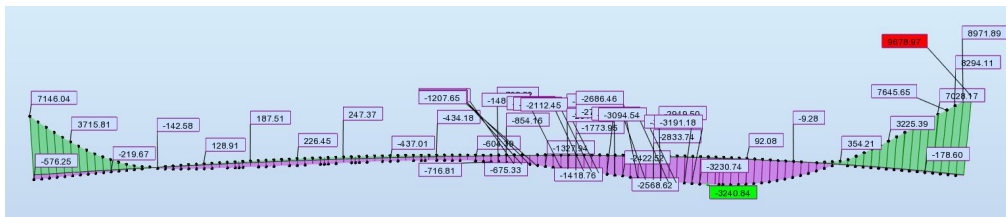
Figure 5.11: Diagram of M_y for the inner tubular beam using Robot. Loading: 16(C)

Values of M_y at sectional points along the inner tubular beam using Robot

M_y at sectional points	Value [kNm]
M_A	7146.04
M_B	-650.45
M_C	-434.18
M_D	-3240.84
M_E	9678.97

Table 5.13: Values of M_y at sectional points along the inner tubular beam using Robot

Diagram of M_y for inner tubular beam of the pedestrian deck using Karamba

Figure 5.12: Diagram of M_y for the inner tubular beam using Karamba. Loading: 16(C).

Values of M_y at sectional points along the inner tubular beam using Karamba

M_y at sectional points	Value [kNm]
M_A	7647.34
M_B	-594.89
M_C	-408.97
M_D	-3460.88
M_E	10390.39

Table 5.14: Values of M_y at sectional points along the inner tubular beam using Karamba

Comparison of the results in tables 5.13 and 5.14 shows a largest deviation when applying load combination 16(C) for M_B, in per cent, for the inner tubular beam of the pedestrian deck. The value of deviation is 8.5 per cent from the results in Robot for the Karamba model. The largest difference as a numeric value is that of M_E, having a difference of 711.42 kNm, corresponding to a deviation of 7.3 per cent.

Note 4: The deviation in results for bending moment about y-axis in the inner tubular beam of the pedestrian deck with load combination 16(C) are reasonably small, and in coherence with the values of deviation for the arch, in per cent. The same arguments as for the arch can therefore be applied for the inner tubular beam of the pedestrian deck.

Evaluation

Given that the results are conclusive also for all other structural parts, and for all force diagrams and displacements, even though not presented here, it can be concluded that despite observing consistent variations in numeric

values for displacements and load diagrams for the structure, the quality of the results are good, as the deviations are fairly small in addition to all diagrams having the same behavioural nature. The structure is in other words responding in the same manner in both instances, and differences in values might be due to differences in definition of material properties, standard cross-sections or load application.

Result: Verification has been made that the bridge design, with its specifications, is modelled properly in Karamba, producing good quality results when comparing with state-of-the-art industrial FE-software.

5.3   Developing an ideal solution for the deck

To determine a solution for the design that would provide favourable results for the structure in regards to deformations, there was at an earlier point during the thesis work carried out some experiments in the Robot Structural Analysis software. The focus was on limiting deformations, as large deformations due to the long span of the bridge was observed.

The first step involved loading the steel frame with its self-weight to have a reference point. The result of this analysis was global extreme values of displacement 50.6 cm in y-direction (horizontal perpendicular to deck bridge span) and -16.3 cm in z-direction (vertical downwards) for the decks.

Thereafter, transverse stiffeners was applied in both decks in order to analyze the structures response with regards to the deformation. The deformation changed, slightly decreasing, but was still unsatisfactory. The result was 21.2 cm in y-direction and -10.0 cm in z-direction.

Additional transverse stiffeners was then applied in both decks, creating a cross between every set of transverse beams. The result was that the structure significantly improved with regards to deformations. The result was 9.9 cm in y-direction and -8.4 cm in z-direction.

If these results are compared to the serviceability limit state requirement for vertical displacement of a bridge deck as previously defined in equation 2.3 as $\frac{L}{350}$ [1], giving an allowed displacement of no more than $\frac{120m}{350} = 34.3$ cm in y-direction when loaded with the crowd load. Considering that this experiment was carried out using simply self-weight, it stands to reason that a solution for stiffening of the structure must be applied.
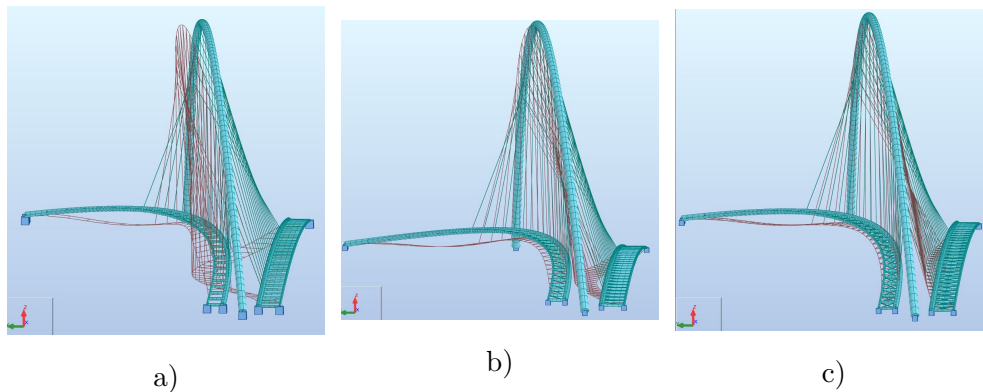
Figure 5.13: a) Def. with no stiffeners, b) def. with diagonal stiffeners, c) def. with cross-stiffeners.

Figure 5.13 a) shows the deformation of the structure without stiffeners when loaded with self-weight, 5.13 b) shows the deformation with only diagonal stiffeners between the transverse beams, and 5.13 c) shows the deformation with cross-stiffeners between all transverse beams. All deformations (see red lines) are scaled up x30.

Conclusion: Creating a stiff deck is crucial in order to achieve desired deformations in the structure. This is likely due to its long span, but also the fact that the placement of the arch in the middle of the two decks leads to the decks, and especially the straight deck, being pulled towards the centre (arch placement) when loaded.

One suggestion can be to use a plate material as deck, attaching it in such a way that the plate itself works as a "cross-stiffener". Another solution could be to design a composite, or joint material deck, using concrete with steel reinforcement.

For this design, it is however chosen to use stiffeners in a truss-pattern, which after tests proved to achieve close to the same results as for cross stiffeners, but at the same time saves the use of material. These stiffeners will be modelled as having a pinned connection to the corners where the transverse beams joins with the tubular pipes of the decks. The idea is then for the deck to simply act as flooring in order to allow people to walk on the bridge - not significantly adding to the stiffness of the structure. Assuming that there is no particular need for increased weight of the deck due to dynamic aspects of the structure, it is chosen to use a light-weight sandwich deck composed of a balsa plate core within plastic cover plates. The top surface of the composite deck plate has a carbonized sheet layer with grip for covering and walking purposes, as delivered by COLEVO [4].

The load to the structure from the deck can be determined based on the

weight of the deck plates, which is $43 \frac{kg}{m^2}$ for a plate spanning $2.4m \times 2.4m$ being used as a deck surface for a footbridge, having a thickness of 70 mm [4]. This means that adjustments must be made to the weight of the plate as the required thickness of it changes depending on the length of the plate span in both directions, and based on requirements for deformation.

When modelling this solution in the Karamba software, the weight of the deck can then be applied as a uniformly distributed load to the transverse beams, and have an algorithmic definition that allows automatic adjustment of the size of the load as the spacing distance between transverse beams potentially are changed. What becomes important in the design is then that the cross-sections of the stiffeners are small enough compared to the transverse beams that deformations of the deck plates do not reach the stiffeners when loading to the plates is applied, seeing as the stiffeners have pinned connections.

a)   b)   c)
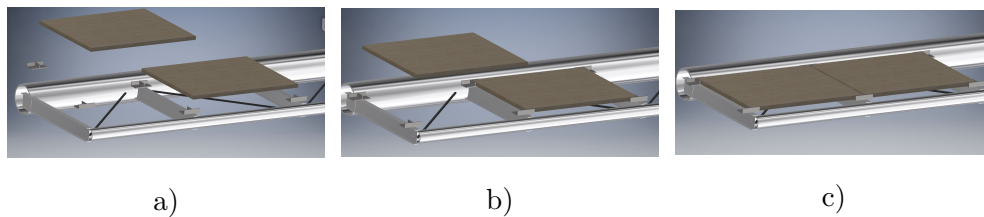
Figure 5.14: a-c) Steel frame with truss-patterned diagonal stiffeners with shelf-like supports for deck plates.

Figure 5.14 shows the steel frame of the bridge deck with a diagonal, truss-patterned solution for transverse stiffening of the deck, and is a solution that is developed by the authors in the Autodesk software, Inventor. To achieve that the deck plates should not act as stiffeners and that they should not affect the deformation pattern significantly, it is chosen that the deck plates shall rest on "corner-shelf supports" seen in figure 5.15, which are made out of steel and creates corners for the deck plates to be fitted into. It is here important that there is some space between the steel corners supporting the deck plates, and the deck plate itself. It is here suggested a 1-2 cm thick rubber-like walling which allows slight movement of the plates as the steel frame structure deforms. This way the structure can be modelled with the steel frame and simply adding load from the weight of the deck plates to the frame to simulate the decks.

<div align="center">a)   b)</div>
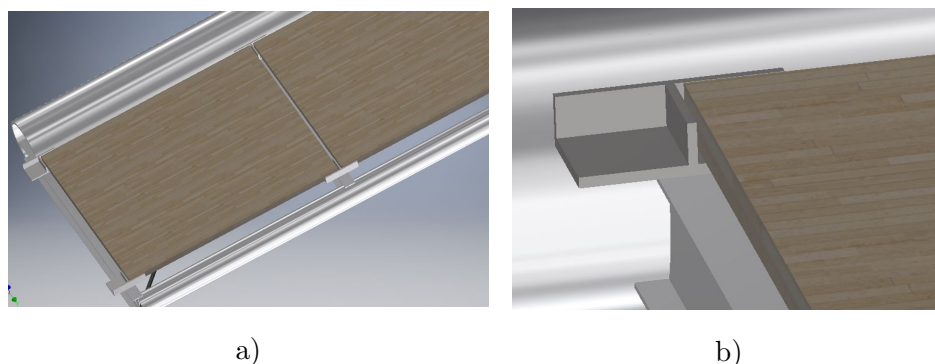
Figure 5.15: a) Top view deck solution, b) Close view of deck plate supports (shelves).

5.4 Changing of the support conditions

During further investigations of the developed footbridge bridge concept, it was found interesting to see how the structure responds to changing of the support conditions, both in relation to thermal loading and in general. Seeing as the structure is prevented from any movement at all supports, it will be interesting to see how the pattern of deformation changes as movement in one of the directions is allowed, and to see how the forces in the structure changes. It is also thought interesting to see if a conclusion can be made as to whether the structure's ability to withstand the changes in temperature improves or not when movement in one of the directions is not prevented.

When changing the support conditions to sliding joint in x-direction, it is done by allowing expansion in the global x-direction for the bridge, i.e. in the direction of the span for the straight deck, previously referred to as the pedestrian deck. Furthermore, it is done so only for the supports of the decks, and only at the side of the bridge span where the two decks are situated closest together, i.e. where both of the decks are oriented parallel to the global x-direction. At the opposite side of the structures span, the supports of the decks remains fixed, whereas the arch remains fixed at both its supports.

As there is a need of limiting the presented results, the presented data in this section will therefore be limited to patterns of deformations and maximum values of displacement of larger structural parts such as the arch and the two separate decks as a whole.

5.4.1 Deformation

Fixed at all supports - all load combinations
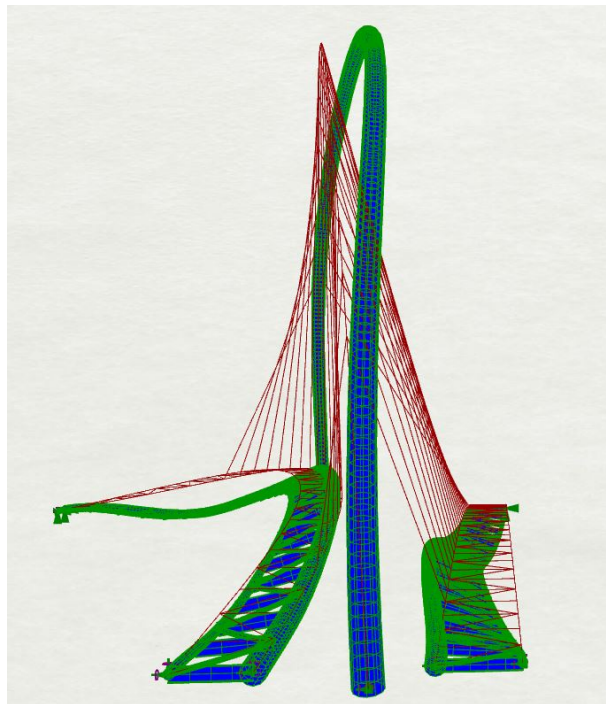
Figure 5.16: Pattern of deformation for the bridge when fixed at all supports.

Structural part	U_x [mm]	U_y [mm]	U_z [mm]
Arch	58	317	63
Pedestrian deck	17	111	250
Bicycle deck	21	55	177

Table 5.15: Values of displacement of the bridge when fixed at all supports.

Sliding joint for expansion in x-direction, all load combinations
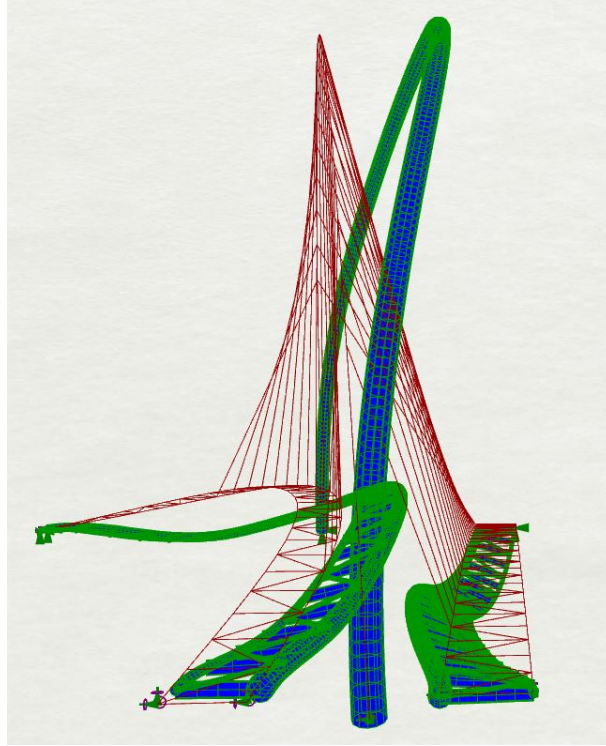
Figure 5.17: Pattern of deformation for the bridge with sliding joint in x-direction.

Structural part	U_x [mm]	U_y [mm]	U_z [mm]
Arch	56	576	62
Pedestrian deck	31	174	365
Bicycle deck	157	241	206

Table 5.16: Values of displacement of the bridge with sliding joint in x-direction.

The figures 5.16 and 5.17 show the worst deformation pattern of the footbridge structure when it is fixed at all supports, and when it has the freedom do slide in x-direction at the decks' near-end side of support from the point of view of the figures, respectively. All figures throughout this section will show the original geometry of the bridge as red lines, and display the deformation pattern for the bridge with cross-sections in green and blue colours.

Note: We observe that the pattern of deformation for the bridge with exclusively fixed supports, seen in figure 5.16, seems to be favourable to

the pattern of deformation for the bridge with sliding joints, seen in figure 5.17, when loaded with all the previously defined load combinations and evaluating the most critical result.

Supporting the observation with comparing the results in tables 5.15 and 5.16, gives a difference of 259 mm in maximum displacement in y-direction, i.e. sideways displacement, for the arch. The maximum displacement of the arch in the longitudinal and vertical, or x- and z-direction respectively, remains insignificantly changed.

Comparison of values of deformation of the pedestrian deck also shows signs of deterioration when changing from fixed to sliding joint for the decks' supports at the near-end of the decks from the point of view seen in figures 5.16 and 5.17. The largest change in maximum deformation for the pedestrian deck is in vertical direction, increasing with 115 mm when changing from fixed to sliding supports.

One of the more severe changes can be seen when comparing the sideways and longitudinal displacement of the bicycle deck for the two instances. This displacement increases from 55 mm to 241 sideways, in y-direction, and from 21 mm to 157 mm in longitudinal, or x-direction.

The conclusion is that it is favourable to maintain the fixed supports of all structural parts based on the results from the above comparison.

5.5 Changing the arch cross-section based on previous theories

For the bridge structure's arch, the pattern of deformation consistently shows that the sideways displacement, i.e. in y-direction, is significantly larger that the displacements in the other directions. This phenomenon seems a quite natural respond the sideways pull on the arch in y-direction as the decks are loaded, and especially when only the pedestrian deck has applied loading, as the cables are oriented more vertically for the connection between arch and bicycle deck compared to between the arch and the pedestrian deck.

In light of the observed pattern of deformation, and inspired of the hypothesis testing of the Gateshead Millennium Bridge, there has been performed an analysis of whether or not a customized cross-section for the arch might be beneficial in order to either reduce the use of material thus increasing the efficiency of the arch, by basing the shape of the cross-section on the bending moment diagrams for the arch.

5.5. CHANGING THE ARCH CROSS-SECTION BASED ON PREVIOUS THEORIES

One of the main instigators for having a more detailed look at this cross-section has been concerns regarding the feasibility of producing such a large tubular beam as initially chosen for the arch in order to reach the requirements of utilization. The tubular beams such as it is, has a cross section with outer diameter 1500 mm, and has a 150 mm thickness. These dimensions are not any standard issue of pipes, and would potentially merely occur in the construction of an oil rig or in similar types of structures. The assumption is that a potential cross-section of this dimension would have to be custom made, and there is a concern regarding the process of welding such a thick-walled pipe. It has therefore been a desire to look into a cross-section more similar to the one seen in the reference structure Gateshead Millennium Bridge.

In figure 5.18, the general behaviour of the bending moment in a beam that is fixed at both supports and have a uniformly distributed load is show. This behaviour is what the hypothesis is based on, although the combined bridge structure has somewhat more complex behaviour. As an example, the bridge has point loads, thought the cables, that are not equal for every cable as a load, and the arch is not a beam - but an arch, which makes the values shown in figure 5.18 not entirely representative. However, it is a basis for a theory.
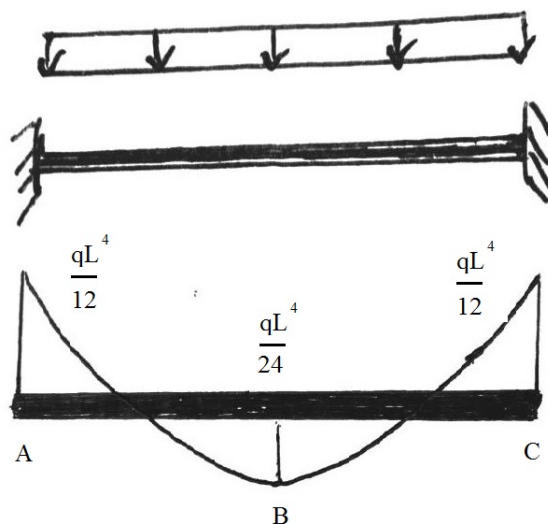
Figure 5.18: Expected behaviour of arch bending moment diagrams to base the hypothesis on.

The idea is that the bending moments will differ in size along the arch, and that a shape for the cross-section of the arc can be based on the bending moment diagram.

The load combinations resulting in the largest bending moment about z-axis in the arch has been found to be load combination 168(C). Critical combination for bending about y-axis was observed to be load combination 16(C). These combinations have been applied, and the resulting critical diagrams is presented in figures 5.19 and 5.20. The values at the supports and at mid span are presented in tables 5.17 and 5.18.

It can be observed that the diagram for bending moment about z-axis in figure 5.19 is behaving very much like expected, however with some variations. The value of the bending moment at mid-span is slightly less than half the value at the near-end support. The value of the bending moment at the far-end support is however closer to the value of the bending moment at mid-span than it is to the value at the near-end support. Here, the hypothesis becomes simple: the cross-section can be larger less wide (dimension in y-direction) towards the middle and support at far-end compared to at the support at the near-end.

For the moment about y-axis in figure 5.20 on the other hand, a more complex behavioural pattern for the bending moment is observed. Notice how the amount of bending moment M_y has increased in value from the section where the Karamba model was verified, shown in figure 5.10. This is interesting, as the only change made to the model between these two checks is the addition of stiffeners in a truss pattern. It can be observed that the flow of bending moment about y-axis in many cases along the arch is doubled in size as a result of the increased stiffness of the deck, and thus the structure. However, here the hypothesis becomes that some increase in height (dimension in z-direction) of the cross-section toward the mid-span might be beneficial, as the moment about y-axis is larger "around the middle", and more specifically at point D.

**Bending moment about z-axis in the arch for critical load combination
168(C)**
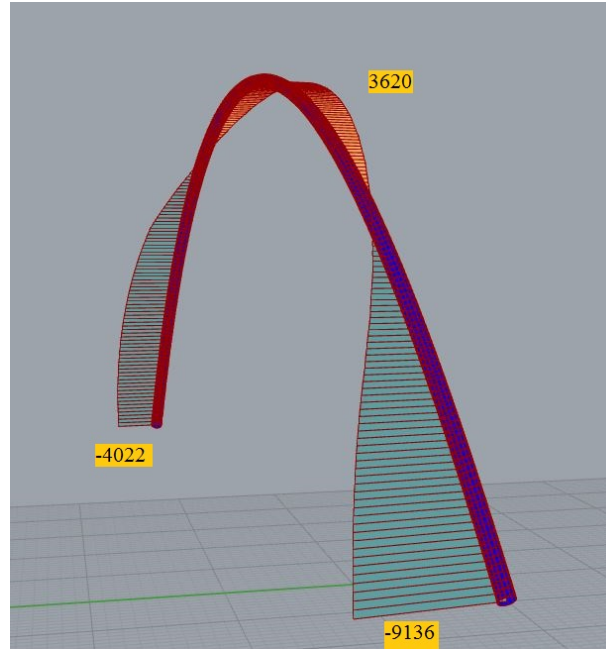
Figure 5.19: Bending moment about z-axis in the arch for critical load combination 168(C).

Values of M_z at sectional supports and mid-span of the arch

M_y at sectional points	Value [kNm]
$M_{support,near-end}$	-9136
$M_{mid-span}$	3620
$M_{support,far-end}$	-4022

Table 5.17: Values of M_z at sectional supports and mid-span of the arch

Bending moment about y-axis in the arch for critical load combination 16(C)
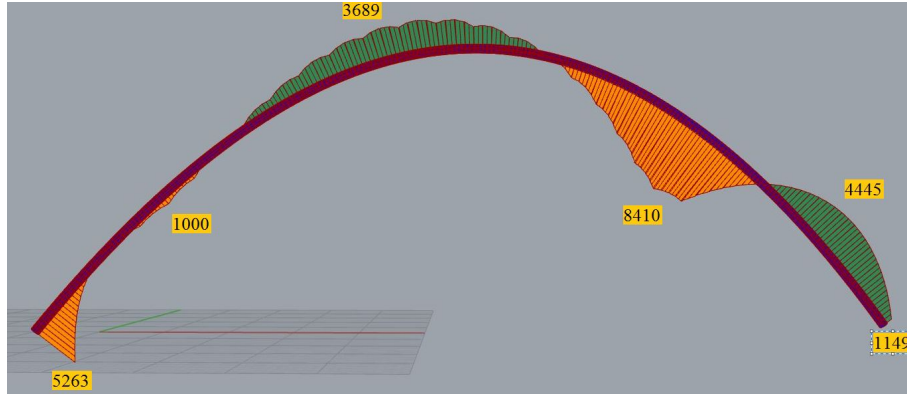
Figure 5.20: Bending moment about y-axis in the arch for critical load combination 16(C).

Following the same patter of sectioning as previously, the values start form the left hand side of the diagram, and every value of a curve top or bottom receives a value and a sectioning letter.

Values of M_y at sectional supports and mid-span of the arch

M_y at sectional points	Value [kNm]
$M_{support,leftside}$	5263
M_B	1000
M_C	-3689
M_D	8410
M_E	-4445
$M_{support,rightside}$	-1149

Table 5.18: Values of M_y at sectional supports and mid-span of the arch

After some preliminary optimization of the new cross-section, it is observed that in order to achieve results near the same quality of deformation, a cross section of the following measurements found in table 5.19 is required. Note that the wall thickness of the cross-section is constant, and has the value $t = 60mm$. For the cross-section shape, see figure 3.20 in section 3.4.

Customized cross-section measurements

Point of measurement	Height (local z-dir)	Widh (local y-dir)
Support near-end	1.5 m	4.2 m
Mid-span	1.9 m	3.0 m
Support far-end	1.5 m	4.2 m

Table 5.19: Values of M_y at sectional supports and mid-span of the arch

The resulting deformation pattern is illustrated in figure 5.21.

Deformation of the bridge when using the newly defined customized arch cross-section
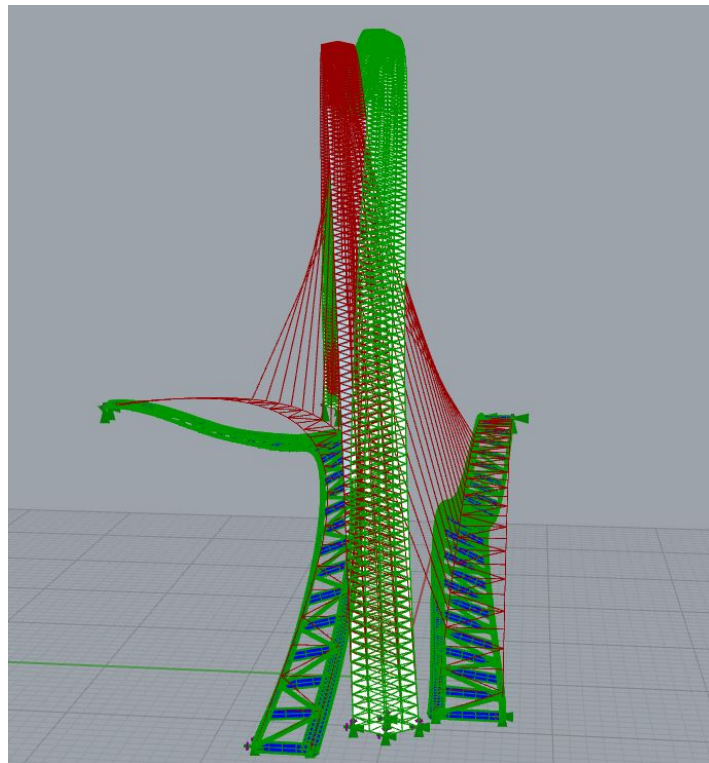
Figure 5.21: Deformation pattern of the bridge when using the newly defined customized cross-section.

Structural part	U_x [mm]	U_y [mm]	U_z [mm]
Arch	53	335	70
Pedestrian deck	20	107	307
Bicycle deck	16	61	212

Table 5.20: Values of displacement of the bridge when customized arch is applied.

Comparing the values of displacement for the bridge with the new arch cross-section, seen in table 5.20, with the values of maximum displacement with the previous tubular arch, found in table 5.23, an increase in displacement can be observed.

Deformation of the bridge when using tubular arch
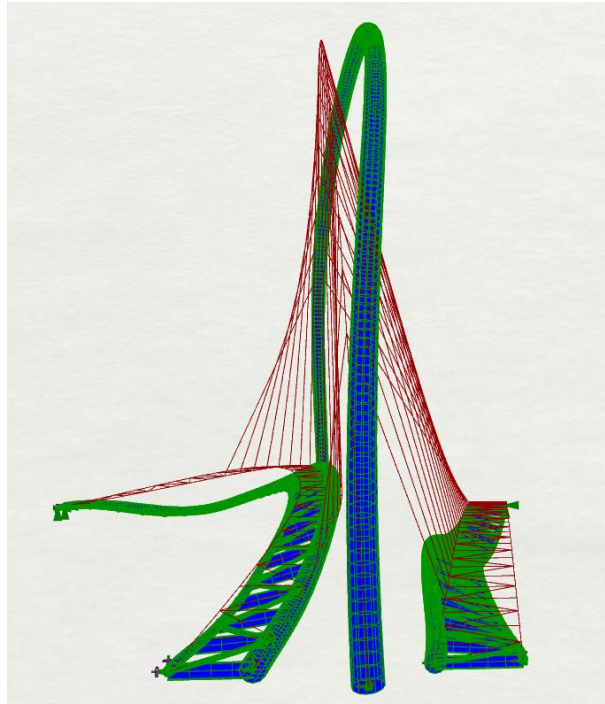
Figure 5.22: Pattern of worst deformation for the bridge with tubular pipe.

Structural part	U_x [mm]	U_y [mm]	U_z [mm]
Arch	58	317	63
Pedestrian deck	17	111	250
Bicycle deck	21	55	177

Table 5.21: Values of worst displacement for the bridge with tubular pipe.

The largest increase is for vertical displacement of the pedestrian deck, and the decrease is merely 57 mm. The value of maximum vertical displacement of 307 mm for the pedestrian deck is still within the previously defined requirement in serviceability limit state requirement for vertical displacement of 342 mm with quite some margin, considering the applied load in this case is not simply crowd load, which has been used to determine the SLS requirement.

5.5. CHANGING THE ARCH CROSS-SECTION BASED ON PREVIOUS THEORIES

Considering that the weight of the structure is measured to have a reduction from $1.625 \times 10^6 kg$ with the tubular arch, to $1.394 \times 10^6 kg$ with the customized arch, reducing the use of steel with 229 tons, the results can be considered satisfactory.

If looking at table 5.22, one can see that the utilization of structural components has increased for all components except the outer tubular beam of the pedestrian deck, which has decreased slightly.

Increase or decrease in utilization of structural components in per cent when customized arch is applied

Structural component	Percentage
Transverse beams	+10.5 %
Stiffeners	+2.7 %
Inner tubular beam pedestrian	+8.8 %
Inner tubular beam bicycle	+4.9 %
Outer tubular beam pedestrian	-0.7 %
Outer tubular beam bicycle	+3.2 %

Table 5.22: Values of increase or decrease in utilization of components

Evaluation It has been seen that the hypothesis about the cross-section being possible to customize based on the diagrams of the bending moments to some degree seems accurate. It is also observed that when doing so, an improved solution in regard to deformation is not achieved in this instance, though the results in this regard are quite close to one another. The fact that there has not been performed deep analysis of how to reach the best possible optimization of the customized cross-section for this experiment may be the reason for the results of displacements not improving.

It has been observed that the applied solution in this instance reduced the use of steel with 229 tons, showing a potential for cost reduction, particularly when considering the potential costs of creating a tubular arch with thickness 150 mm and outer diameter 1500 mm as well.

One must also consider the increase in utilization of structural components, showing consistent increase of 0-10 % for most components, which may lead to an increase in cost in relation to need for increased or reinforced cross-sections of certain components. This thus weakens the argument of potential cost reduction by changing the arch to the customized cross-section. More detailed cost-analysis would have to be performed to evaluate and determine the potential savings.

Conclusion If the design is to be altered in regard to the arch cross-section,

it should mainly be as a consequence of the tubular arch cross-section being difficult to manufacture, or too expensive to manufacture. The proposed alternative does however offer potential savings through a weight reduction of 229 tons, and should be considered.

5.6   Adding compression elements between the decks

To prevent the deformation pattern described in the previous sections, a solution that has been tested is the adding of compression elements connecting the two separate decks. The idea was initially also for this solution to have an additional effect, which is illustrated in figure 5.23, of counteracting the torsional forces produced by loading the decks without suspending them on both sides. The amount of torsion produced in this case has however proven insignificant seen in perspective of the large cross-section of the inner tubular beams of the decks, and bending moment about y- and z-axis has turned out to be critical instead. In light of this, the additional desired effect has not been subject for further analysis, but would however be quite interesting were the inner beams of the decks of a smaller cross-section.
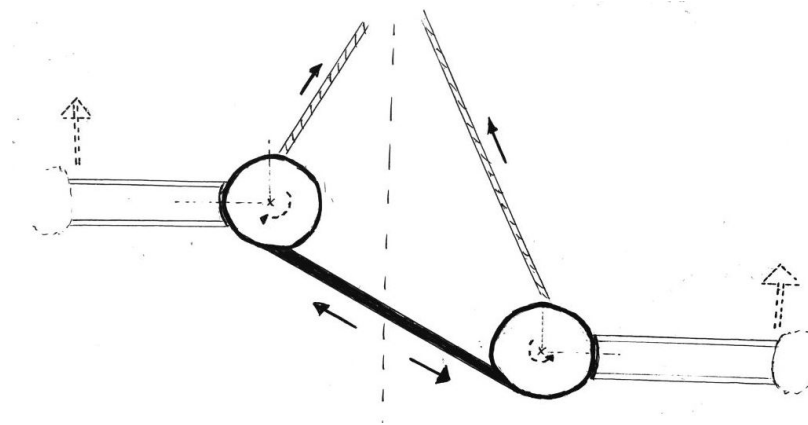
Figure 5.23: Desired additional effect of connecting decks with compression bars.

The hypothesis has here become that the adding of compression elements between the two decks will result in a reduction of sideways displacement of the pedestrian deck.

The connecting compression elements have been found to be most effective when placed where the two decks starts to severely depart in opposite directions from one another, seen in figure 5.24.
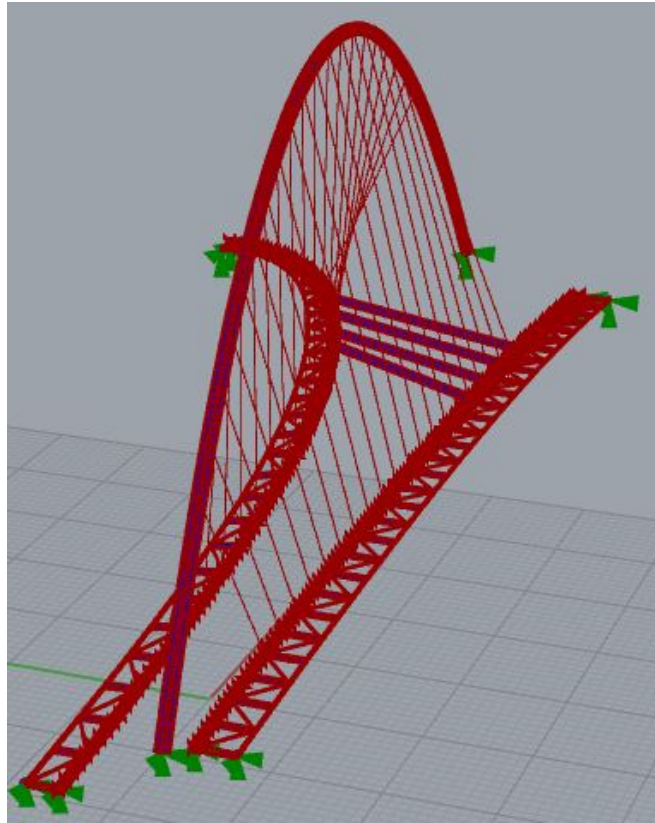
Figure 5.24: Placement of compression elements for connection between decks.

As one might expect, there is quite a large amount of forces being distributed through the compression elements. When arbitrarily adding four compression beams, the result becomes that a cross-section of at least HEB1000 is required when they are placed where they most efficiently affect the sideways displacement. As opposed to come up with an optimal solution for the cross-section, it has here been focused on highlighting the effects of compression elements being present on the structure.

The resulting reduction of displacements is show in figure 5.25 and can be compared to the previously shown displacement in figure 5.22. The values of maximum displacements are presented in table 5.23 and can be compared with the results presented in table 5.23.

It is observed that the sideways displacement in y-direction increases with 2.4 cm, though at the same time decreasing the sideways displacement of the pedestrian deck with 4.5 cm. Also the sideways displacement of the bicycle deck is improved by 2.8 cm. Where the vertical displacement of the of the bicycle deck improves, i.e. decreases with 3.0 cm, the pedestrian deck worsens, having an increase of 2.8 cm in vertical z-direction.
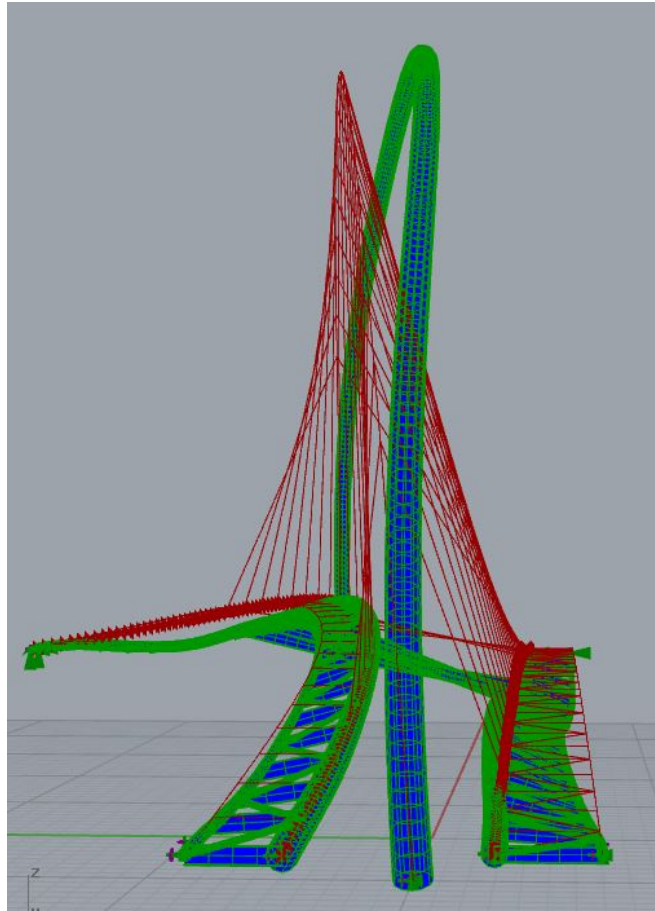
Figure 5.25: Deformation of the bridge with the presence of compression elements for connection between decks.

Structural part	U_x [mm]	U_y [mm]	U_z [mm]
Arch	56	361	69
Pedestrian deck	15	66	278
Bicycle deck	4	27	147

Table 5.23: Values of worst displacement for the bridge with compression elements connecting the two decks.

In addition, connecting the two decks leads to a maximum difference of vertical displacement between the inner and outer tubular beams of the decks of 9 cm over a width of 4 m. This result has been assumed to be acceptable. It can be compared to a value of 11 cm over a width of 4 m when the decks were not connected. By modelling in such a way as to offset the point of connection between the compression elements and the inner tubular beams from the center, as illustrated in figure

refadditional.effect, it would be expected that a nullification of the 9 cm difference in vertical displacement of the inner and outer tubular beams to be possible.

As a result of connecting the two decks, thus preventing sideways displacement of the pedestrian deck especially, an increase in bending moments about y- and z-axis, i.e. "in-plane" and "out-of-plane" bending, from 10 - 20 % is observed in the arch. This result is quite as expected, seeing as the pedestrian deck is no longer yielding to the pull of the cables to the same degree in terms of displacement. This will naturally result in the pull being larger on the arch.

Evaluation In light of adding comfort for the users of the bridge in terms of displacements, and then especially in regard to the sloping resulting from difference in vertical displacement of the inner and outer tubular beams, the addition of compression elements connection the two decks might be a viable option to consider. Seeing as there is no finite requirement of displacement of the arch, and considering that the displacements are relatively small even in the ultimate limit state, this solution may be wise simply to reduce the rotational deformation of the decks. On the other hand, the downside to this solution is that it increases the amount of bending moments in arch significantly, resulting in the need of larger cross-sectional capacities. This in turn leads to increased costs, in addition to the cost of adding the compression elements in itself.

Conclusion The disadvantages of the solution may outweigh the benefits. Considering that the displacements in the ULS were not large to begin with, the proposed solution might seem more costly than the the potential benefits are worth.

6. Summary

The parametric design software Grasshopper 3d and Karamba 3d have been used to carry out the main activities of hypothesis testing, development of conceptual design contribution for the footbridge Conference contribution and further analysis of the final design.

During the course of this thesis, an array of interesting bridges that are asymmetrically suspended has been investigated. Using parametric design for hypothesis testing on four different footbridges, the following results could be derived:

Clavières footbridge: Angular deformations tend to create big deflections as spans grow long in this kind of footbridges.

Jiak Kim bridge: Lean of arch counter to the curvature of the deck is beneficial, both with regards to bending moments out of plane in the arch, and to deflections.

Gateshead Millennium bridge: Fastening the cables on the outside of the decks curvature instead of on the inside might be beneficial, and angle of incidence between the cables and plane drawn by deck benefits from being around 90 degrees.

Liberty bridge: No analysis except "back-of-envelope" conceptual drawings was done, but it showcases that well thought through solutions can slim down potentially heavy designs with clever direction of tensile forces.

This shows us that parametric design tools are very useful when wanting to rapidly explore conceptual design ideas. It allows us to dissect the designs in exploration of how they work mechanically. Most of the operations, when modelling is finished, are simply plug and play. The hypothesis testing provided a general insight into the mechanical workings of an asymmetrically suspended footbridge. The above results provided a basis to make decisions on how the final footbridge design should be analyzed, in order to further investigate its plausibility in chapter V.

Participating in the "Footbridge 2017 Berlin" conference provided a great opportunity to explore the use of parametric design in the actual develop-

ment of a structural design. Many designs were easily (after some initial learning) produced and tested. After having used both parametric design software as well as traditional modelling and analysis software (Robot Structural Analysis during this thesis, and many more in the past), it has become clear that going through this many different designs would be very time consuming without the use of parametric software. Each design would have to be much more developed and conceptualized on paper before modelling and analysis. Using traditional structural analysis software directly and explicitly in the early design phase has proven cumbersome and time-consuming to the authors' experience, whereas with parametric software, the geometry is easily adapted as the concept is developing.

Especially useful is the possibilities of being able to rapidly change the geometry of the structure, getting instant results, and thus indicators on the structures respond to changes, as the conceptual designs are being developed.

Through further analysis of the Footbridge 2017, the Karamba model was verified using a traditional FE-software for modelling as a reference. Furthermore, the plausibility of the concept as a realistic structure was more thoroughly verified through application of a more realistic load situation. It was shown that in order to reduce large deformation of the footbridge's decks, it was necessary to apply sideways (y-directional) stiffening of the decks.

By applying an already investigated cross-section as replacement for the tubular arch, it was found that potential reduction of costs could be achieved, though the solution did not seem to improve efficiency of the structure from a mechanical point of view. It did however potentially add to the structures plausibility, through knowledge of a similar use of cross-section in the reference structure Gateshead Millennium Bridge.

Further analysis also indicated that the assumption of exclusively fixed supports for the structure seemed to be viable solution. Lastly, analysis showed that connecting the two decks with compression elements would have benefits in regards to deformation of the decks, though at the same time leading to a significant increase of forces to be absorbed by the arch.

Although not arriving on any revolutionary discoveries in the further analysis of the final footbridge design, insight into how the parametric deign software can be used for preliminary structural analysis in conceptual design was achieved. It was noticed that applications and testing of different types of solutions to an already existing design concept was quite user friendly once the software had been learned.

6.1 Conclusion

Having experienced the flexibility and accuracy of these types of software, we are confident that some version of this kind of modelling will be dominating also in the field of structural engineering in the coming years, with the possible exception of highly specialized applications. When one has gained some experience in algorithmic thinking, much can be achieved in a short amount of time, especially when it comes to preliminary structural analysis. It is certainly useful for exploring forms and their variants, although caution must be taken to not forget basic engineering knowledge.

6.2 Further work

In order to make the final footbridge design buildable, further work concerning concerning optimization would have to be performed. In regards to parametric design in general, it would have been natural to develop the algorithms here for use in smaller footbridges, both with regards to taking use of the knowledge gained in the testing of hypotheses and to small scale automated production.

List of Figures

95

Conceptual structural design of footbridges:

Bibliography

[1] Statens-Vegvesen. *Håndbok N400: Bruprosjektering - Prosjektering av bruer, ferjekaier og andre bærende konstruksjoner.*, chapter 3.6 Funksjonskrav for bruer, 3.6.1 Deformasjoner, page 44. Vegdirektoratet, 2015.

[2] Per Kr. Larsen, Arild H. Clausen, and Arne Aalberg. *Stålkonstruksjoner - profiler og formler*, pages 24+43. Tapir Akademiske Forlag, 3rd edition, 2003.

[3] Eugenio Merzagora. Online: `http://www.pwcspics.se/switzerland.html`, 2014.

[4] Sebastien Lavachy, Sylvain Plumey, and Thierry Beuchat. *LIGHTWEIGHT DURABLE COMPOSITE DECK OFFERS SOLUTION ON BRIDGE DYNAMICS*, chapter 1, page 7. Footbridge 2014, 2014.

[5] Structurae.net. Jiak kim bridge. Online: `https://structurae.net/structures/jiak-kim-bridge`, accessed 15 June 2017.

[6] Terence Ong. Online: `https://commons.wikimedia.org/wiki/File:Jiak_Kim_Bridge_2.jpg?uselang=nb`, 03 2007.

[7] Andy Williamson. Online: `http://www.picturesofgateshead.co.uk`, 07 2002.

[8] Ramboll. Online: `http://www.ramboll.com/projects/ruk/gateshead%20millennium%20bridgea`, 2003.

[9] Structurae.net. Gateshead millennium bridge. Online: `https://structurae.net/structures/gateshead-millennium-bridge`, accessed 9 June 2017.

[10] Wojtek Gurak. Online: `http://www.mimoa.eu/projects/United%20Kingdom/Newcastle%20upon%20Tyne/Gateshead%20Millennium%20Bridge/`.

[11] John Johnson and Peter Curran. *Proceedings of the Institution of Civil Engineers - Civil Engineering*, volume 156, Issue 1, chapter Gateshead Milenium Bridge - an eye-opener for engineering, pages 16–24. ICE Publishing, February 2003.

[12] Lee Parks. Online: `https://www.flickr.com/photos/peacefultraveler/6915441713/`.

[13] Per Kr. Larsen. *Dimensjonering av stålkonstruksjoner*, chapter Torsjon, pages 115–125. Fagbokforlaget, 2nd edition, 2010.

[14] TriPyramid Structures Inc. Structural tension assemblies. rod & cable mechanical properties. Online: `http://www.tripyramid.com/?q=tension-elements#`.

DIE BROMMY-KREUZUNG

Kristian M. EICK
Student at the Institute of Structural Engineering
Norwegian University of Technology and Science
Trondheim, Norway
kristeic@stud.ntnu.no

Herman E. AAS
Student at the Institute of Structural Engineering
Norwegian University of Technology and Science
Trondheim, Norway
hermanea@stud.ntnu.no

Figure 1: Bridge design "Die Brommy-Kreuzung". rendering by Eick & Aas, 2017.

LOCATION

The crossing between the Berlin downtown districts of Kreuzberg and Friedrichshain over the river Spree. The width of the river is approximately 110 m.

PURPOSE

With the planned development of the previous industrial area to the north and south of the old river-crossing, a bridge connecting the two areas is attractive. Situated with the old bridge-pier in the south-end and the remainings of the Berlin Wall near the north-end, the bridge will benefit tourists taking in the views of the area as well. In crossing the bridge, pedestrians will pass and see the remaining pier as a monument of the old Brommybrücke which was destroyed during the war.

APPROACH

As the design of the bridge is part of a master thesis concerning conceptual design in genereal and parametric design in particular, it was largely conceived with the software Grasshopper and assorted plug-ins to make changes to the design quick and easily assesed. The main focus was on accentuating the remains of the old Brommybrücke for pedestrians in addition to giving a good view of the old berlin wall, as well as getting cyclists from one side to the other separately from the pedestrians.

THE LOAD BEARING SYSTEM

To give the sensation of openness to each side in addition to not disturbing already established routes of travel on the river, decks suspended on one side from an arch were chosen, necessating a very prominent arch and very torsionally stiff decks.

THE ONE-SIDED BEARING OF THE DECKS

The idea of having cables attached on one side of the deck is inspired by reference bridges such as Jiak Kim Bridge in Singapore and Gateshead Milenium Bridge in Newcastle. The idea is to give the sense of a more open space both when using the bridge and when viewing it from either riverbed. It also enables the use of different directions for the two decks using one arch, as connecting cables on the outsides of the decks would have physically obstructed the path.
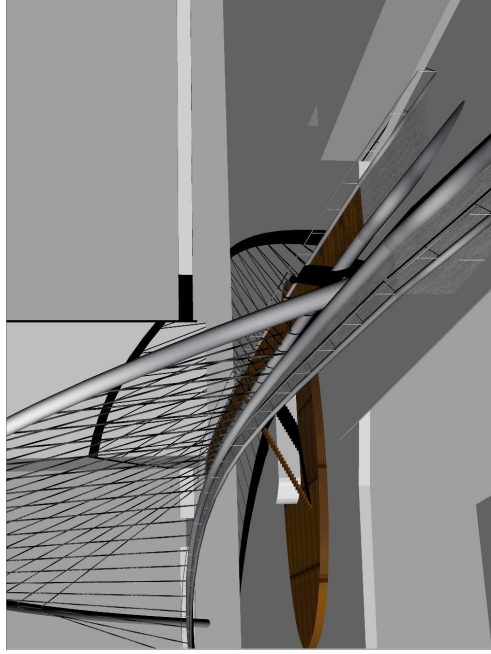
Figure 2: Bridge design "Die Brommy-Kreuzung". Rendering by Eick & Aas, 2017.

THE TWO SEPERATE DECKS

The idea of the curved deck sprung from wanting to highlight the remaining abutment of the old Brommybrücke as a monument for those using the bridge as well as leading cyclists smoothly from crossing the river to cycling along it. To prevent larger groups of pedestrians pausing to view the pylon from interferring with bicycle traffic, two decks are used. The pedestiran deck spans the Spree in a straight line, giving a walking distance of ~134 m, while the deck for cycling, with both more vertical and lateral curvature, has a total length of ~162 m. Staircases leading down to the existing pier with a platform provide a place to enjoy the afternoon sun along the river. Structurally the two decks work together as a seesaw, as in cases with high loading on one deck the other deck's stiffness counteracts the loaded deck's deflection.
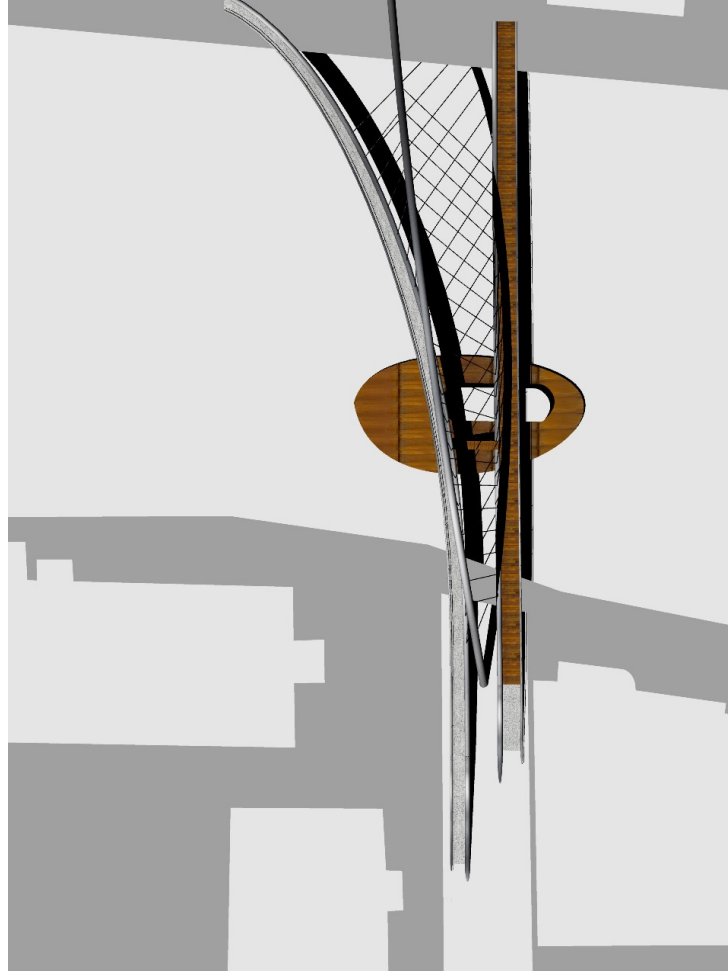
Figure 3: Bridge design "Die Brommy-Kreuzung". Rendering by Eick & Aas, 2017.

ABUTMENTS

On each end of the bridge there are concrete abutments, giving the bridge solid anchoring as well as separation of pedestrians and cyclists. On the south side of the river a ramp, through which pedestrians can walk, leads up to the elevated cycling deck, thereby giving access to the pedestrian deck from all sides.

SUGGESTIONS FOR ADDITIONAL RAMPS

To gain access to the old pier, stairs descending from the pedestrian deck to a platform around the pier suspended from the decks is suggested. Additional stairs ascending up to the cyclist deck is another element that will provide a place to rest, party, eat or enjoy the view from the river.

THE LOAD BEARING ARCH

Tasked with being the load-bearer for both decks, initial analysis indicates that a circular hollow cross-section 150 cm in diameter required. A total height of ~42 meters makes it a big feature in the landscape.

TORSIONAL STIFFNESS OF DECKS

One-sided sagging of the decks is prevented by pipes spanning along the decks. They take the brunt of the torsion experienced by the decks and thusly end up at a size big enough to become a dominating part of the design.

MEASUREMENTS

Figure 5: Bridge design "Die Brommy-Kreuzung". Model sketch by Eick & Aas, 2017.
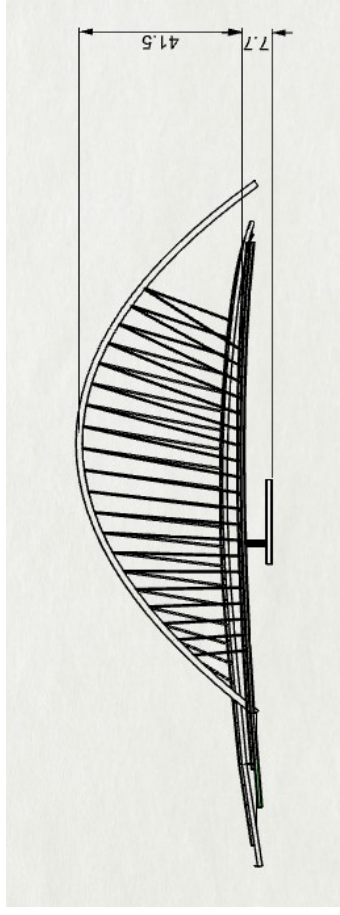
Figure 6: Bridge design "Die Brommy-Kreuzung". Model sketch by Eick & Aas, 2017.

Dimensions of circular hollow cross-sections	Diameter [cm]	Wall thickness [cm]
(Deck: Outer sections)	40	5
Deck: Suspended inner sections	100	10
Arch	150	15

Table 1: Dimensions of the circular cross-sections used in the model.

Figure 4: Bridge design "Die Brommy-Kreuzung", rendering by Eick & Aas, 2017.

Attachment B: Snow load

NS-EN 1991-1-3:2003/NA:2008

<u>Classification of snow load:</u>

(NA.2) In Norway, snow load is generally neither treated as an exceptional load nor an accidental load. It is assumed that the same applies for Germany.

3.2: Assuming normal conditions leads to determination of snow load by using 5.2(3)P a) and 5.3.

5.2(3)P a): Persistent/transient design situation

$(5.1)\ s := \mu_i \cdot C_e \cdot C_t \cdot s_k$

5.2(8): No heating of the decks that leads to the melting of snow
$C_t := 1.0$

$$1.0 \tag{1}$$

Table 5.1: Conservatively assuming that the structure is situated lower than its surroundings, so that snow is not removed by wind
$C_e := 1.2$

$$1.2 \tag{2}$$

Assuming that the deck is flat and that no snow slides off due the shape, resulting in shape factor:
$\mu_i := 1.0$

$$1.0 \tag{3}$$

Table C.1: Characteristic snow load on ground based on region and height above sea level

Germany is located in Central-Europe, east
The Brommy site is located 36.8 meters above sea level according to the site information

Zone number:
$Z := 3$

$$3 \tag{4}$$

Sites height above sea level [m]:
$A := 36.8$

$$36.8 \tag{5}$$

Resulting in characteristic snow load on the ground for the Brommy site:

$$s_k := (0.264 \cdot Z - 0.002) \cdot \left(1 + \left(\frac{A}{256}\right)^2\right) \cdot \frac{kN}{m^2}$$

$$\frac{0.8063246090\ kN}{m^2} \tag{6}$$

NS-EN 1991-1-3 (5.1) gives characteristic snow load on the bridge:
s

$$\frac{0.9675895308 \; kN}{m^2} \tag{7}$$

NS-EN 1990:2002+A1:2005+NA:2016 Table A2.4(A) gives safety factor for where relevant

$\gamma_s := 1.50$

$$1.50 \tag{8}$$

Resulting in design load for snow:

$S := \gamma_s \cdot s$

$$\frac{1.451384296 \; kN}{m^2} \tag{9}$$

Attachment C: Traffic load

NS-EN 1991-2:2003+NA:2010

Table 2.1: **Footbridge**

Uniformly distributed load as a nominal value to represent a crowd given in 5.3.2.1.

Load model for representing a service vehicle as a nominal value given in 5.3.2.3 and 5.6.3.

Section 3: Design cases shall be made out of critical combinations.

Section 5: Footbridges

5.3.2.1 Crowd loading (uniformly distributed load)

For the given footbridge situated in the center of Berlin, it is evaluated that one must take into account that the entire bridge is loaded with a continuous crowd, which means that the recommended value of

$$q_{fk} := 5\frac{kN}{m^2}$$

$$\frac{5\ kN}{m^2} \tag{1}$$

as a characteristic value for the crowd loading applies.

5.3.2.2 Concentrated load

(3) Since the bridge requirements specify that a service vehicle shall be taken into account, a concentrated load Q_{fwk} is not applicable.

5.3.2.3 Service vehicle

Since no other information about the service vehicle is provided, except that it is to be accounted for, combined with the fact that there is nothing to prevent an accidental car appearance on the bridge, the load situation for an accidental car given in 5.6.3 applies for the service vehicle.
Note 1: when the load situation for an accidental car is used for the service vehicle, there is no need to apply 5.6.3 to consider an accidental car, i.e. it is assumed that considering the one is sufficient and accounts for both events.

5.6.3(2) Load model for vehicle
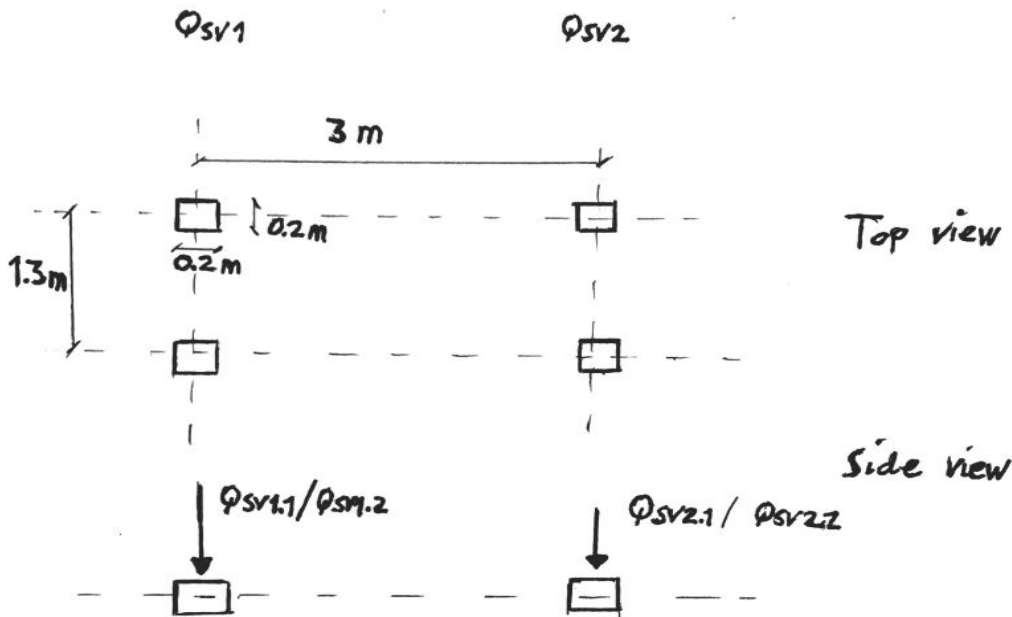
Figure C.1 "Simplified wind load model".

Vertical loads Qsv1 and Qsv2 are the loads working on each shaft of the vehicle and have recommended values as follows:

$$Q_{SV1} := 80 \ kN$$

$$80 \ kN \tag{2}$$

$$Q_{SV2} := 40 \ kN$$

$$40 \ kN \tag{3}$$

Each shaft load is distributed equally to each of the shafts' two wheels, working over a surface 0.2 x 0.2 $\left[m^2 \right]$ for transference to the surface of the deck.

$$Q_{SV1.1=SV1.2} := 40 \ kN$$

$$40 \ kN \tag{4}$$

$$Q_{SV2.1=SV2.2} := 20 \ kN$$

$$20 \ kN \tag{5}$$

or subsequently

$$q_{SV1.1=SV1.2} := \frac{40 \ kN}{0.2 \cdot 0.2 \cdot m^2}$$

$$\frac{1000.000000 \ kN}{m^2} \tag{6}$$

$$q_{SV2.1=SV2.2} := \frac{20 \ kN}{0.2 \cdot 0.2 \cdot m^2}$$

$$\frac{500.0000000 \ kN}{m^2} \tag{7}$$

5.4 Horizontal force (footbridges only) to ensure horizontal longitudinal stability

Q_{flk} is the greater value out of

10% of total vertical loading due to the crowd load
60% of total vertical loading due to the vehicle

An approximation of the the area of each of the bridge decks has been estimated to be roughly no larger than 150 m x 3 m.

$Q_{flk1} := 0.1 \cdot q_{fk} \cdot 150 \cdot m \cdot 3 \cdot m$

$$225.0 \ kN \tag{8}$$

$Q_{flk2} := 0.6 \cdot (Q_{SV1} + Q_{SV2})$

$$72.0 \ kN \tag{9}$$

Resulting in horizontal loading
$Q_{flk} := Q_{flk1}$

$$225.0 \ kN \tag{10}$$

working at the same height as the pavement 5.6.3(2).

5.4(3)
The horizontal loading should work together with the corresponding vertical force.

5.6.3(3)
No variable action should be taken into account simultaneously with the load model for an accidental car.

5.6 Collision forces on piers

5.6.2.1 (1) b)
Impact force has a recommended value of 1000 kN in vehicle traffic direction or 500 kN perpendicular to vehicle traffic direction and has a height of impact of 1.25 m.
This applies in general if the footbridge crosses a trafficated road etc.

For a road located in a city environment, table 4.1 in NS-EN 1991-1-7 for accidental loads recommends a value of respectively 500 kN and 250 kN parallel and perpendicular to the vehicle traffic direction for an accidental crash from a vehicle to a structure's piers.

Attachment D: Thermal load

NS-EN 1991-1-5:2003+NA:2008

As the Karamba and Robot software takes input ΔT and the material to account for thermal forces, ΔT is what is relevant to extract from the Standard.

5 Temperature variations in structures

Table 5.2 Recommended outdoor temperature for buildings above terrain.

Assuming a dark surface due to coating of the steel for the relative absorption factor, so that all coatings may chosen later without any problem.

Temperature summer: $T_{max} + T_5$

Temperature winter: T_{min}

Recommended value for T_5 for surfaces oriented towards south-west or horizontal surfaces

$T_5 := 42\ °C$

As the available eurocode applies for Norwegian regions, temperatures T_{max} and T_{min} for Berlin is found using the record maximum and record minimum temperatures in Berlin as published by RM, 2011 on the BBC Weather internet page, and found to be

$T_{max} := 37\ °C$

$T_{min} := -21\ °C$

Average Conditions data © Copyright RM, 2011. All rights reserved. Helicon Publishing is a division of RM.
http://www.bbc.com/weather/2950159

Resulting in ΔT

$\Delta T = T_{max} + T_5 - T_{min}$

$\Delta T := 37 + 42 - (-21)$

<div align="center">100</div> **(1)**

$\Delta T := 100\ °C$

<div align="center">$100\ °C$</div> **(2)**

Furthermore it is assumed that a logical approach will be to build the bridge so that no thermal forces will act on the bridge at the mean temperature, T_{build}, between T_{max} and T_{min}

$$T_{mean} = \frac{T_{max} - T_{min}}{2}$$

$$T_{mean} := \frac{37 - (-21)}{2}$$

<div align="center">29</div> **(3)**

$$T_{build} = T_{min} + T_{mean}$$

$$T_{build} := (-21) + 29$$

<div align="center">8</div> **(4)**

$$T_{build} := 8\ °C$$

<div align="center">$8\ °C$</div> **(5)**

Meaning that the temperature can swing from $8\ °C \pm \frac{\Delta T}{2}$, causing thermal forces in the structure.

This results in the temperature input being $\pm 50\ °C$, which is $\frac{\Delta T}{2}$, when considering the thermal loading in the software.

Attachment E: Wind load

NS-EN 1991-1-4:2005+NA:2009

Since the available standard contains data for Norwegian regions, the simplification of assuming that wind loads for downtown Berlin can be compared with Oslo, Norway.

4.2 Reference values

(4.1)

$c_{dir} := 1.0$

$$1.0 \tag{1}$$

$c_{season} := 1.0$

$$1.0 \tag{2}$$

Table NA.4(901.1) Reference wind velocity $v_{b,0}$ for regions - Oslo

$v_{b,0} := 22 \dfrac{m}{s}$

$$\dfrac{22 \; m}{s} \tag{3}$$

$v_b := c_{dir} \cdot c_{season} \cdot v_{b,0}$

$$\dfrac{22.00 \; m}{s} \tag{4}$$

4.3 Average wind

4.3.2

Assuming terrain class IV due to heavily populated city environment

$z_0 := 1.0 \; m$

$$1.0 \; m \tag{5}$$

$z_{0,II} := 0.05 \; m$

$$0.05 \; m \tag{6}$$

$z_{min} := 10 \; m$

$$10 \; m \tag{7}$$

$z_{max} := 200 \; m$

There is created a simplified model of the wind load on the bridge structure as seen below (right hand side shows simplified model)
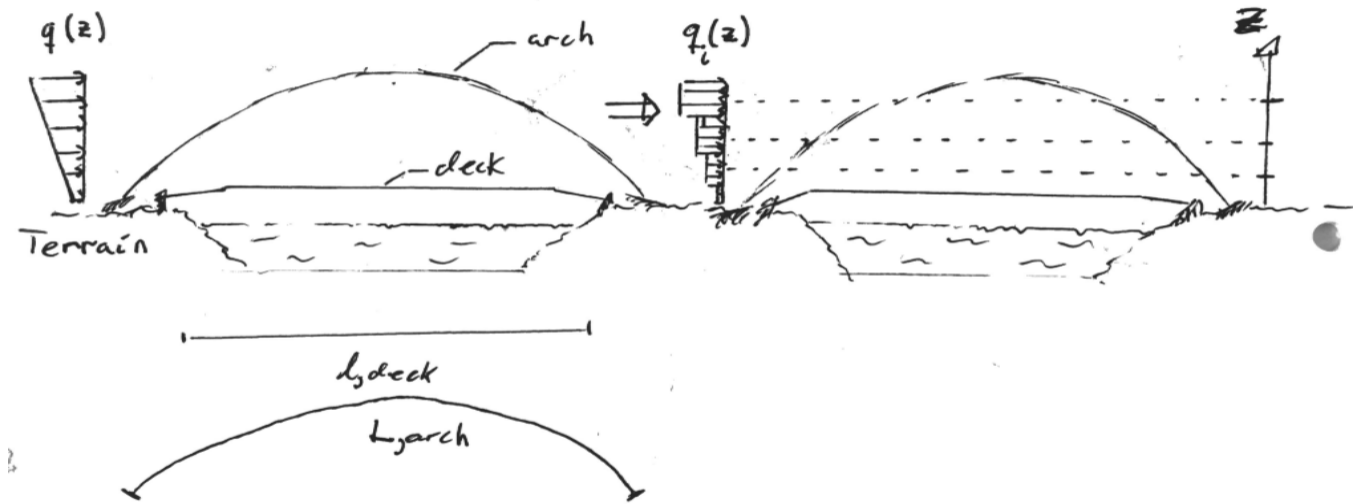
Figure E.1 "Simplified wind load model".

Neither of the two bridge decks reaches a height, z, above the terrain significantly larger than 10 m during the span, L. The wind load for the decks is therefore most accurately calculated using the value of z_{min}.

$$z \leq z_{min} \implies q_p(z_{min})$$

The arch has a total height of 46 m according to the current model. It has been chosen to divide the arch into three separate parts with regards to the height for the simplified model of the wind load. The height of each part of the arch then becomes 46/3 m which is approximately 15.3 m. There is then two approaches for calculating the values of the wind load for each part of the arch. Either one can choose the reference height to be at the midpoint (z-direction) of the arch part, or one can choose a more conservative approach and choose that the reference height is at the top of each part.

Here, the more conservative assumption is chosen, resulting in the following reference heights for each of the arch parts:

$z_{e,arch,lower} := 15.3\ m$

$$15.3\ m \tag{8}$$

$z_{e,arch,middle} := 30.6\ m$

$$30.6\ m \tag{9}$$

$z_{e,arch,upper} := 45.9\ m$

$$45.9\ m \tag{10}$$

$$z_{min} \leq z_{e,arch,i} \leq z_{max}$$

(4.5)

$$k_r := 0.19 \cdot \left(\frac{z_0}{z_{0,II}} \right)^{0.07}$$

<div align="center">0.2343288174</div>   **(11)**

(4.4)

$$c_{r,deck} := k_r \cdot \ln \left(\frac{z_{min}}{z_0} \right)$$

<div align="center">0.5395620418</div>   **(12)**

$$c_{r,arch,lower} := k_r \cdot \ln \left(\frac{z_{e,arch,lower}}{z_0} \right)$$

<div align="center">0.6392145272</div>   **(13)**

$$c_{r,arch,middle} := k_r \cdot \ln \left(\frac{z_{e,arch,middle}}{z_0} \right)$$

<div align="center">0.8016388864</div>   **(14)**

$$c_{r,arch,upper} := k_r \cdot \ln \left(\frac{z_{e,arch,upper}}{z_0} \right)$$

<div align="center">0.8966510457</div>   **(15)**

4.3.1

Wind velocity for site

$$c_0 := 1.0$$

<div align="center">1.0</div>   **(16)**

$$v_{m,deck} := c_0 \cdot c_{r,deck} \cdot v_b$$

<div align="center">$11.87036492 \; \frac{m}{s}$</div>   **(17)**

$$v_{m,arch,lower} := c_0 \cdot c_{r,arch,lower} \cdot v_b$$

<div align="center">$14.06271960 \; \frac{m}{s}$</div>   **(18)**

$$v_{m,arch,middle} := c_0 \cdot c_{r,arch,middle} \cdot v_b$$

<div align="center">$17.63605550 \; \frac{m}{s}$</div>   **(19)**

$$v_{m,arch,upper} := c_0 \cdot c_{r,arch,upper} \cdot v_b$$

<div align="center">$19.72632301 \; \frac{m}{s}$</div>   **(20)**

4.4 Wind turbulence

(4.7)

$$k_l := 1.0$$

$$1.0 \qquad\qquad\qquad\text{(21)}$$

$$I_{v,deck} := \frac{k_l}{c_0 \cdot \ln\left(\dfrac{z_{min}}{z_0}\right)}$$

$$0.4342944819 \qquad\qquad\qquad\text{(22)}$$

$$I_{v,arch,lower} := \frac{k_l}{c_0 \cdot \ln\left(\dfrac{z_{e,arch,lower}}{z_0}\right)}$$

$$0.3665886919 \qquad\qquad\qquad\text{(23)}$$

$$I_{v,arch,middle} := \frac{k_l}{c_0 \cdot \ln\left(\dfrac{z_{e,arch,middle}}{z_0}\right)}$$

$$0.2923121886 \qquad\qquad\qquad\text{(24)}$$

$$I_{v,arch,upper} := \frac{k_l}{c_0 \cdot \ln\left(\dfrac{z_{e,arch,upper}}{z_0}\right)}$$

$$0.2613378064 \qquad\qquad\qquad\text{(25)}$$

4.5 Pressure from wind gust velocity

(4.10)

Recommended value for air density is
$$\rho := 1.25 \frac{kg}{m^3}$$

$$\frac{1.25\ kg}{m^3} \qquad\qquad\qquad\text{(26)}$$

Pressure from wind gust velocity for site (NA.4.5(1))

$$q_b := \frac{1}{2} \cdot \rho \cdot v_b^{\,2} \quad [\text{Pa}]$$

$$\frac{302.5000000\ kg}{m\,s^2} \qquad\qquad\qquad\text{(27)}$$

(4.8)

Short-term top value for pressure from wind gust velocity

$$q_{p,deck} := \left(1 + 7 \cdot I_{v,deck}\right) \cdot \frac{1}{2} \cdot \rho \cdot v_{m,deck}^2 \quad [\text{Pa}]$$

$$\underline{355.7919522 \ \frac{kg}{m \, s^2}} \tag{28}$$

$$q_{p,arch,lower} := \left(1 + 7 \cdot I_{v,arch,lower}\right) \cdot \frac{1}{2} \cdot \rho \cdot v_{m,arch,lower}^2 \quad [\text{Pa}]$$

$$\underline{440.7727201 \ \frac{kg}{m \, s^2}} \tag{29}$$

$$q_{p,arch,middle} := \left(1 + 7 \cdot I_{v,arch,middle}\right) \cdot \frac{1}{2} \cdot \rho \cdot v_{m,arch,middle}^2 \quad [\text{Pa}]$$

$$\underline{592.1602510 \ \frac{kg}{m \, s^2}} \tag{30}$$

$$q_{p,arch,upper} := \left(1 + 7 \cdot I_{v,arch,upper}\right) \cdot \frac{1}{2} \cdot \rho \cdot v_{m,arch,upper}^2 \quad [\text{Pa}]$$

$$\underline{688.1153095 \ \frac{kg}{m \, s^2}} \tag{31}$$

(4.9)

Exposure factor relevant for calculation of the forces working on the decks

$$c_e := \frac{q_{p,deck}}{q_b}$$

$$\underline{1.176171743} \tag{32}$$

8 Wind load on bridges

Decks

Lets assume for the sake simplicity that each deck has a rectangular cross-section with measurements

$$d_{height} := 0.5 \ m$$

$$\underline{0.5 \ m} \tag{33}$$

$$b_{width} := 3 \ m$$

$$\underline{3 \ m} \tag{34}$$

and an average length of approximately (can be arbitrarily chosen since we want the result in $\frac{kN}{m^2}$ by dividing with the length later $\Rightarrow$ length superfluous)

$$l := 140 \ m$$

$$140 \ m \tag{35}$$

Results in a reference area of

$$A_{ref,z} := l \cdot b_{width}$$

$$420 \ m^2 \tag{36}$$

for wind in vertical direction, and

$$A_{ref,x} := l \cdot d_{height}$$

$$70.0 \ m^2 \tag{37}$$

for wind in horizontal direction.

Wind force in horizontal direction perpendicular to the bridge span

(8.1)

$$\frac{b_{width}}{d_{height}}$$

$$6.000000000 \tag{38}$$

$$c_{f,x} := 1.0$$

$$1.0 \tag{39}$$

$$C_x := c_{f,x} \cdot c_e$$

$$1.176171743 \tag{40}$$

(8.2)
Assuming that dynamic response calculations not necessary (Simplified solution)

$$F_W := q_b \cdot C_x \cdot A_{ref,x}$$

$$\frac{24905.43666 \ kg \ m}{s^2} \tag{41}$$

Excluding the reference area, a horizontal planar load more applicable for the software is found:

$$q_{W,horizontal} := q_b \cdot C_x$$

$$\frac{355.7919523 \ kg}{m \ s^2} \tag{42}$$

which is equal to $q_{W,horizontal} = 0.356 \ \dfrac{kN}{m^2}$

Wind force in horizontal direction parallel to the bridge span

8.3.4 (1)

Assuming structure is a beam bridge, the wind force on the deck horizontally and parallel to the span of the deck is 25 % of the wind force perpendicular to the span of the deck.

$0.25 \cdot F_W$

$$\frac{6226.359165 \; kg \; m}{s^2} \tag{43}$$

which is equal to 6.2 kN. This value is quite low, especially compared to the required horizontal load parallel to the span due to the traffic load. It is therefore neglected for the sake of simplicity.

Wind force in vertical direction perpendicular to the deck surface

8.3.3

$c_{f,z} := 0.9$

$$0.9 \tag{44}$$

$C_z := c_{f,z} \cdot c_e$

$$1.058554569 \tag{45}$$

$F_W := q_b \cdot C_z \cdot A_{ref,z}$

$$\frac{1.344893580 \; 10^5 \; kg \; m}{s^2} \tag{46}$$

Excluding the reference area, a vertical planar load more applicable for the software is found:

$q_{W,vertical} := q_b \cdot C_z$

$$\frac{320.2127571 \; kg}{m \, s^2} \tag{47}$$

which is equal to $q_{W,vertical} = 0.320 \; \dfrac{kN}{m^2}$

Wind load on the arch as a structural member

6.2 Determination of structure factor:

As there are no standard recommended values for the given arch, and as we are missing information for manual calculation, we shall have to assume a factor for the structural member, no less than 0.85.

A generally recommended value would be 1.0, and is what will be assumed for the calculation for the force on the arch.

$c_s c_d := 1.0$

7.9.1 Outer shape-factor

$b := 1.5 \; m$

$$1.5 \; m \tag{48}$$

$v := 15 \cdot 10^{-6} \cdot \dfrac{m^2}{s}$

$$\frac{3}{200000} \quad \frac{m^2}{s} \tag{49}$$

$v_{Ze} := \sqrt{\dfrac{2 \cdot q_{p,arch,upper}}{\rho}}$

$$33.18108640 \; \sqrt{\frac{m^2}{s^2}} \tag{50}$$

(7.15) Reynold's value

$R_e := \dfrac{b \cdot v_{Ze}}{v}$

$$\frac{3.318108640 \; 10^6 \; \sqrt{\dfrac{m^2}{s^2}} \; s}{m} \tag{51}$$

(7.19) Force factor for cylinder with ∞ slenderness

$\psi_\lambda := 0.99$ (fig. 7.36)

$$0.99 \tag{52}$$

Roughness k for steel is 0.05 (table 7.13)

$$\frac{k}{b} = \frac{0.05}{1.5} = 0.033 \approx 10^{-2}$$

(fig. 7.28)

$c_{f,0} := 1.05$

$$1.05 \tag{53}$$

$c_f := c_{f,0} \cdot \psi_\lambda$

$$1.0395 \tag{54}$$

Note: as the entire arch has the same k/b and ψ_λ value, the only thing affecting the force factor is the Reynold's value through v_{Ze}. As the Reynold's value does not differ significantly enough to be able to read a different value for $c_{f,0}$ than 1.05, the force factor c_f remains unchanged for all three parts of the arch.

Wind load on arch

Length of the entire arch from software measurement
$L := 190 \ m$

$$190 \ m \tag{55}$$

$A_{ref,arch} := L \cdot b$

$$285.0 \ m^2 \tag{56}$$

However, in this case, the desired result is the force working for each part of the arch over its length, i.e. in $\dfrac{kN}{m}$, for a more applicable result for the software. This means that L is superfluous and can be excluded as follows:

(5.3) Wind load working on the arch

$$F_{W,arch} = c_s c_d \cdot c_f \cdot q_p \cdot A_{ref,arch}$$

$$Q_{W,arch} = \frac{F_{W,arch}}{L}$$

$c_s c_d = 1.0$ as previously found in (6.2)

Wind load for each part of the arch

$$Q_{W,arch,i} := c_s c_d \cdot c_f \cdot q_{p,arch,i} \cdot b$$

$$Q_{W,arch,lower} := 1.0 \cdot c_f \cdot q_{p,arch,lower} \cdot b$$

$$\frac{687.2748638 \ kg}{s^2} \tag{57}$$

$$Q_{W,arch,middle} := 1.0 \cdot c_f \cdot q_{p,arch,middle} \cdot b$$

$$\frac{923.3258714 \ kg}{s^2} \tag{58}$$

$$Q_{W,arch,upper} := 1.0 \cdot c_f \cdot q_{p,arch,upper} \cdot b$$

$$\frac{1072.943796 \ kg}{s^2} \tag{59}$$

Estimation of the wind force acting over the length of each of the arch parts:

$$Q_{W,arch,lower} = 0.687 \ \frac{kN}{m}$$

$$Q_{W,arch,middle} = 0.923 \ \frac{kN}{m}$$

$$Q_{W,arch,upper} = 1.073 \ \frac{kN}{m}$$